The Oxidative Dehydrogenation of *n*-Octane using Manganese Oxide Supported on SBA-15 Catalysts

Kershen Naicker

June 2014

The Oxidative Dehydrogenation of *n*-Octane using Manganese Oxide Supported on SBA-15 Catalysts

By

Kershen Naicker

Submitted in fulfilment of the academic requirements for the degree of
Master of Science in the
School of Chemistry and Physics
University of KwaZulu-Natal
Durban
South Africa

June 2014

As the candidate's supervisor/s I have approved this thesis/dissertation for submission.

Signed: _____ Name: Prof. H.B. Friedrich Date: _____

Signed: _____ Name: Dr. S. Singh Date: _____

Abstract

Supported metal oxides have been widely used in heterogeneous catalysis, particularly for the activation of paraffin's. For this study, manganese oxide supported on SBA-15 was used to investigate the oxidative dehydrogenation of *n*-octane. Wet impregnation was used firstly to synthesize catalysts with clusters of manganese oxide on the surface of the SBA-15 support. Thereafter, deposition precipitation was used to prepare catalysts with metal oxides in the pores of the SBA-15 support. Weight loadings of 2, 5 and 9 weight percent were synthesized for both groups of catalysts.

Catalysts were characterized by inductively coupled plasma – optical emission spectroscopy, Raman spectroscopy, powder and *in situ* X-ray diffraction, temperature programmed analyses, oxygen chemisorption, nitrogen physiorption, Brunauer-Emmet-Teller surface analyses, transmission electron microscopy and scanning electron microscopy with energy dispersive X-ray spectroscopy. With most characterization techniques, clear differences were seen for catalysts with metal oxide on the surface of the support when compared to those with metal oxide in the pores of the SBA-15 support at the same weight loadings. However, the dominant phase present at room temperature was found to be Mn_3O_4 for both groups of catalysts, with a phase change to MnO taking place after reduction similarly for both groups of catalysts.

The catalysts were tested in a continuous flow fixed-bed reactor system. The support and all catalysts were found to be active for the oxidative dehydrogenation of *n*-octane. Dominant product groups obtained were octene isomers, aromatic compounds, cracked products and carbon oxides. Desired products groups were octene isomers and aromatic compounds and based on this and conversions of *n*-octane, reaction conditions were optimized and all catalysts were tested and compared under optimum conditions. From the results obtained, insight into product pathways were obtained and a reaction mechanism was proposed for this metal oxide system. The 9 weight percent catalysts were found to provide the best conversions for both groups of catalysts, with catalysts having metal oxide on the surface displaying greater conversion than catalysts with metal oxides in the pores of the SBA-15 support, likely due to the enhanced accessibility of the active site. The lower accessibility of the active site did however lead to one product group having high selectivity for catalysts with metal oxide in the pores, with carbon oxides and octenes being the most selective product group for the 2 and 9 weight percent catalysts respectively.

Preface

The experimental work described in this thesis was carried out in the School of Chemistry and Physics, University of KwaZulu-Natal, Westville Campus from March 2012 to November 2013, under the supervision of Prof. Holger B. Friedrich and the co-supervision of Dr. Sooboo Singh.

This study represents original work by the author and has not otherwise been submitted in any form for any degree or diploma to any tertiary institution. Where use has been made of the work of others, it is duly acknowledged in the text.

Declaration – Plagiarism

I, Kershen Naicker, declare that:

1. The research reported in this thesis, except where otherwise indicated, is my original work.

2. This thesis has not been submitted for any degree or examination at any other university.

3. This thesis does not contain any other person's data, pictures, graphs or other information, unless specifically acknowledged as being sourced from other persons.

4. This thesis does not contain other person's writing unless specifically acknowledged as being sourced from other researchers. Where other written sources have been quoted, then:

(a). Their words have been re-written but the general information attributed to them has been referenced.

(b). Where the exact words have been used, then their writing has been placed in italics and inside quotation marks, and referenced.

5. This thesis does not contain text, graphics or tables copied and pasted from the internet, unless specifically acknowledged, and the source being detailed in the thesis and in the Reference sections.

Signed:

_____

Kershen Naicker

Conference Contributions

Parts of this work have been presented at conferences as detailed below:

1. Poster presentation, Catalysis Society of South Africa (CATSA) conference, Langebaan, RSA, November 2012, titled "The synthesis and characterization of SBA-15 supported catalysts".

2. Poster presentation, European Congress of Catalysis (Europacat) conference, Lyon, France, September 2013, titled "The oxidative dehydrogenation of *n*-octane over manganese oxide supported on SBA-15 catalysts".

3. Discussion symposia oral presentation, European Congress of Catalysis (Europacat) conference, Lyon, France, September 2013, titled "The influence of the position of the active site for the oxidative dehydrogenation of *n*-octane over manganese oxide supported on SBA-15 catalysts".

4. Oral presentation, Catalysis Society of South Africa (CATSA) conference, Port Edward, RSA, November 2013, titled "The oxidative dehydrogenation of *n*-octane over manganese oxide supported on SBA-15 catalysts – effect of the active site position".

Acknowledgements

First and foremost I would like to thank my supervisors, Prof. Friedrich and Dr. Singh. This research work would not have been possible if not for your effort. Thank you for your patience, advice, motivation, criticism, time and immense pool of knowledge. I could not have chosen a better collaboration for the supervision of this research project.

A sincere and heartfelt thanks goes out to Dr. Abdul S. Mahomed for his help throughout this research project. Thank you for your time, patience, input, assistance and direction for the completion of this research project.

This work would not have been possible, if not for the University of KwaZulu-Natal, which allowed me to register for the MSc degree, SASOL, NRF and THRIP for funding throughout this project.

I would like to thank my mentors at the Catalysis Research Group at UKZN, Dr. Venkata Dasireddy and Dr. Thashini Chetty, for their guidance and support throughout this project. I would also like to thank Mr. Drushan Padayachee, Mr. Ziyaad Mohamed and Mr. Ajij Golandaj for assistance with experimental work and support and also thank other members of the Catalysis Research Group for their assistance.

I wish to thank academic, support and technical staff of the School of Chemistry and Physics (UKZN), in particular Mr. A. Bissessur, Mr. G. Moodley, Mrs. T. Naidoo and Mrs. V. Reddy. I would also like to thanks all the members of the Electron Microscopy unit at UKZN for assistance with microscopy.

I would also like to thank Dr. Michael Datt, Dr. Johnathan Chetty, Dr. Pheladi Mohlala and Ms. Alisa Govender of SASOL for their time, direction and input into the research project.

To my parents, Melanie and Ruben, for their love, for raising me into the man I have become and being the best role models a person could ask for.

Thank you to my brother, Edwin, sister, Sharice and extended family for their support throughout my studies.

A special thank you to Christina for her love, care, motivation and always being there for me. A much needed smile and reassurance in times of doubt will forever and always be appreciated.

To my friends, Sabena, Chrisanne, Darrel, Dukhi, Dunesha, Krissy, Leeven, Letisha, Mzamo, Shirveen, Sofiah, Terelle and Vashen for your motivation and much needed distractions at times.

Dedication

To my late great grandmother, Mrs. D, Gounden

for her love, care and support.

Forever loved and always missed.

Table of Contents

	Page No.
Abstract	i
Preface	ii
Declaration – Plagiarism	iii
Conference Contributions	iv
Acknowledgements	v
Dedication	vii
Table of Contents	viii
List of Figures	xiii
List of Tables	xiii
Abbreviations	xix
Calculations	xxi
Chapter 1 - Introduction and literature review	**1**
1.1 Introduction to catalysis	1
1.2 Homogeneous and heterogeneous catalysis	3
1.2.1 Homogeneous catalysis	3
1.2.2 Heterogeneous catalysis	4
1.3 The four tradeoffs of heterogeneous catalysis	5
1.3.1 Activity	5
1.3.2 Selectivity	5

Page No.

1.3.3 Stability 6

1.3.4 Accessibility 6

1.4 Industrial applications of heterogeneous catalysis 7

1.4.1 Fischer-Tropsch 7

1.4.2 Fluid catalytic cracking 8

1.4.3 Hydrogenation 9

1.4.4 Preferential oxidation 9

1.4.5 Paraffin activation 10

1.5 Diverse methods of heterogeneous paraffin activation 11

1.5.1 Cracking 11

1.5.2 Dehydrogenation 11

1.5.3 Oxidative dehydrogenation 12

1.6 Previous research on oxidative dehydrogenation of paraffin molecules 13

1.7 The choice of SBA-15 as a catalyst support 15

1.8 Manganese in heterogeneous catalysis 17

1.9 Aim and objectives of study 20

Chapter 2 - Experimental Procedure **21**

2.1 SBA-15 synthesis 21

2.2 Catalyst synthesis by wet impregnation 22

2.3 Catalyst synthesis by deposition precipitation 22

Page No.

2.4 Catalyst characterisation 22

2.5 Reactor Design 24

2.6 Product analysis 26

Chapter 3 - Characterisation **27**

3.1 Wet impregnation and deposition precipitation catalyst characterisation 27

3.1.1 Inductively coupled plasma – optical emission spectroscopy 27

3.1.2 Fourier Transform - Infrared 27

3.1.3 Raman spectroscopy 28

3.1.4 XRD 28

3.1.5 Nitrogen physisorption 30

3.1.6 BET Analyses 30

3.1.7 Transmission Electron Microscopy 31

3.1.8 Scanning Electron Microscopy 33

3.1.9 Temperature programmed analysis (TPR and TPO) 37

3.1.10 Chemisorption analyses 38

3.2 Spent catalyst characterisation 39

3.2.1 Inductively coupled plasma – optical emission spectroscopy 39

3.2.2 Brunauer–Emmett–Teller studies 39

3.2.3 Transmission Electron Microscopy analysis 40

Page No.

Chapter 4 - Preliminary catalytic testing and determination of optimum reaction conditions **41**

4.1. Investigation of non-catalytic activation of *n*-octane 41

4.2. Catalytic testing of the SBA-15 support 43

4.3 Catalytic testing of the 2W catalyst 45

4.3.1 Determination of optimum reaction conditions 48

4.3.1.1 The role of pellet particle size 48

4.3.1.2 The influence of varying space velocities 49

4.3.1.3 The effect of changing carbon to oxygen ratio 56

4.3.2 Experiments to determine catalyst stability 69

4.4 Proposed reaction pathway 71

Chapter 5 - The role of active metal loading and position in support **72**

5.1 Catalytic results of catalysts prepared by wet impregnation (2W, 5W and 9W catalysts) 72

5.1.1 Catalytic results of the 5W catalyst 72

5.1.1 Catalytic results of the 9W catalyst 74

5.2 Catalytic results of catalysts prepared by deposition precipitation (2D, 5D and 9D catalysts) 78

5.1.1 Catalytic results of the 2D catalyst 78

5.1.1 Catalytic results of the 5D catalyst 80

Page No.

5.1.1 Catalytic results of the 9D catalyst 83

5.3 The effect of the position of the metal oxide 86

5.4 Product selectivity at isoconversion 88

Chapter 6 - Summary and Conclusion **90**

Chapter 7 - Summary and motivation for future work **92**

References **98**

Appendix **106**

List of Figures

	Page No.
Figure 1.1 A simplified catalytic cycle	1
Figure 1.2 Energy profile of an exothermic chemical reaction in the presence and absence of a catalyst	2
Figure 1.2 3D arrangement of silica channels and hexagonal structure in SBA-15	15
Figure 2.1 Schematic of reactor used	25
Figure 2.2 Schematic of reactor tube used	26
Figure 3.1 Powder XRD analysis of 2W and 2D catalysts	28
Figure 3.2 Reduction *in situ* XRD analysis of 2W catalyst	29
Figure 3.3 N_2 adsorption/desorption isotherms of SBA-15, 2W and 2D catalysts	30
Figure 3.4 TEM images of (A) SBA-15, (B) 9W catalyst showing hexagonal mesopores (C) 2W catalyst, (D) 5W catalyst, (E) 9W catalyst, (F) 2D catalyst, (G) 5D catalyst and (H) 9D catalyst.	32
Figure 3.5 Metal oxide particle size measurements of 9W and 9D catalyst	33
Figure 3.6 SEM-EDX and line scan of the 9W catalyst	34
Figure 3.7 Point scan of the 9W catalyst	34
Figure 3.8 SEM-EDX and line scan of the 9D catalyst	35
Figure 3.9 Point scan of the 9D catalyst	36
Figure 3.10 TPR-TPO of 9W catalyst	37
Figure 3.11 TPR-TPO-TPR of 9D catalyst	38
Figure 3.12 TEM images of spent catalyst (A) 9W catalyst and (B) 9D catalyst	40
Figure 4.1 Effect of temperature on *n*-octane conversion and product selectivity in the carborundum packed reactor (N_2 gas, GHSV = 4000 h^{-1} and C:O = 8:0)	41
Figure 4.2 Effect of temperature on *n*-octane conversion and product selectivity in carborundum packed reactor (Air and N_2 gas, GHSV = 4000 h^{-1} and C:O = 8:2)	42
Figure 4.3 Effect of temperature on *n*-octane conversion and product selectivity over SBA-15 (GHSV = 4000 h^{-1}, C:O = 8:2 and pellet particle size = 600 - 1000 μm)	43

Page No.

Figure 4.4 Selectivity of octene isomers as a function of temperature over SBA-15 (GHSV = 4000 h^{-1} and C:O = 8:2). 44

Figure 4.5 Aromatics selectivity as a function of temperature over SBA-15 (GHSV = 4000 h^{-1} and C:O = 8:2) 44

Figure 4.6 Conversion of *n*-octane and selectivity to products as a function of temperature over the 2W catalyst (GHSV = 4000 h^{-1}, C:O = 8:2 and pellet particle size = 600 - 1000 μm) 45

Figure 4.7 Selectivity of octene isomers as a function of temperature over the 2W catalyst (GHSV = 4000 h^{-1} and C:O = 8:2) 47

Figure 4.8 Aromatics selectivity as a function of temperature over the 2W catalyst (GHSV = 4000 h^{-1} and C:O = 8:2) 47

Figure 4.9 Conversion of *n*-octane and selectivity to products at different temperatures over the 2W catalyst (GHSV = 2000 h^{-1} and C:O = 8:2) 49

Figure 4.10 Selectivity towards octene isomers at different temperatures over the 2W catalyst (GHSV = 2000 h^{-1} and C:O = 8:2) 50

Figure 4.11 Aromatics selectivity at different temperatures over the 2W catalyst (GHSV = 2000 h^{-1} and C:O = 8:2) 50

Figure 4.12 Conversion of *n*-octane and selectivity to products at different temperatures over the 2W catalyst (GHSV = 6000 h^{-1} and C:O = 8:2) 51

Figure 4.13 Selectivity towards octene isomers at different temperatures over the 2W catalyst (GHSV = 6000 h^{-1} and C:O = 8:2) 51

Figure 4.14 Aromatics selectivity at different temperatures over the 2W catalyst (GHSV = 6000 h^{-1} and C:O = 8:2) 52

Figure 4.15 Conversion of *n*-octane and selectivity of octene isomers over the 2W catalyst (Temperature = 450 ºC and C:O = 8:2 at 8000 h^{-1} and 10000 h^{-1} GHSV) 53

Figure 4.16 Aromatics selectivity over the 2W catalyst (Temperature = 450 ºC and C:O = 8:2 at 8000 h^{-1} and 10000 h^{-1} GHSV) 53

Table 4.17 Conversion of *n*-octane and selectivity to products with varying GHSV over the 2W catalyst (Temperature = 450 ºC and C:O = 8:2) 54

Figure 4.18 Conversion of *n*-octane and selectivities toward desired products with varied GHSV's at 450 ºC 55

Page No.

Figure 4.19 Conversion of *n*-octane and selectivity towards products as a function of temperature over the SBA-15 (GHSV = 4000 h^{-1} and C:O = 8:0) 56

Figure 4.20 Selectivity of octene isomers as a function of temperature over the SBA-15 support (GHSV = 4000 h^{-1} and C:O = 8:0) 57

Figure 4.21 Conversion of *n*-octane and selectivity towards products as a function of temperature over the 2W (GHSV = 4000 h^{-1} GHSV and C:O = 8:0) 58

Figure 4.22 Selectivity of octene isomers as a function of temperature over the 2W catalyst (GHSV = 4000 h^{-1} GHSV and C:O = 8:0) 59

Figure 4.23 Conversion of *n*-octane and selectivity towards products as a function of temperature over the 2W catalyst (GHSV = 4000 h^{-1} and C:O = 8:1) 59

Figure 4.24 Selectivity of octene isomers as a function of temperature over the 2W catalyst (GHSV = 4000 h^{-1} and C:O = 8:1) 60

Figure 4.25 Ethylbenzene as a function of temperature over the 2W catalyst (GHSV = 4000 h^{-1} and C:O = 8:1) 60

Figure 4.26 Conversion of *n*-octane and selectivity towards products as a function of temperature over the 2W catalyst (GHSV = 4000 h^{-1} and C:O = 8:3) 61

Figure 4.27 Selectivity of octene isomers as a function of temperature over the 2W catalyst (GHSV = 4000 h^{-1} and C:O = 8:3) 62

Figure 4.28 Aromatics selectivity as a function of temperature over the 2W catalyst (GHSV = 4000 h^{-1} and C:O = 8:3) 62

Figure 4.29 Conversion of *n*-octane and selectivity of products as a function of temperature over the 2W catalyst (GHSV = 4000 h^{-1} and C:O = 8:4) 63

Figure 4.30 Selectivity of octene isomers as a function of temperature over the 2W catalyst (GHSV = 4000 h^{-1} and C:O = 8:4) 64

Figure 4.31 Aromatics selectivity as a function of temperature over the 2W catalyst (GHSV = 4000 h^{-1} and C:O = 8:4) 64

Figure 4.32 Mars and van Krevelen cycle of metal oxide phases and formation of primary product 67

Figure 4.33 Effect of time with the conversion of *n*-octane over 2W catalyst (Temperature = 450 ºC, GHSV = 4000 h^{-1} and C: O = 8:2) 69

Page No.

Figure 4.34 Conversion of *n*-octane and selectivity towards products over the 2W catalyst for recycle test (GHSV = 4000 h^{-1} and C:O = 8:2) 70

Figure 4.35 Scheme of individual product formation 71

Figure 5.1 Conversion of *n*-octane and selectivity towards products as a function of temperature over the 5W catalyst (GHSV = 4000 h^{-1} and C:O = 8:2) 72

Figure 5.2 Octenes selectivity as a function of temperature over the 5W catalyst (GHSV = 4000 h^{-1} and C:O = 8:2) 73

Figure 5.3 Aromatics selectivity as a function of temperature over the 5W catalyst (GHSV = 4000 h^{-1} and C:O = 8:2) 74

Figure 5.4 Conversion of *n*-octane and selectivity towards products as a function of temperature over the 9W catalyst (GHSV = 4000 h^{-1} and C:O = 8:2) 75

Figure 5.5 Octenes selectivity as a function of temperature over the 9W catalyst (GHSV = 4000 h^{-1} and C:O = 8:2) 75

Figure 5.6 Aromatics selectivity as a function of temperature over the 9W catalyst (GHSV = 4000 h^{-1} and C:O = 8:2) 76

Figure 5.7 Conversion of *n*-octane and selectivity towards products as a function of temperature over catalysts prepared by wet impregnation (GHSV = 4000 h^{-1} and C:O = 8:2) 77

Figure 5.8 Conversion of *n*-octane and selectivity towards products as a function of temperature over the 2D catalyst (GHSV = 4000 h^{-1} and C:O = 8:2) 79

Figure 5.9 Octenes selectivity as a function of temperature over the 2D catalyst (GHSV = 4000 h^{-1} and C:O = 8:2) 79

Figure 5.10 Aromatics selectivity as a function of temperature over the 2D catalyst (GHSV = 4000 h^{-1} and C:O = 8:2) 80

Figure 5.11 Conversion of *n*-octane and selectivity towards products as a function of temperature over the 5D catalyst (GHSV = 4000 h^{-1} and C:O = 8:2) 81

Figure 5.12 Octenes selectivity as a function of temperature over the 5D catalyst (GHSV = 4000 h^{-1} and C:O = 8:2) 82

Figure 5.13 Aromatics selectivity as a function of temperature over the 5D catalyst (GHSV = 4000 h^{-1} and C:O = 8:2) 82

Page No.

Figure 5.14 Conversion of *n*-octane and selectivity towards products as a function of temperature over the 9D catalyst (GHSV = 4000 h^{-1} and C:O = 8:2) 83

Figure 5.15 Octenes selectivity as a function of temperature over the 9D catalyst (GHSV = 4000 h^{-1} and C:O = 8:2) 83

Figure 5.16 Aromatics selectivity as a function of temperature over the 9D catalyst (GHSV = 4000 h^{-1} and C:O = 8:2) 84

Figure 5.17 Conversion of *n*-octane and selectivity towards products as a function of temperature over catalysts prepared by deposition precipitation (GHSV = 4000 h^{-1} and C:O = 8:2) 85

Figure 5.18 Conversion of *n*-octane and selectivity towards products for all catalysts (Temperature = 450 ºC, GHSV = 4000 h^{-1} and C:O = 8:2) 87

Figure 5.19 Isoconversion results of 9W and 9D catalysts catalyst at 12% conversion of *n*-octane and 400 °C 89

Figure 5.20 Isoconversion results of 2W and 2D catalysts catalyst at 8.5 % conversion of *n*-octane and 450°C 89

Figure A1 XRD pattern of 5D catalyst 106

Figure A2 XRD pattern of 5W catalyst 107

Figure A3 XRD pattern of 9D catalyst 107

Figure A4 XRD pattern of 9W catalyst 108

Figure A5 N_2 adsorption/desorption isotherm of 5D catalyst 108

Figure A6 N_2 adsorption/desorption isotherm of 5Wcatalyst 109

Figure A7 N_2 adsorption/desorption isotherm of 9D catalyst 109

Figure A8 N_2 adsorption/desorption isotherm of 9W catalyst 110

Figure A9 Raman spectrum of 2W catalyst 110

Figure A10 Electron mapping graph of 9D catalyst 110

Figure A11 Electron mapping graph of 9W catalyst 111

Figure A12 Picture of micro-reactor set-up used 111

Figure A13 Sample chromatograms 112

List of Tables

	Page No.
Table 1.1 A comparison of homogeneous and heterogeneous catalysis	3
Table 1.2 Heterogeneous catalytic processes used in various industries	7
Table 2.1 List of reagents used	21
Table 3.1 Weight loading of metal oxide for all catalysts prepared	27
Table 3.2 Dominant band and band assignment for support and catalysts	27
Table 3.3 Surface area, pore volume and pore diameter for support and catalysts	31
Table 3.4 Relative metal composition of different points for 9W catalyst	35
Table 3.5 Relative metal composition of different points for 9D catalyst	36
Table 3.6 H_2/O_2 titration results for SBA-15, 2W and 2D catalysts at atmospheric pressure	38
Table 3.7 Surface areas, pore volume and pore diameter for spent support and spent catalysts	40
Table 4.1 Conversion of *n*-octane and selectivities to products for 300 – 600 μm pellets	48
Table 4.2 Conversion of *n*-octane, selectivities toward desired products and contact time of this feed with varying GHSV's at 450 °C	54
Table 4.3 Conversion of *n*-octane and selectivity toward octenes and aromatics of the 2W catalyst with varying carbon to oxygen ratios at 450 °C	65
Table 4.4 Conversion of *n*-octane and selectivities for time-on-stream analysis	70
Table A1 Sample calculation for moles of 1-octene obtained	106

Abbreviations

Å : Angstroms

AR : Analytical Reagant

atm : Atmospheres

ATR : Attenuated total reflectance

BET : Braunauer-Emmet-Teller

cm : Centimetre

EDX : Energy-dispersive X-ray spectroscopy

EO : Ethylene oxide

FT-IR : Fourier Transform - Infrared

GC : Gas chromatography

GHSV : Gas hourly space velocity

g : Gram

h : Hour

HPLC : High performance liquid chromatography

ICP-OES : Inductively coupled plasma-optical emission spectroscopy

kV : Kilovolt

L : Litre

μ : Micron

mA : Milliamperes

m : Metre

MCM41: Mobil Composition of Matter - type 41

mg : Milligram

min : minute

mL : Millilitre

M : Molar (concentration in mole per litre)

Nm : Nanometre

No. : number

ODH : Oxidative dehydrogenation

ppm : Parts per million

PO : Propylene oxide

PR : Pressure regulator

rpm : revolutions per minute

SBA-15 : Santa Barbara Amorphous – type 15

SEM : Scanning electron microscopy

SR : Steam reforming

TPR : Temperature programmed reduction

TCD : Thermal conductivity detector

TGA : Thermogravimetric analysis

TEM : Transmission electron microscopy

TEOS: Tetraethyl Orthosilicate

UOP : Universal Oil Products

wt : Weight

XRD : X ray diffraction

2W : 2 weight percent catalyst prepared by wet impregnation

5W : 5 weight percent catalyst prepared by wet impregnation

9W : 9 weight percent catalyst prepared by wet impregnation

2D : 2 weight percent catalyst prepared by deposition precipitation

5D : 5 weight percent catalyst prepared by deposition precipitation

9D : 9 weight percent catalyst prepared by deposition precipitation

Calculations

Conversion was calculated based on moles of *n*-octane reacted using the formula:

$$\text{Conversion} = \frac{\text{No. of moles of } n-\text{octane reacted}}{\text{Total no. of moles of } n-\text{octane}} \times \frac{100}{1}$$

with the answer obtained expressed as mol%

Selectivity was calculated based on moles of individual product obtained compared to the no. of moles of all products using the formula:

$$\text{Selectvity} = \frac{\text{No. of moles of individual product obtained}}{\text{Total no. of moles of product obtined}} \times \frac{100}{1}$$

with the answer obtained expressed as mol%

GHSV was calculated based on the total gaseous flow rate, in ml/h, divided by the volume of catalyst, in ml, to obtain an answer expressed in h^{-1}:

$$\text{GHSV} = \frac{\text{Total gaseous flow rate}}{\text{Volume of catalyst}}$$

Percentage yield was calculated based on conversion and selectivity and expressed as a percentage:

$$\text{Percentage Yield} = \frac{\text{Conversion} \times \text{Selectivity}}{100}$$

Chapter 1

Introduction and literature review

1.1 Introduction to catalysis

Catalytic processes have been taking place for a considerable length of time and it was only in 1835 that Jöns Jacob Berzelius gave a formal definition to the word "catalysis" [1, 2]. Sixty years later, Ostwald recognized the phenomenon of catalysis as something that could be explained by the laws of chemistry and polished the definition of a catalyst to "a material that would accelerate a chemical reaction without affecting its equilibrium position". At present, catalysts are engaged in the manufacture of value added chemicals and materials in order to better the commercial productivity of over 90 % of large-scale industrial processes [3]. There are practical applications in many large scale processes today, including outside of the chemical industry. For example, the 3-way catalyst used in the motor industry, which has proven to be effective in reducing the emissions given off by car exhausts [4].

The commonly known definition of a catalyst is a substance that that can speed up therate of a chemical reaction without itself being used up during the process or its chemical state altered at the end of it [4]. Originally, it was presumed that the catalyst stayed the same throughout the extent of the reaction it was involved in. However, further probing revealed that the catalyst chemically bonded with the reactants and so formed a catalytic process.

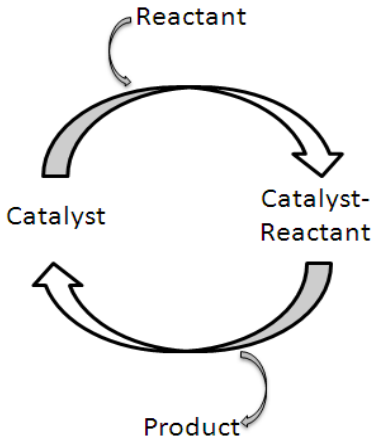

Figure 1.1 A simplified catalytic cycle [5].

The simplified catalytic cycle, shown in Figure 1.1, describes how the binding site of the reactant interacts with catalyst to form an unstable intermediate which reacts further to form the products of the

reaction. These products are then released and the catalyst is returned to its initial state. This process might seem simple, but in practice is much more complicated. Catalysis classically begins with a single reactant molecule adsorbing onto the surface of the catalyst from the bulk reactant. This is then followed by migration to an active site of the catalyst where the surface reaction can take place to form products. The final step in this general process is desorption of the products from the active site and returning to the bulk [2, 3]. When a reactant molecule specifically adsorbs onto a surface and there is an interaction with the active site of the catalyst, typically there are three processes that can occur. These are bond forming, bond weakening and bond breaking, which ultimately results in the formation of product molecules. It is the active site that allows the reactant to react more easily and once the products diffuse from it, another reactant molecule can adsorb or migrate onto it and the catalytic process begins once again. The active site merely assists the reaction to take place on it and it, along with the catalyst as a whole, does not change. This feature of catalytic reactions is one of the main aspects that make them desirable for application. However, in practice, there are many factors in a reaction that can cause a catalyst to undergo chemical changes that cannot be reversed while the reaction is taking place. This can affect the performance of a catalyst and may result in it being undesirable for prolonged use [5, 6].

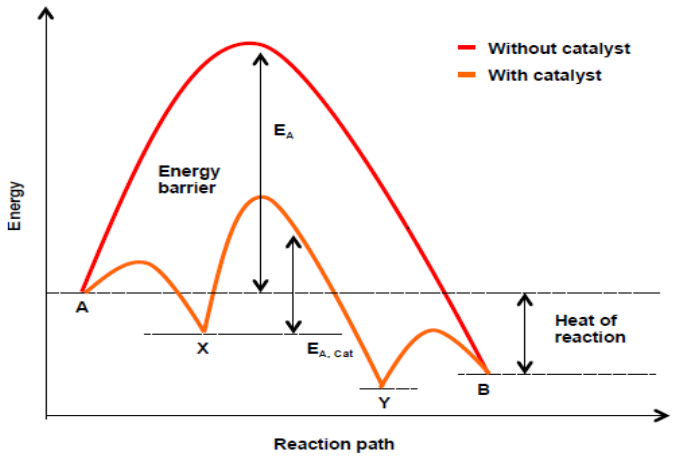

Figure 1.2 Energy profile of an exothermic chemical reaction in the presence and absence of a catalyst [7].

The procedure by which a catalyst is able to speed up the rate of a chemical reaction is illustrated in Figure 1.2, with A being the starting material, X and Y intermediate compounds and B is the reaction product. In the absence of a catalyst, the energy barrier or activation energy E_a, for product formation is high and this results in product formation being slow, if any are formed at all by the uncatalysed reaction.

On the other hand, in the presence of a catalyst, the energy required for product formation is lower due to the catalyst lowering the activation energy required for the given reaction. This results in products forming at a higher rate than would be possible without a catalyst. [6, 7].

1.2 Homogeneous and heterogeneous catalysis

Catalysis can be divided into two main categories, namely homogeneous and heterogeneous catalysis. In homogeneous catalysis, the catalyst and reactants are present in the same phase while the reaction takes place, whereas with heterogeneous catalysis, they are present in different phases. Both types of catalysis have distinct advantages and disadvantages that often complement each other and the key characteristics typically exhibited by both groups of catalysts are summarized in Table 1.1

Table 1.1 A comparison of homogeneous and heterogeneous catalysis [6].

Characteristic	**Homogeneous**	**Heterogeneous**
Active centers	All metal atoms	Surface atoms
Selectivity	High	Low
Reaction temperatures	Low to mild(~ 50 - 200°C)	Moderate to high(~≥250°C)
Diffusion limitations	Very few	Mass transfer limitations exist
Thermal stability	Low	High
Cost of lost catalyst	High	Low
Catalyst separation	Difficult	Simple, often unnecessary
Catalyst recycling	Possible	Simple
Catalyst regeneration	Difficult, if possible	Possible
Application	Low range of applications	Wide range of applications

1.2.1 Homogeneous catalysis

Homogeneous catalysts have a higher degree of dispersion when compared to heterogeneous catalysts, due the the catalyst and reactant being in the same phase. This, in theory, means that each individual atom of the catalyst can be active, as opposed to heterogeneous catalysts, where only surface atoms are

active. However, the fact that the catalyst and reactant are in the same phase leads to one of the major disadvantages of homogeneous catalysts, namely the separation of the catalyst and reactant products. Heterogeneous catalysts can easily be removed from a reactor or reaction mixture, either by physically removing the catalyst from its location or by simple methods such as filtration or centrifuge. More complex processes are required for the removal of homogenous catalysts from reaction mixtures such as liquid-liquid extraction and distillation [5].

Homogeneously catalyzed processes are synonymous with high selectivity; the Monsanto acetic acid process is probably one of the most commonly known examples of such a process. It involves a rhodium and iodide catalyzed carbonylation of methanol to acetic acid and an estimated 60% of the world production of acetic acid is synthesized in this way [8, 9]. Another well-known example of a homogeneously catalyzed industrial process is the Oxo synthesis. This involves the coupling of an olefin and CO in the presence of hydrogen to form an aldehyde, It originally used a $[Co_2(CO)_8]$ catalyst, which was later modified with phosphine ligands to improve the yield of the aldehyde produced [5].

Due to the drawbacks with thermal stability, cost of catalyst loss, catalyst separation and regeneration, homogeneously catalyzed processes are not widely used in industry. From an industrial point of view, heterogeneous catalysis is far more favourable, in particular the low cost of catalyst loss and ease of separation [10].

1.2.2 Heterogeneous catalysis

Heterogeneous catalysis is suitable for large-scale, industrial applications. The reaction temperatures employed, thermal stability attained and ease of separation are a few of the positive characteristics of heterogeneous catalysts that make them advantageous for application. Heterogeneous catalysts can be a variety of materials including metals, metal oxides and zeolites to name a few. Supported metal oxides are well known industrially in the field of heterogeneous catalysis and this will be looked at in more detail from section 1.6 till the end of Chapter 1. Well known processes in heterogeneous catalysis include the Haber and Contact processes, for the production of ammonia and sulphuric acid respectively [11, 12]. There are numerous applications for heterogeneous catalysts, with current developments and discoveries only expanding the range of applications in fields such as preferential oxidation and paraffin activation.

1.3 The four tradeoffs of heterogeneous catalysis

Ertl *et al* [6] described what they refer to as the 4 tradeoffs in heterogeneous catalysis, which are accessibility, activity, stability and the selectivity. These principles are the basis for which a catalyst can be designed in order to optimize the performance of the catalyst. This is, in theory, ideal but when it comes to actual catalyst design and performance, all four of these conditions cannot necessarily be met. For example, a catalyst can be more active with an increase in temperature but this may result in a change in stability and selectivity. Finding a balance between these parameters is key for an efficient process.

1.3.1 Activity

Activity is a measure of how fast or to what extent a reaction proceeds in the presence of a catalyst. The most apt measure of the activity of a catalyst is the conversion of the catalyst. Conversion is defined as the amount of reactant that is transformed into products during a reaction. It can be calculated based on moles or mass and is usually presented in the form of a percentage. The activity of a catalyst can be affected by many factors in heterogeneous catalysis. Temperature affects activity greatly, with an increase in temperature leading to an increase in the average kinetic energy of reactant molecules which in turn increases conversion [13]. The time that a catalyst is in contact with the reactant also affects conversion, a greater contact time generally increasing the conversion. There are also many other reaction conditions that can be altered to affect conversion, for example fuel to reactant ratios and catalyst particle size. From an industrial point of view, activity of a catalyst can be altered in a number of different ways for different catalysts and reactions.

1.3.2 Selectivity

Selectivity is assigned to individual products or groups of products from a reaction and is defined as the proportion of an individual product formed to all products formed from the reaction. It is usually calculated based on moles or mass and is also usually expressed as a percentage. For example, if a catalytic reaction formed only one product, that product is said to have 100 mol% selectivity. Selectivities can vary with changing reaction conditions and catalysts, and these are optimized to provide the highest selectivity toward desired products of the reaction and/or provide lowest selectivity toward undesired products. A selective catalyst is one that can provide a reasonably high selectivity toward

desired products and currently, research and industry places a greater prominence on the development of selective catalysts [5, 14].

1.3.3 Stability

The stability of a catalyst is the measure of the active lifetime of a catalyst. If a catalyst loses activity, it is said to deactivate and any process that causes a catalyst to do so, is a deactivation process. There are 3 major types of deactivation processes. Firstly, mechanical, which is caused by breaking or abrasion of catalyst particles. The impact of this deactivation is minimal as it can easily be avoided by proper packing of a catalyst into a reactor. Secondly, deactivation can occur physically by agglomeration or sintering in supported metal catalysts [12]. This results in an irreversible loss of surface area and in turn lowers the activity of the catalyst. The third type of deactivation that can occur is chemical deactivation that mainly comes about by a catalyst being poisoned by the presence of an impurity. A loss of stability can lead to a loss in activity of the catalyst and catalysts that cannot be regenerated will ultimately end up as waste. This is why there is a great demand in industry for stable catalysts with long lifetimes to avoid the increasing cost of catalyst that will need to be subsequently replaced and to reduce the downtime of a reactor.

1.3.4 Accessibility

The accessibility parameter with regards to the four tradeoffs of heterogeneous catalysis is one that can have a great influence on two of the other parameters, namely activity and selectivity. Accessibility refers to the ability of the reactant molecule to come into contact with the active site of a heterogeneous catalyst. A highly accessible active site improves contact time between the reactant and site, allowing for higher conversion to products. This will increase the activity of the catalyst, however, with this increased activity, the catalyst may be less selective towards desired product groups due to the large amounts of different products being formed. On the other hand, a catalyst with a poorly accessible active site may result in lower activity but improved selectivity toward desired products, ultimately improving the yield or production rate.

1.4 Industrial applications of heterogeneous catalysts

Table 1.2 Heterogeneous catalytic processes used in various industries [5].

Process	**Catalyst**	**Product**
Steam reforming of methane	Ni/Al_2O_3	H_2 gas and CO gas
Haber process	Fe_3O_4 promoted with K_2O, Al_2O_3	NH_3 gas
Oxidation of SO_2	Supported V_2O_5	SO_3 gas
Dehydrogenation of ethylbenzene	Fe_3O_4 promoted with Cr, K oxide	Styrene
Oxidation of butene	Supported V_2O_5	Maleic anhydride
Polymerisation of ethene	Cr_2O_3/SiO_2 or Cr_2O_3/MoO_3	Polyethylene
Ammoxidation of methane	Pt/Rh nets	HCN
Alkylation of benzene	H_3PO_4/SiO_2	Cumene
Fischer–Tropsch	Co/Fe based catalysts	Hydrocarbons

There are many different heterogeneously catalyzed reactions that have been commercialized into large-scale industrial processes for the production of a wide range of industrial gases, organic chemicals and inorganic chemicals. The bulk of heterogeneously catalyzed industrial processes are used for the production of organic chemicals. A few examples of industrial processes are summarized in Table 1.2 and a brief description of some of them follows [5].

1.4.1 Fischer-Tropsch

The Fischer–Tropsch process was first developed in Germany in 1925 by Franz Fischer and Hans Tropsch and involves a series of chemical reactions to convert a mixture of natural gas into liquid hydrocarbons. Carbon monoxide and hydrogen react to produce a variety of hydrocarbons, having the general formula ($C_nH_{(2n+2)}$) formed by the reaction:

$$(2n + 1)H_2 + nCO \rightarrow C_nH_{(2n+2)} + nH_2O$$

However, there are other concurrent reactions that take place to form low amounts of alkenes, alcohols and oxygenated products. The bulk of products obtained are straight chain hydrocarbons, which find use mainly in fuels [3].

There are many catalysts that have shown to be active for the Fischer-Tropsch process, but the most common commercial catalysts used are cobalt and iron-based catalysts. Iron-based catalysts are more widely used in industry but are less stable than cobalt-based catalysts, which have been incorporated into industry in the last 20 years. Both types of catalysts contain a number of promoters, such as potassium and copper and are supported on high surface area supports such as silica or alumina in order to improve catalytic performance. For commercialized Fischer-Tropsch processes, iron-based catalysts can operate at higher temperatures when compared to cobalt based catalysts [5, 10].

1.4.2 Fluid catalytic cracking

Fluid catalytic cracking is widely used to convert hydrocarbon fractions of crude oil to more valuable products such as gasoline. Initially, cracking of hydrocarbons was carried out thermally. This has been replaced by catalytic cracking as it produces a higher yield of gasoline with higher octane numbers. The by-products of fluid catalytic cracking of hydrocarbons are also more valuable than by-products obtained from thermal cracking. Modern catalysts for fluid catalytic cracking are zeolite-based catalysts in the form of a fine powder that are highly active with good resistance to attrition and produce low amounts of coke [11].

A modern fluid catalytic cracking catalyst is made up of four major components: a zeolite, binder, matrix and filler [11].The zeolite is the active component of the catalyst and it can make up between 15 to 50 weight percent of the catalyst. The catalytic sites in the zeolite are acidic sites, which form during the synthesis of the catalyst. In some catalysts for fluid catalytic cracking, metals such as cerium and lanthanum have been used to provide enhanced activity and catalyst stability. The matrix component of the catalyst is made up of amorphous silica. The larger pores present in the silica allow entry for larger molecules, which cannot fit into the zeolite and thus, enhances the activity [5, 10].

1.4.3 Hydrogenation

Catalytic hydrogenation takes place when molecular hydrogen reacts with an unsaturated organic molecule in the presence of a catalyst [15]. Harsh reaction conditions, such as high temperatures and pressures, are required in order to carry out these reactions and therefore catalysts were developed in order to carry out these reactions under milder conditions. Catalytic hydrogenation has been well reported and is one of the most widely studied chemical reactions to date [14, 16]. There have been many advances in the field and selective hydrogenation of a mixture of organic compounds has been of interest in recent years [17].

1.4.4 Preferential oxidation

Preferential oxidation has increasingly become a field of great interest lately due to a need for looking at alternative energy resources and one such application is the use of fuel cell technology. A fuel cell converts the chemical energy of fuel directly into electrical energy and is thus an electrochemical energy converter. It has a large potential for highly efficient power generation [18]. Currently, proton exchange membrane fuel cells are the most sought after type of fuel cells for use due to their low emission of pollutants, high power output and quick response times that lead to it having enhanced capabilities and performance over other types of fuel cells [19]. This type of fuel cell uses hydrogen as a fuel and at present, hydrogen production takes place mainly from the reforming of natural gas, followed by the water gas shift reaction [20]:

$$CH_4 + H_2O \rightarrow CO + 3H_2 \qquad \Delta H_{298K} = +206 \text{ kJ/mol}$$

$$CO + H_2O \rightarrow CO_2 + H_2 \qquad \Delta H_{298K} = -36 \text{ kJ/mol}$$

The drawback to this process is that due to the thermodynamic factors of this reaction, CO is produced, which can adsorb onto the active site of the electrodes present in the fuel cell and lead to a loss of cell productiveness.

Chronic exposure to CO, even in low concentrations, can also lead to electrode degradation. This results in a need for preferentially oxidizing CO to CO_2 in hydrogen rich streams, as CO_2 does not poison the electrodes present in the fuel cell [21]. This need for purifying the feed gas to the fuel cellhas sparked

great interest and research into preferential oxidation, since it is closely related with developments in the field of alternative energy.

Noble group metals were looked at earlier for preferential oxidation of CO [22], however, later research showed that supported transition metal oxides such as Pt, Rh and Ru had promising results [23-25], with Marino *et al.* [26] reporting that Pt catalysts have been widely looked at for this type of reaction. However, due to the interest in fuel cell technology only sparking greater interest in recent years, research into preferential oxidation has grown greatly and intense research is on-going.

1.4.5 Paraffin activation

Alkanes or paraffins are saturated hydrocarbon molecules with the general formula C_nH_{2n+2} and are known to be less reactive than the subsequent alkene (C_nH_{2n}) and alkyne (C_nH_{2n-2}) molecules [27, 28]. Alkanes are largely produced as by products in coal-to-liquid, gas-to-liquid and petrochemical plants worldwide and with the number of these plants increasing each year, more and more of these alkane compounds are being produced [29]. Branched alkanes can be used in fuels due to their high octane numbers but the octane numbers of linear alkanes are low and as a result find less use in fuels. Instead, these compounds can be used as feedstocks for other industrial processes.

Aromatic, oxygenated and olefinic compounds are well known feedstocks for many industrial processes [30]. However, these compounds are far more valuable than alkane molecules, which are precursors to these compounds. This has led to research into paraffin activation to develop catalysts that can convert alkanes to these value added products so that they can be replaced as feedstocks for various industrial applications. There has been extensive research carried out in paraffin activation, which will be discussed further on in this chapter, but the field is still vast and some areas unexplored. There can still be some uniqueness and novelty found in this field of heterogeneous catalysis, while still having substantial knowledge from previous research endeavors. This sense of further exploration has given impetus to this study.

1.5 Diverse processes of heterogeneous paraffin activation

1.5.1 Cracking

A simplified method of converting paraffins is via cracking. This is a process whereby the paraffin molecule is broken down into smaller molecules. For example, if a long chain linear paraffin molecule with carbon chain length of 6 or greater was broken down into smaller, shorter chain paraffin molecules, such as ethane, propane or butane, the reactant molecule is said to have "cracked" due to this break down. The cracking of paraffin compounds can either take place thermally or chemically. Thermal cracking takes place when the molecule is broken down using high temperatures. Chemical cracking takes place catalytically, where the molecule is broken down in the presence of a catalyst [5]. For example, the acid catalyzed cracking of hydrocarbons can take place via the following general reaction [31].

$$C_nH_{2n+2} + H^+ \rightarrow C_xH_{2x+2} + C_{n-x}H^+_{2(n-x)+1} \qquad \text{(where } x<n\text{)}$$

1.5.2 Dehydrogenation

The catalytic dehydrogenation of paraffin molecules takes place anaerobically via the following general reaction:

$$C_nH_{2n+2} \rightarrow C_nH_{2n} + H_2$$

These processes have been in existence on an industrial scale from the 1930s, an example being the UOP Pacol process for the production of linear olefins from paraffins [32]. The reaction involves removal of H_2 from an alkane molecule and as a result an alkene is formed. In some cases, the alkene may cyclise to form an aromatic ring, but this would depend on the nature of the catalyst present and the reaction conditions. There are many catalysts that have been reported to show high yields of desired products from the dehydrogenation reaction of paraffin molecules [33-35].

The products of dehydrogenation reactions of paraffins are olefin and aromatic compounds, which are known to be more reactive than the paraffin precursors due to the electron rich double bonds present in these molecules. This is one of the major drawbacks with dehydrogenation reactions. Others include the reaction being endothermic and requiring large amounts of energy input on an industrial scale. The high

temperatures required for dehydrogenation reactions also lead to cracking taking place as unwanted side reactions.

Coke formation is also more apparent with dehydrogenation reactions, which result in regeneration steps being required [32]. With environmental awareness and energy efficiency being major concerns currently and the high energy input required for dehydrogenation reactions, among other factors, dehydrogenation was not considered as an appealing pathway for the activation of paraffins. However, the desirable reaction products and high yields obtained from dehydrogenation could not be ignored. This suggested an investigation into oxidative dehydrogenation as a method for paraffin activation.

1.5.3 Oxidative dehydrogenation

The oxidative dehydrogenation of paraffin molecules takes place via the following general reaction:

$$2C_nH_{2n+2} + O_2 \rightarrow 2C_nH_{2n} + 2H_2O$$

The products of these reactions are olefin compounds and water, with the olefins formed being able to react further to aromatic compounds. There are numerous advantages to oxidative dehydrogenation reactions when compared to dehydrogenation reactions. These reactions are exothermic and would not require the high energy input required by commercialized dehydrogenation reactions. This makes it appealing industrially from an economic and green chemistry point of view. Coking is also minimal, which makes commercialization of these types of reactions more desirable [36]. However, certain negatives to oxidative dehydrogenation need to be noted. Side reactions are more apparent, with carbon oxide formation being the most prevalent unwanted side reaction [37]. However, the potential benefits of oxidative dehydrogenation of paraffin molecules far outweigh the drawbacks and there is a great demand for industrial applications. This has lead to research and development into trying to produce catalysts that can provide high selectivities toward desired products at reasonable conversions while hindering the formation of unwanted side reactions such as carbon oxides. There are still areas that are far off the mark, but the overall aim is to establish a system that is suitable for the oxidative dehydrogenation of paraffin molecules.

1.6 Previous research on oxidative dehydrogenation of paraffin molecules

Paraffin activation has been widely researched globally, particularly with oxidation and oxidative dehydrogenation. This is guided primarily by the need for stable catalysts that can be commercialized that provide good activity and high selectivity toward desired products. There has been extensive work done all around the world in the oxidative dehydrogenation of paraffin molecules. There are numerous studies by various academic and industrial groups globally looking at alkane activation via oxidative dehydrogenation providing a wealth of knowledge.

Friedrich and co-workers have studied various catalytic systems for paraffin activation via oxidative dehydrogenation. These include transition metal promoted VPO, VMgO, hydrotalcite-like compounds, molybdates and many other catalytic systems. [9, 29, 30, 34, 38-52].Activation of *n*-butane [38-43] was initially looked at first by this research group, due to the commercial production of maleic anhydride from this linear alkane [5].The choices of catalysts at the time were Co, Fe and Ru promoted VPO catalysts for the activation of *n*-butane, with the desired target product being maleic anhydride. The best results found was a 32.85% yield to maleic anhydride obtained with a Co promoted VPO catalyst and this was found while varying reaction parameters, such as space velocity and temperature [39].

Pillay *et al.*, Friedrich and co-workers used nickel molybdate catalysts for *n*-hexane activation [29, 45] and used different reaction conditions to promote selectivity toward hexenes. Contact time, flammability limits, oxidant ratios and nitrogen dilution were factors investigated, with results obtained showing 55% selectivity towards hexenes, 27% of which was 1-hexene.

Mahomed and Friedrich [47] studied *n*-octane activation with hydrotalcite-like compounds containing Mg/V which showed enhanced selectivity towards styrene. They were also able to infer and propose a mechanism for styrene formation based on the dehydrogenation of ethylbenzene. Chetty and Friedrich [9] looked at the effect of varying weight loadings of vanadium in VMgO catalysts and the effect of promoters with the activation of *n*-hexane and *n*-octane. Their work showed that metal weight loading plays a critical role in catalytic activity and weight loading needs to be optimized for a catalyst system. They found a weight loading of 19% V_2O_5as the optimum, since higher weight loadings showed a loss in activity. Weight loadings lower than 19% showed lower conversion of *n*-hexane when compared to the catalyst containing 19 wt% catalyst, at the temperatures where complete conversion of *n*-hexane was not observed. This catalyst was chosen to be promoted with other metal oxides, e.g. Te and Mo. Makatini and Friedrich [51] looked at mixed metal oxide catalysts using MoVTeNbO catalysts, following work

by Lopez-Nieto *et al.* [53, 54]. Vanadium content and reaction conditions were manipulated to find the highest conversion and selectivity toward oxygenated products, in this case methanol, with a selectivity of 12%. Ekhalifa and Friedrich [49] looked at the effect of varying reaction parameters such as carbon to oxygen ratio on the activity and product selectivity with a 15 wt% VMgO catalyst that showed good selectivity toward olefin and aromatic products. This research effort showed that reaction parameters, such as *n*-octane to oxygen ratio, can influence activity and selectivity greatly.

Hutchings and co-workers have made great contributions to research in catalysis and in particular alkane activation. They studied many diverse catalytic systems starting initially with short chain paraffins and moving to longer chains [55-63]. In terms of higher linear alkanes, work was done and published primarily on *n*-decane [62, 63]. Iron molybdate catalysts were found to be effective at 350ºC for producing oxygenated aromatics from *n*-decane [62], whereas ceria based catalysts provided enhanced selectivities toward alcohols under relatively mild reaction conditions [63].

Lopez-Nieto *et al.* have also made a significant impact in the field of oxidation catalysis, especially in the oxidation of lower paraffins [53, 54, 64-68].Using vanadium based and supported vanadium catalysts, they have shown that the acid-base properties and redox nature of a catalyst directly influences a catalyst's performance for alkane activation.

Cavani and Trifiro [69] have studied the redox properties of mixed metal oxide systems by looking at the selective oxidation of C1 – C5 linear paraffins, with focus on gas phase interaction at the support surface. They found that the factors that affect catalytic performance where structural defects, concurrent effects of different phases, the meta lto oxygen bond strength and redox properties of the active sites. Corma *et al.* [70-73] have looked at microporous materials, mesoporous material and zeolites for their use in selective oxidation. This research looked into shape selective catalysis and Corma's work delved into tackling some of the issues within this field, also using materials with large pores so that it could handle bulkier reactants [70].

Supported transition metal oxides have been widely reported and these types of catalysts have been effective for the oxidative dehydrogenation of *n*-octane, as shown by Friedrich and co-workers, which is why this type of catalyst was chosen. However, the use of high surface area, mesoporous supports like SBA-15 with transition metals have been less reported for the oxidative dehydrogenation of *n*-octane. Furthermore, certain metal oxides such as manganese oxide have also been less studied, being the reason to choose this type of catalyst.

1.7 The choice of SBA-15 as a catalyst support

Ordered mesoporous silica based solids have become a widely researched group of materials since the disclosure of the M41S family in1992 [74, 75]. Since then, a great deal of work has been done to synthesize a wide range of mesoporous materials with different frameworks, pore sizes and shapes, with MCM-41 and SBA-15 being 2 examples of such materials [76, 77]. SBA-15 is a high surface area, well ordered arrangement of SiO_2 synthesized in an acidic medium. It is a mesoporous silica that has a regular arrangement of open channels, hexagonal mesopores as well as thicker silica walls and higher thermal stability when compared to MCM-41 [76]. It has been reported to possess weak acidity on its amorphous silica wall [78] and has been discovered due to research into molecular sieves for applications in separations and catalysis [79]. The desirable properties of SBA-15 such as high surface area, high thermal stability, well ordered mesoporous structure, open channels and relatively thick silica walls make it suitable for use as a catalyst support. A generalized structure of SBA-15 with ordered, open channel pores of even diameter was first reported by Samran *et al.* [80], shown in Figure 1.3.

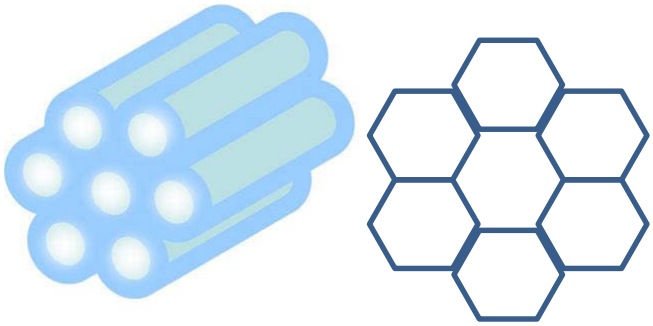

Figure 1.3 3D arrangement of silica channels and hexagonal structure in SBA-15 [80].

SBA-15 has been used in a number of different applications in the field of heterogeneous catalysis, such as molecular sieves or catalyst supports for different heterogeneous catalysis reactions. The most common method for the synthesis of SBA-15 was developed by Stucky and co-workers [76] using an amphiphilic triblock copolymer as structure-directing agent in highly acidic media and based on a hydrothermal treatment method. However, once this material was developed there was still a large amount of research put in to manipulating the properties of SBA-15 in order to make it more effective in its application. Colilla *et al.* [81] showed that using different mixtures of H_3PO_4 and HCl to obtain acidic media would provide different surface areas based on the mixtures used. Stucky and co-workers [82] also found different methods of synthesis that provided different morphologies for SBA-15. Samran

et al. [80] also developed a novel room temperature approach to SBA-15 synthesis from silatrane. In addition, SBA-15 modified with transition metals Al [83], Fe[77, 84], Ti [85], and Ga [86] into the framework by direct synthesis or post grafting has been extensively studied as a novel approach to alter the acid/base properties of the support.

SBA-15 was used as a support for heterogeneous catalysis, in particular with transition metals. Vasiliadou *et al.* [87] used SBA-15 as a support for copper catalysts for the hydrogenolysis of glycerol to propylene glycol. They showed that the dispersion of Cu on the support directly affected the conversion, whereas selectivities between 92 – 97% towards propylene glycol was achieved for all supported catalysts. Huang *e. al.* [88] used incipient wetness impregnation to load Fe on SBA-15. The structure of the support remained after impregnation, as shown by low angle XRD and N_2 adsorption-desorption isotherms. The Fe/SBA-15 catalyst was found to be active for the ozonation of dimethyl phthalate in aqueous solution.

Lou *et al.* [89] also used impregnation to support molybdenum oxides on SBA-15 as catalysts for the oxidation of ethane. This study again showed that the structure of SBA-15 was maintained, even with weight loadings as high as 9.5 wt%. However, for a 15.4 wt% MoO_x/SBA-15 catalyst various characterizations techniques showed changes in the SBA-15 framework, which suggested that too high weight loadings may destroy the SBA-15 framework. Wet impregnation was the common method of supported metal oxides on SBA-15. Ressler *et al.* [90] also used wet impregnation to prepare MoO_x/SBA-15 catalysts for the selective oxidation of propene. On the other hand, Melero *et al.* [91] used a co-condensation method to synthesize molybdenum containing SBA-15 catalysts for the epoxidation of olefins. These catalysts showed different characterization results indicative of Mo incorporated in the SBA-15 framework.

In terms of oxidative dehydrogenation, Dinse and co-workers [92] used SBA-15 supported vanadia catalysts for a kinetic investigation on the oxidative dehydrogenation of propane. These catalysts were prepared by a grafting ion-exchange procedure that incorporate the vanadium species into the silica matrix and resulted in high dispersion of the metal throughout the support. This type of catalyst worked well for the kinetic investigation due to its predictable reaction behavior.

SBA-15 is a well-used support for many different catalytic applications. Its desirable properties make it appealing as a support and it has been well reported to be used with transition metals. The use of SBA-

15 as a support with a transition metal oxide is not well reported which provided an opportunity to explore SBA-15 in higher paraffin activation.

1.8 Manganese in heterogeneous catalysis

Manganese is well known for having the most number of stable oxidation states from the first row transition metals. These large number of stable oxidation states enhance the reductive and oxidative properties of a catalyst incorporating Mn and thus making it easier to manipulate its redox potential, serving as a better redox catalyst [69].

Manganese oxide was used as a catalyst itself by Sun *et al.* [93] for the combustion of dimethyl ether. This reaction was used to probe the effect of different crystalline phases of manganese oxide, namely α-, β- and γ-, with the α-MnO_2possessing a nanorod shape showing enhanced catalytic activity. Unsupported Mn_3O_4 has also shown good catalytic activity in many reactions, for example, the selective reduction of nitrobenzene to nitrosobenzene [94, 95]. Kung and Mcbride [96] also described the oxidation of hydroquinone in aqueous solutions of Mn_3O_4at pH 6. Lamaita *et al.* [97] also used synthesized MnO_2 for the complete oxidation of ethanol to carbon dioxide and water. They showed that the catalytic activity of the MnO_2 prepared by $MnCO_3$ decomposition and oxidation of acid $MnSO_4$ solution was better than β-MnO_2 and Mn_2O_3 due to the presence of Mn^{3+} and Mn^{4+} ions and OH species generated by Mn^{4+} vacancies.

Supported manganese oxide catalysts have also been used in many types of catalytic reactions. Wang *et al.* [98] supported Mn_3O_4on alumina by wet and dry impregnation. They found that manganese acetate was an effective precursor salt in order to obtain an effective dispersion of manganese oxide throughout the high surface area alumina support. They also found from TPR that the state of dispersion was affected by some factors in catalyst preparation, e.g. drying rate and decomposition period.

Boot *et al.* [99] prepared zirconia supported cobalt and manganese oxide catalysts for the dehydrogenation of 1-butene to 1, 3-butadiene. Good dispersion was obtained by using a pre-shaped zirconia support and by a preparation method using complex organic precursors. It was also found that the Co and Mn catalysts had similar behavior in terms of catalytic performance. For the oxidative dehydrogenation of propane to propene, Cadus and Ferretti [100] used manganese oxide catalysts impregnated with molybdenum. They found that surface area of the catalysts decreased with increasing

amounts of molybdenum and different Mn-Mo phases were found with XRD with increased Mo content. Catalysts with greater Mo content however did show the best activity. Zhou *et al.* [101] prepared a series of manganese oxide octahedral molecular sieves for the oxidative dehydrogenation of ethanol. They also doped these sieves with various first row transition metals, with the Co doped sieves showing the best activity.

Manganese has also been widely used with SBA-15 in previous research in a number of different catalytic studies [102-111]. Rosal *et al.* [102] used the minimum volume method to synthesize MnO_x/SBA-15 catalysts and compare them to MnO_x/Al_2O_3 catalysts for the catalytic ozonation of atrazine and linuron in a fixed bed reactor. Both catalyst types were found to have no effect on the rate of the hydroxyl-mediated ozonation as this process was found to be a non-catalytic one which took place in a homogeneous phase. However, the MnO_x/SBA-15 catalysts did significantly increase the ozone decomposition rate.

Zhang *et al.* [103] prepared a series of SBA-15 catalysts promoted with noble and *3d*-transition metals, including Mn, via an impregnation method for the catalytic combustion of acetonitrile. The XRD patterns obtained showed no metal oxide peaks present and this in combination with N_2 adsorption/desorption analyses showed that the structure of SBA-15 remained intact after impregnation for all catalysts. For this study, Cu proved to be the most effective metal. Tang *et al.*[104] prepared SBA-15 modified with manganese pyrazolyl pyridine complexes by a covalent grafting method for the catalytic epoxidation of terminal alkenes. Testing showed that these catalysts were effective for a wide range of alkenes, including terminal ones. For these catalysts, FT-IR, Raman spectroscopy and XRD clearly showed the manganese complexes present on the SBA-15 support, with the support framework maintained.

Satish-Kumar *et al.* [105, 106] described a synthesis method for incorporation of manganese into the SBA-15 framework. This was done by pre-hydrolyzing the silica precursor(tetraethyl orthosilicate) and manganese salt above the isoelectric point of silica, whilst employing triblock copolymer as the template for the structure. The effect of washed and unwashed samples as well as pH of synthesis was looked at, with higher pH resulting in more of the Mn being incorporated. Tang *et al.* [107] used a controlled post-synthesis grafting method to prepare manganese oxide catalysts supported on SBA-15 for the catalytic epoxidation of *trans*-stilbenzene. The transmission electron micrographs in this study clearly showed the well-ordered structure and hexagonal mesopores of SBA-15, with the manganese oxide particles clearly present after the grafting synthesis.

Tsoncheva *et al.* [108] used incipient wetness impregnation to prepare a range of copper and manganese oxide SBA-15 catalysts for the oxidation of ethyl acetate and the decomposition of methanol. They found that the ordered mesoporous structure of SBA-15 facilitates the interaction between different metal oxide nanoparticles and increases their dispersion but ethyl acetate oxidation was suppressed due to the lower accessibility of the metal oxide particles, which were located in the pores of the support. Visuvamithiran *et al.* [109] also synthesized a bimetallic Mn-Ti-SBA-15 catalyst for the oxidation of ethylbenzene using a hydrothermal method with pH adjustment. A combination of various characterization techniques showed the incorporation of both metals into the framework of the support without affecting the mesoscopic nature of the material.

Benzene oxidation with ozone was also looked into using MnO_x/SBA-15 catalysts by Jin *et al.* [110]. The effect of nitrate and acetate precursor salts were looked at and it was found that the precursor salts directly affected the particle size and dispersion of the manganese oxide particles on the support, with the acetate precursor yielding smaller particles and a higher dispersion, ultimately resulting in a more active catalyst. Pérez *et al.* [111] also presented a similar study, looking into the effect of precursors on the synthesis and activity of MnO_x/SBA-15 catalysts for the complete oxidation of ethyl acetate. They found that the manganese oxide dispersion depended on the precursor, however the metal oxide particles were deposited on the surface as well as inside the pores for all precursor salts used. The most active catalyst was found to be the one with Mn^{4+}/Mn^{3+} pairs.

Manganese oxide catalysts supported on SBA-15 have not been looked into for the oxidative dehydrogenation of *n*-octane and due to the novelty of this work and potential industrial impacts, this was deemed a unique research endeavor. However, there can be further unique aspects to this work. Since SBA-15 has a well ordered structure, different synthesis methods were used to specifically prepare two groups of catalysts. The first would contain metal oxide atoms on the surface of the SBA-15 support and the second would contain metal oxide atoms in the pores of the SBA-15 support. These two groups of catalysts were compared and the effect of the metal oxide position with respect to the SBA-15 support was determined.

1.9 Aim and objectives of study

The amount of long chain linear paraffins produced as by-products from coal to liquid and gas-to-liquid plants worldwide is increasing annually. A process that is able to convert paraffins to more valuable products or compounds that are feedstocks for industrial process would be of great interest. Oxidative dehydrogenation has been an effective route for production of these compounds from paraffins. Oxidative dehydrogenation of *n*-octane will be looked at using manganese oxide supported on SBA-15 catalysts.

The main objectives of this study were:

1. To synthesize and characterize of SBA-15 and manganese oxide supported on SBA-15 catalysts.

2. To explore the influence of pellet particle size, gas hourly space velocity, carbon to oxygen molar ratios on conversion of *n*-octane and selectivity of octene isomers and aromatic compounds and to evaluate the stability of the catalyst.

3. To investigate the effect of varying the weight percentage of manganese and to establish the effect of the active site position for the oxidative dehydrogenation of *n*-octane.

Chapter 2

Experimental Procedure

There were various chemicals and reagents used for the synthesis, characterisation and catalytic testing of the support and catalyst, as shown in Table 2.1.

Table 2.1 List of reagents used.

Reagent	**Supplier**	**Grade / Purity**
Pluronic P123 copolymer	Sigma-Aldrich	>98%
NH_4F	Sigma-Aldrich	>98%
Acetone	Merck	>98%
Manganese Nitrate solution	Polychem supplies	50%
HNO_3	SaarChem	AR
HCl	SaarChem	AR
Tetraethyl Orthosilicate	Sigma-Aldrich	>98%
HF	SaarChem	AR
n-Octane	Merck	>98%
Carborandum powder (24 grit)	Promark Chemicals	-
Sodium Carbonate	Sigma-Aldrich	>98%
Mn 1000 ppm ICP standard	Polychem supplies	AR
Si 1000 ppm ICP standard	Polychem supplies	AR

2.1 SBA-15 synthesis

This synthesis was carried out according to a previously reported method by Stucky *et al.* [76] and Pitchumani *et al.* [112]. For the synthesis, 14.8 g of pluronic P123 copolymer was used. This polymer (containing ethylene oxide and propylene oxide in the ratio EO_{20}–PO_{70}–EO_{20}) was dissolved in 535 mL of 1.3 M HCl. This solution was stirred for 1 h at 1000 rpm. To this solution 0.161 g of NH_4F was added and then 30 ml of TEOS was added drop-wise over a period of 10 minutes. The solution was left to stir for 24 h and thereafter was transferred to a sealed container, with a stirrer bar and placed in an oil bath maintained at 100 °C for 24 h. The resulting product was recovered by filtration after cooling and washed

with 80 ml acetone, to give a white powder. The powder was then calcined under flowing air at 550 °C for 5 h.

2.2 Catalyst synthesis by wet impregnation

The synthesis of the 2 wt% catalyst was done using 4.0049 g of SBA-15 and 50 ml of double distilled water, which was stirred for 30 minutes at 500 rpm. To this, 2.1248 g of manganese nitrate solution added over a period of 10 minutes, stirred for 6 h at 500 rpm and then heated to dryness at 100 °C. The paste that formed was placed in an oven at 100 ºC overnight. The brown powder obtained was calcined under air for 5 h at 550 ºC. The mass of manganese solution used was varied to obtain the desired weight loading for the 5 and 9 wt% catalysts.

2.3 Catalyst synthesis by deposition precipitation

For the synthesis of the 2 wt% catalyst, the following procedure was used. 2.009g of SBA-15 in 50ml of double distilled water was stirred for 30 minutes at 500 rpm. The pH was adjusted to between 7 and 8 with saturated Na_2CO_3 solution. To this, 1.0611g of manganese nitrate solution was added over a period of 10 minutes. The solution was stirred for 6 h at 500 rpm and the pH was maintained between 7 and 8. The excess sodium was washed off with HCl. The solution was heated to dryness at 100 °C and the paste that formed was placed in an oven at 100 ºC overnight. The brown powder was calcined under air for 5 h at 550 ºC. The mass of manganese solution used was varied to obtain the desired weight loading for the 5 and 9 wt% catalysts.

2.4 Catalyst characterisation

Inductively coupled plasma optical emission spectroscopy (ICP-OES) was carried out using a Perkin Elmer Precisely Optical Emission Spectrometer Optima 5300 DV. This was used to determine the weight percentage of metal loading of all the catalysts. The samples were prepared using a mixture of hydrofluoric acid (HF), nitric acid (HNO_3) and hydrochloric acid (HCl) in the ratio HF:HCl:HNO_3 = 4:3:1 in order to dissolve the samples. The standards were prepared from a 1000 ppm ICP standard (Sigma-Aldrich).

Powder X-ray diffraction (XRD) was carried out using a Bruker D8 Advance XRD diffractometer employing Cu K_α radiation (λ = 1.5406 Å). The samples were analyzed as fine powders, which were ground prior to analysis. The diffractometer operated at 40 kV and 40 mA with a scanning rate of 0.5 ° min^{-1} slit (in 2θ) and divergence slit and scatter slit widths of 1°. *In situ* XRD was carried out with 5 % H_2 in N_2 at a flowrate of 30 mL min^{-1} in order to obtain a reducing environment. The temperature was ramped at a rate of 1 °C min^{-1} till 600 °C and thereafter was cooled to 100 °C. The instrument was then purged with N_2 for 2 h at 100 °C to remove any H_2 present. Thereafter, air was used at a flowrate of 30 mL min^{-1} and a temperature ramp of 1 °C min^{-1} until 600 °C for re-oxidation.

A PerkinElmer Spectrum 100 Fourier Transform – Infrared (FT-IR) fitted with a universal attenuated total reflectance (ATR) sampling accessory, equipped with a diamond crystal, was used to record infrared spectra. The powdered samples were placed on the crystal and a force (120 Gauge) was applied to ensure proper contact between the sample and the crystal while the sample was analyzed. Spectrum software was used to analyze the data obtained.

N_2 adsorption and desorption isotherms was obtained using a Micromeritics Tristar instrument. Based on these isotherms and using the BET equation, the surface area, pore volume and pore diameter values were calculated. Prior to analysis, the samples were degassed overnight at 200 °C under nitrogen flow using a Micromeritics FlowPrep 060. The degassed samples were cooled to room temperature before further analysis.

Transmission electron microscopy (TEM) images of the various catalysts were obtained using a Jeol JEM-1010 electron microscope. The images were captured using iTEM software. Sample preparation was carried out by suspending the sample on a formvar coated copper grid using acetone.

The scanning electron microscopy (SEM) analysis was carried out on a Zeiss Ultra Plus Field Emission Gun SEM with a secondary electron detector and was analyzed with Smart SEM software. Prior to analysis, samples were mounted on aluminium stubs with double-sided carbon tape. EDX analysis was carried out using a Jeol JSM-6100 scanning microscope fitted with a Bruker EDX detector and was analyzed using Esprit 1.8 software. All samples were carbon coated using a Jeol JEE-4C vacuum evaporator prior to analysis.

H_2-temperature programmed reduction (TPR) and O_2-temperature programmed oxidation (TPO) analyses were carried out with a Micromeritics 2920 Autochem II Chemisorption Analyzer. Samples were placed on quartz wool located in a U-shaped quartz tube and sample preparation was done in the

instrument and included argon flowing at a rate of 30 mL min^{-1} until 350 °C, which was obtained with temperature ramping rate of 20 °C min^{-1}. Firstly, H_2-TPR was done and the sample was reduced using 5 % H_2 in argon flowing at a rate of 30 mL min^{-1}, whilst the temperature was linearly increased from 80 °C to 1000 °C at a rate of 10 °C min^{-1}. The amount of hydrogen consumed was measured by a thermal conductivity detector (TCD) and a plot of TCD signal vs. temperature was used to determine the reduction peaks of the catalyst. After TPR, the sample chamber was cooled to 80 °C and then the TPO procedure began, with the temperature being increased to 1000 °C at a rate of 10 °C. min^{-1} while 5% O_2 in argon was passed through it at a rate of 30 mL min^{-1}.

Raman spectra were obtained using a Delta Nu Advantage 532 instrument, with the laser source operating at 532 nm and controlled by NuSpec software. Fine powder samples were loaded into a clean quartz tube and placed into the sample holder of the instrument which operated at 22 ºC, the controlled temperature of the room. Analysis parameters were optimised based on number of scans and time-per-scan until clear peaks were observed on the spectra.

Oxygen chemisorption was carried out using a Mircomeretics ASAP 2020 Chemisorption analyser. Before sample analysis, catalysts were degassed using a Micromeritics VacPrep 060 under vacuum in nitrogen at 200 ºC overnight. The samples were then reduced in the instrument under flowing hydrogen at 30 mL min^{-1} for 3 h at 450 °C and then flushed at the same temperature for 30 minutes with helium at 30 mL.min^{-1}. Oxygen was passed at 30 mL min^{-1} through the sample for 3 h until saturation of the sample was attained. The oxygen uptake was quantified using a TCD detector.

2.5 Reactor Design

Figure 2.1 shows a schematic of the reactor used. Gas delivery was done through ¼ inch copper tubing and was regulated to 100 kPa using mini-regulators, while the individual flow rates were carefully controlled using rotameters calibrated for the specific gas used. The feed delivery lines after the rotameters were made using 316-grade ¼ inch stainless steel tubing connected using Swagelok fittings of the appropriate size. The feed was sent in via a High Performance Liquid Chromatography (HPLC) pump that was calibrated for *n*-octane delivery and the mass delivered was monitored via a 3 decimal place balance. The feed was vaporised in the delivery lines to the reactor tube which were heated to 200 °C using heating tape controlled by a CB-100 temperature controller with internal relay output.

The reactor itself was a ½ inch (internal diameter) stainless steel tube (316-grade), 35 cm in length. This was placed in a copper heating block of 30 cm length and was heated using a cylindrical heating

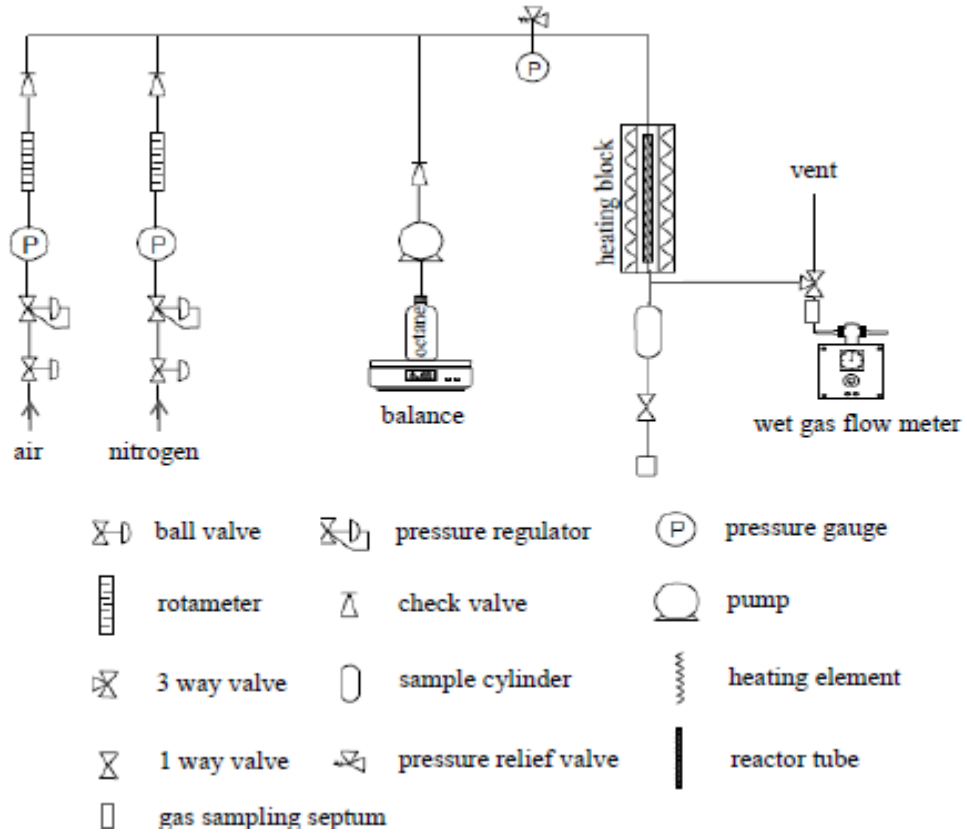

Figure 2.1 Schematic of reactor used [49].

element that served as a furnace. The block was insulated using glass wool and covered in a stainless steel jacket. The heating of the reactor block was controlled by a CB-100 temperature controller equipped with a solid state relay. The product line from the reactor was connected to a 150 mL sample cylinder containing a needle valve. This was cooled to ~ 2 °C to assist the condensation of the gaseous products. All gaseous products that did not condense were vented via a Ritter wet gas flow meter which monitored the volume of gas produced over a given time period.

The reactor tube cross section shown horizontally in Figure 2.2 was situated vertically in the heating block and was used to hold the catalyst at the hottest point or "hot-spot" of the heating block, which was found to be approximately 12 cm below the top of the heating block. Catalyst pellet particles were held in place using glass wool on either side. The catalyst was first ground and then packed together in a dye-press to for a pellet. The pellets were then sieved to the required size (300 – 600 and 600 to 1000 µm) to form catalyst particle pellets. The reactor tube was then filled with inert carborundum powder and

glass wool as a stopper at each end of the reactor tube. The internal temperature of the reactor tube was monitored via a thermocouple inserted into the catalyst bed and covered by a stainless steel thermocouple jacket.

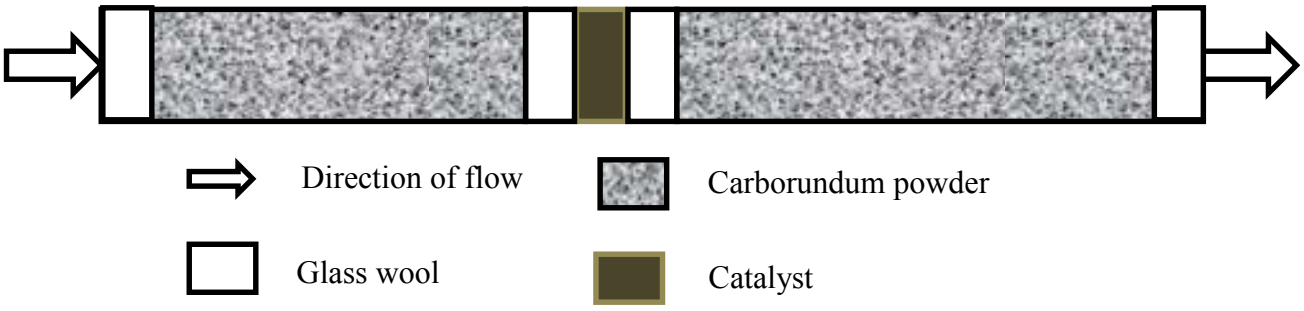

Figure 2.2 Schematic of reactor tube used [49].

Before catalytic testing, the reactor system was pressurised to 1 bar to check for leaks. The pressure was maintained overnight to ensure no leaks were present. The pressure was then released and the gasses were set to their required flow rates. Thereafter, the reactor block and heating tape were taken to their required temperatures for the reaction in 50 °C intervals. Once the adequate temperature was reached, the pump was started and the feed was introduced into the system. The pump was allowed to equilibrate for 2 hours, after which time the sample cylinder was drained and a run was initiated. Reaction time was 2 hours per run at each temperature window and after this time, the sample cylinder was emptied, with the collect liquid used for product analysis. All catalytic runs were done in duplicate or more to ensure reproducibility of results.

2.6 Product Analysis

Both organic liquid and gas samples were collected from the reaction and product analysis was carried out by a gas chromatograph. The GC used was a Perkin Elmer Clarus 580 with a 30 m PONA column and an FID detector to quantify organic products while a Perkin Elmer Clarus 400 GC fitted with a 30 m Supelco Carboxen column and TCD detector was used to quantify carbon oxides formed. Gas samples were injected using a SGE gas-tight syringe. GC-MS analysis was carried out on a Perkin Elmer Clarus 500 using a 50 m PONA column, to identify unknown products that formed during the reaction.

Chapter 3

Characterisation

3.1 Wet impregnation and deposition precipitation catalyst characterisation

3.1.1 Inductively coupled plasma – optical emission spectroscopy

ICP - OES analysis was used to confirm the amount of metal oxide present on the support and to determine the metal loading. For the catalysts prepared by wet impregnation, ICP confirmed the weight loadings as 2, 5 and 9 wt% which were denoted as 2W, 5W and 9W. For catalysts prepared by deposition precipitation, weight loadings of metal oxide were confirmed at 2, 5 and 9 wt% and these catalysts were denoted as 2D, 5D and 9D respectively. The exact weight loadings are listed in Table 3.1.

Table 3.1 Weight loading of metal oxide for all catalysts prepared.

Catalyst	**Weight loading / %**
2W	2.12
5W	5.09
9W	9.23
2D	1.98
5D	5.11
9D	9.07

3.1.2 Fourier Transform - Infrared

Table 3.2 Band assignment for support and catalysts.

Wavenumber / cm^{-1}	**Assignment**
3300	υ OH (H_2O)
1050	υ_{as}(Si-O-Si)
790	υ_s (Si-O-Si)
630	υ_s (Mn-O-Mn)
440	δ (Si-O-Si)

Table 3.2 shows the dominant band assignment for the support and all the catalysts. It was found that all catalysts showed strong peaks at the same wavenumber values as shown in Table 3.1. The peaks at 3300, 1050, 790 and 440 cm^{-1} can be attributed to characteristic peaks of SBA-15, as also seen by Perez *et al* [111]. The peaks at around 630 cm^{-1} was seen for all catalysts but not the support and was assigned as the Mn-O-Mn stretching peak.

3.1.3 Raman spectroscopy

Raman spectroscopy (Figure A9 in Appendix) showed no significant peaks for the SBA-15 support. All catalysts showed two peaks at 480 and 810 cm^{-1} which correspond to the Mn-O-Mn bending and stretching peaks respectively [107].

Both FT-IR and Raman analyses suggest that the SBA-15 support was synthesised correctly and there is a phase of manganese oxide present for all catalysts, however, these techniques do not give further information as to the type of phase present. Other characterisation techniques were thus utilised to establish the phases of manganese oxide present as well as its distribution on the support.

3.1.4 XRD

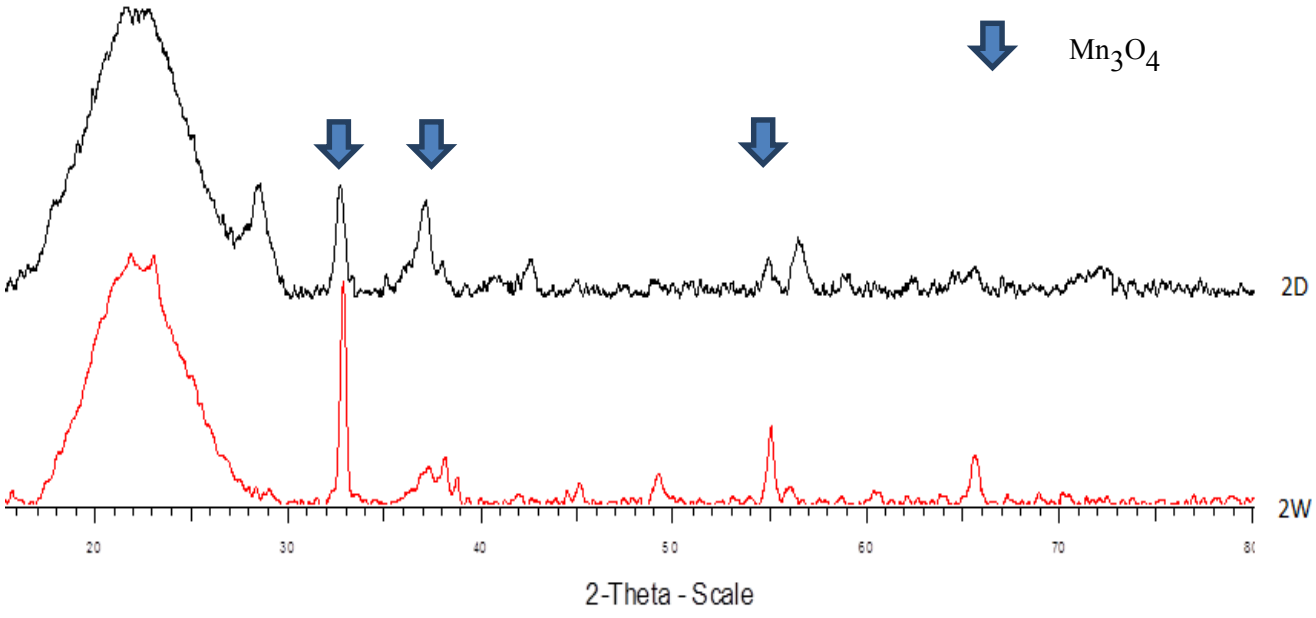

Figure 3.1 Powder XRD analysis of 2W and 2D catalysts.

The powder XRD of the 2W and 2D catalysts are shown in Figure 3.1. The dominant phase present in both groups of catalysts was Mn_3O_4 at room temperature indicated by the peaks at 2θ angles of 33º, 37º and 55º corresponding to d-spacing values of 2.73, 2.42 and 1.67 Å respectively [113]. The large broad peak at lower 2 theta values can be attributed to the SBA-15 support, and when comparing the intensity of this peak to that of the manganese oxide peaks, the intensities of the 2W peaks are higher than those of 2D catalyst peaks, which suggests a different degree of crystallinity of the Mn_3O_4 phase with the respect to the SBA-15 for the different synthesis methods. This phase of manganese oxide was found to be present for all catalysts synthesized by both preparation techniques as indicated by the dominant peaks from the XRD analyses of all the catalysts, as shown in the Appendix A1 – A4. To determine the stability of the dominant phase, *in situ* XRD analysis was used. The redox behavior of the catalyst could easily be monitored by *in situ* XRD and looking at the reduction of the oxide in Figure 3.2, MnO was observed as the dominant phase of manganese oxide at the higher temperature. Complete reduction of the Mn_3O_4 phase took place at 450 °C, which was also observed by Wang *et al* [98].

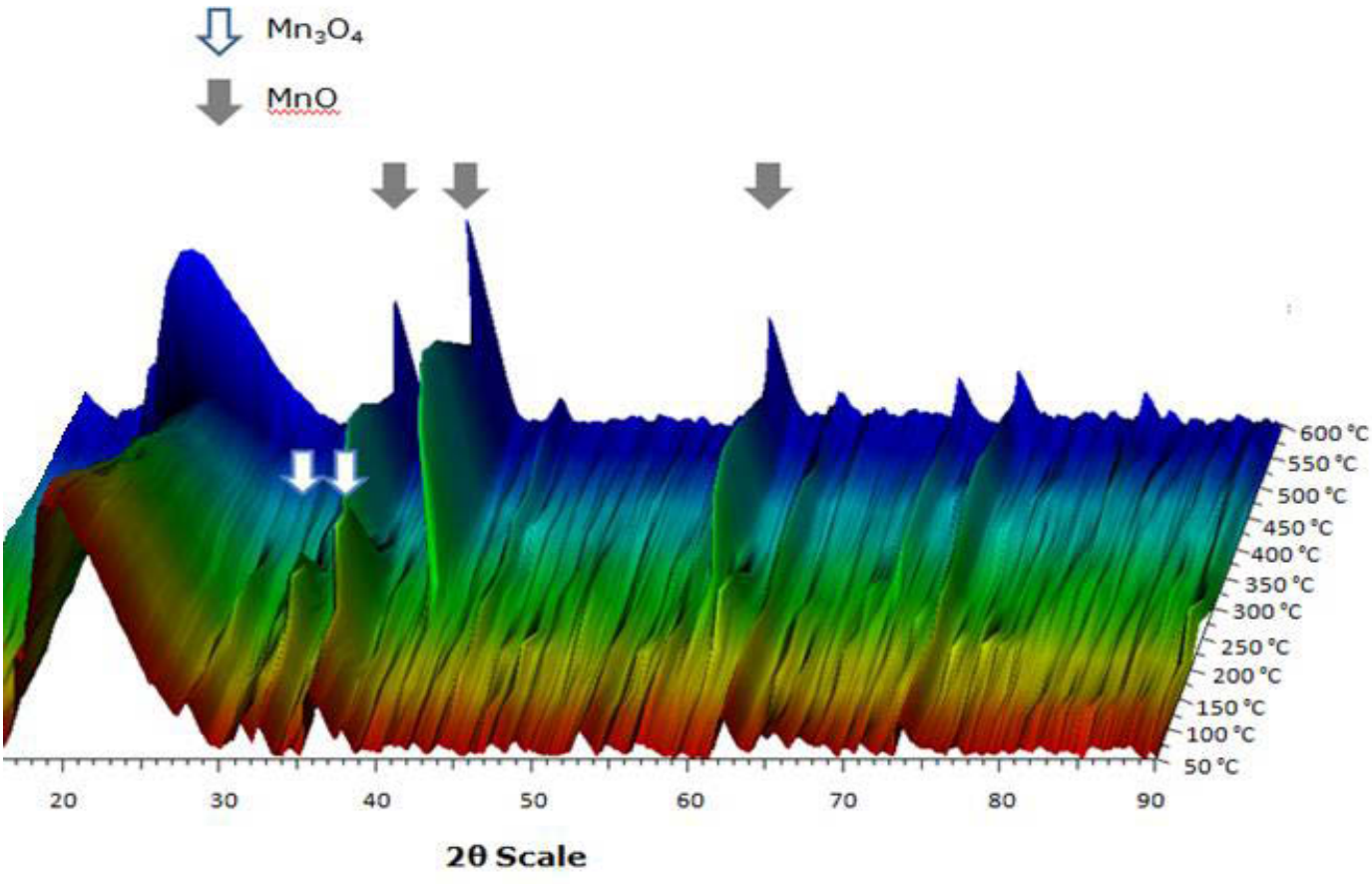

Figure 3.2 Reduction of 2W catalyst under *in-situ* XRD analysis.

3.1.5 Nitrogen physisorption

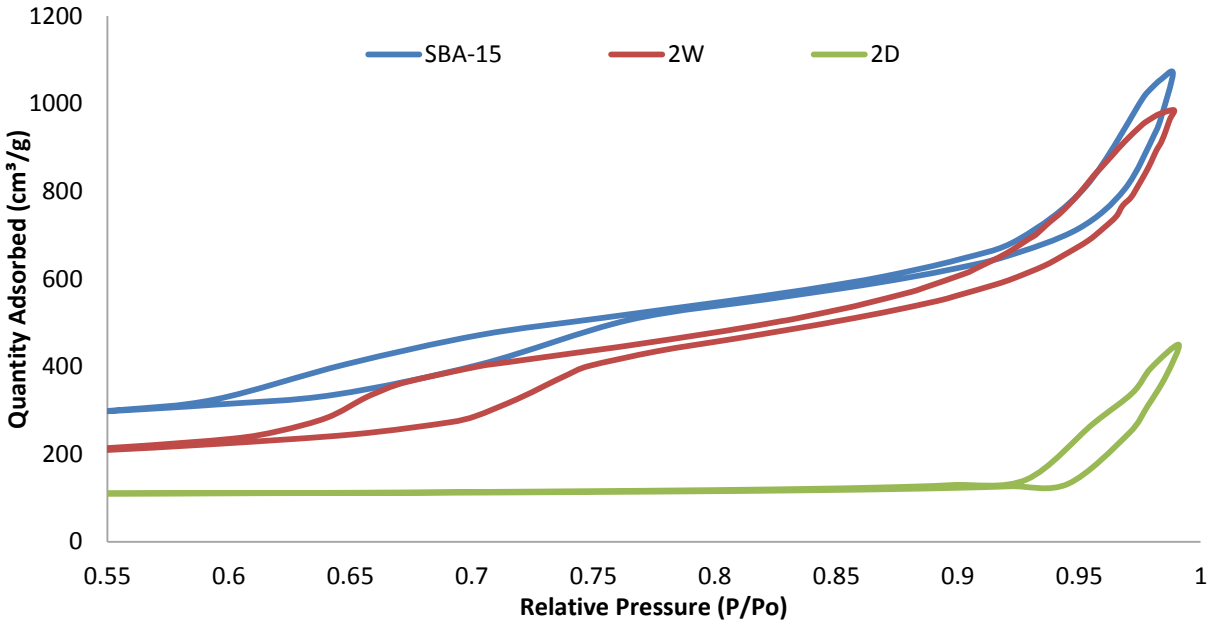

Figure 3.3 N_2 adsorption/desorption isotherms of SBA-15, 2W and 2D catalysts.

Nitrogen physisorption was used to determine the adsorption and desorption isotherms, as shown in Figure 3.3. The SBA-15 and 2W catalyst both have type IV hysteresis loops, indicative of mesopores. The relative amount of nitrogen physisorbed is lower for the 2W catalyst than the SBA-15, which is expected with the addition of the metal [112]. However, for the 2D catalyst the relative amount of nitrogen adsorbed is much lower and the shape of the isotherm changes completely. This is likely because of the channels of the SBA-15 being filled with metal oxide particles. The shape of the isotherms for all catalysts prepared by wet impregnation was the same. Similarly, the shape of the isotherms for all catalysts prepared by deposition precipitation was the same. Isotherms can be seen in Appendix A5-A8.

3.1.6 BET Analyses

Using the BET equation, the surface area, pore volumes and pore diameters were calculated for the support and all the catalysts and the results are shown in Table 3.3. The surface area, pore volume and pore diameter of the synthesized SBA-15 are in correlation with results previously obtained with this system [107].It was found that both surface area and pore volume decreased with increasing metal

loading for both groups of catalysts, while pore diameter remained fairly constant, which indicates there was no change in the porous support structure. The surface areas of the catalysts prepared by deposition precipitation were much lower than for catalysts prepared by wet impregnation. Since the support is primarily mesoporous and if the pores were filled with metal oxide particles, it would account for these lower values. This is confirmed by the much lower pore volumes for catalysts prepared by deposition precipitation when compared to those prepared by wet impregnation at the same metal oxide weight loading.

Table 3.3 Surface area, pore volume and pore diameter for support and catalysts.

Catalyst	**SBA-15**	**2W**	**5W**	**9W**	**2D**	**5D**	**9D**
Surface Area / (m^2/g)	770	450	397	334	339	292	239
Pore Volume / (cm^3/g)	1.2	0.9	0.9	0.8	0.4	0.3	0.4
Pore Diameter / (nm)	14	12	14	11	13	11	12

3.1.7 Transmission Electron Microscopy

For the TEM images in Figure 3.4, images A is of the SBA-15 catalyst and from this image, the well-ordered structure of the SBA-15 can be seen. Image B is of the 9W catalyst, where the hexagonal, open channel mesopores are present. The support appears as a film, perpendicular to the electron beam. Images C, D and E are of the 2W, 5W and 9W catalysts respectively. With these catalysts, the SBA-15 support structure appears intact. This suggests that the method of wet impregnation resulted in fewer metal oxide particles being located within the pores of the sections of the support. On the contrary, when comparing these images to those of the D-series of catalysts (Figure 3.4 images F, G and H showing the 2D, 5D and 9D catalysts respectively), it can be clearly observed that the pores of the support appear collapsed and filled to some extent by metal oxide particles. A similar observation was made by Lou *et al.* with molybdenum oxide supported on SBA-15 [89].

These images were also used to determine the particle size of the metal oxides, shown in Figure 3.5 and it was found that for the 9W catalyst, the metal oxide particle sizes were above 20 nm, higher than the pore diameter of the support, while for the 9D, the particle sizes were all lower than the pore diameter of the support. The difference in particle size measurements of the manganese oxide particles is likely the reason why for wet impregnation, the metal oxide was found to be present on the surface of the support while for deposition precipitation, the metal oxide particles were in the pores of the support.

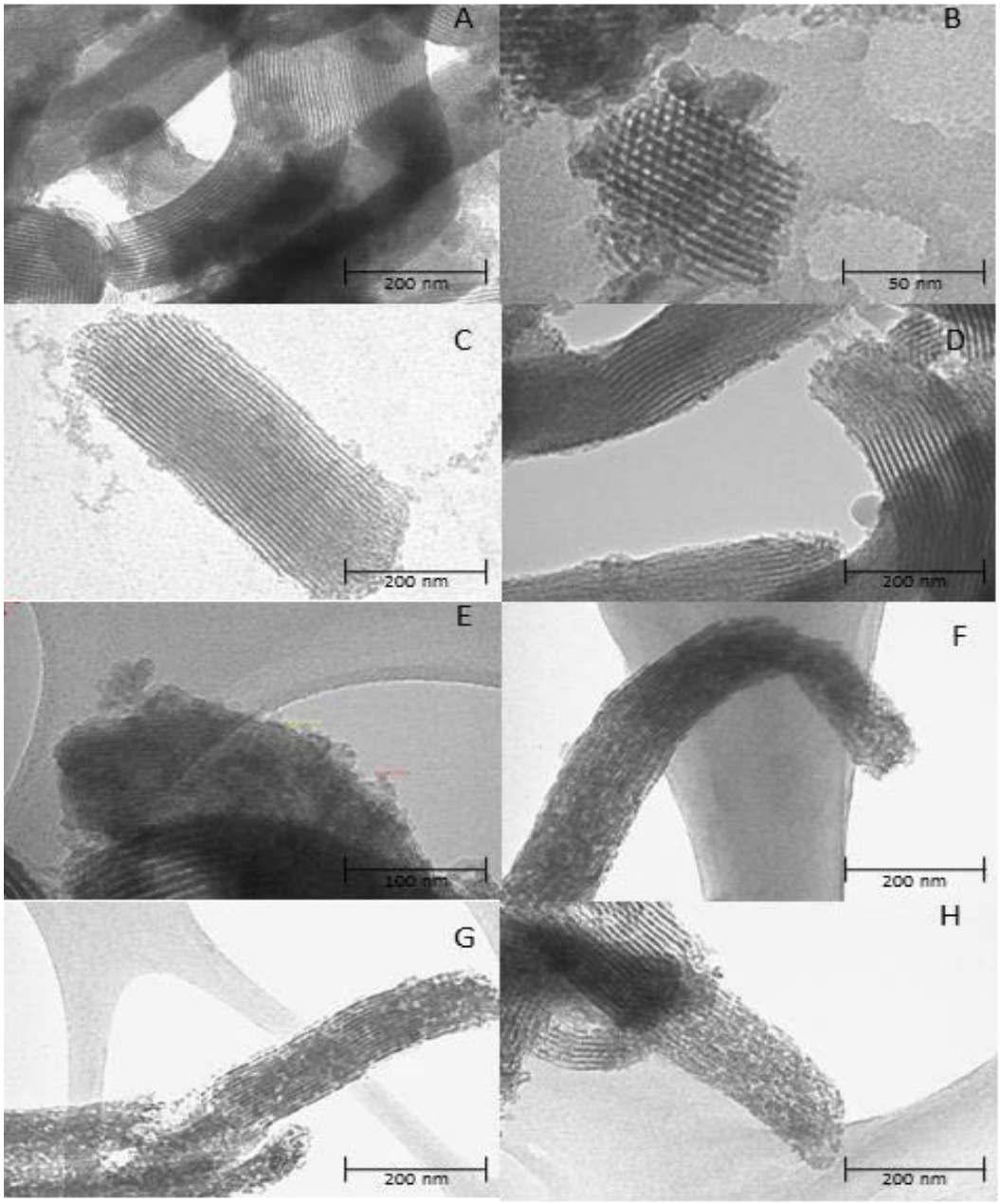

Figure 3.4 TEM images of (A) SBA-15, (B) 9W catalyst showing hexagonal mesopores (C) 2W catalyst, (D) 5W catalyst, (E) 9W catalyst, (F) 2D catalyst, (G) 5D catalyst and (H) 9D catalyst.

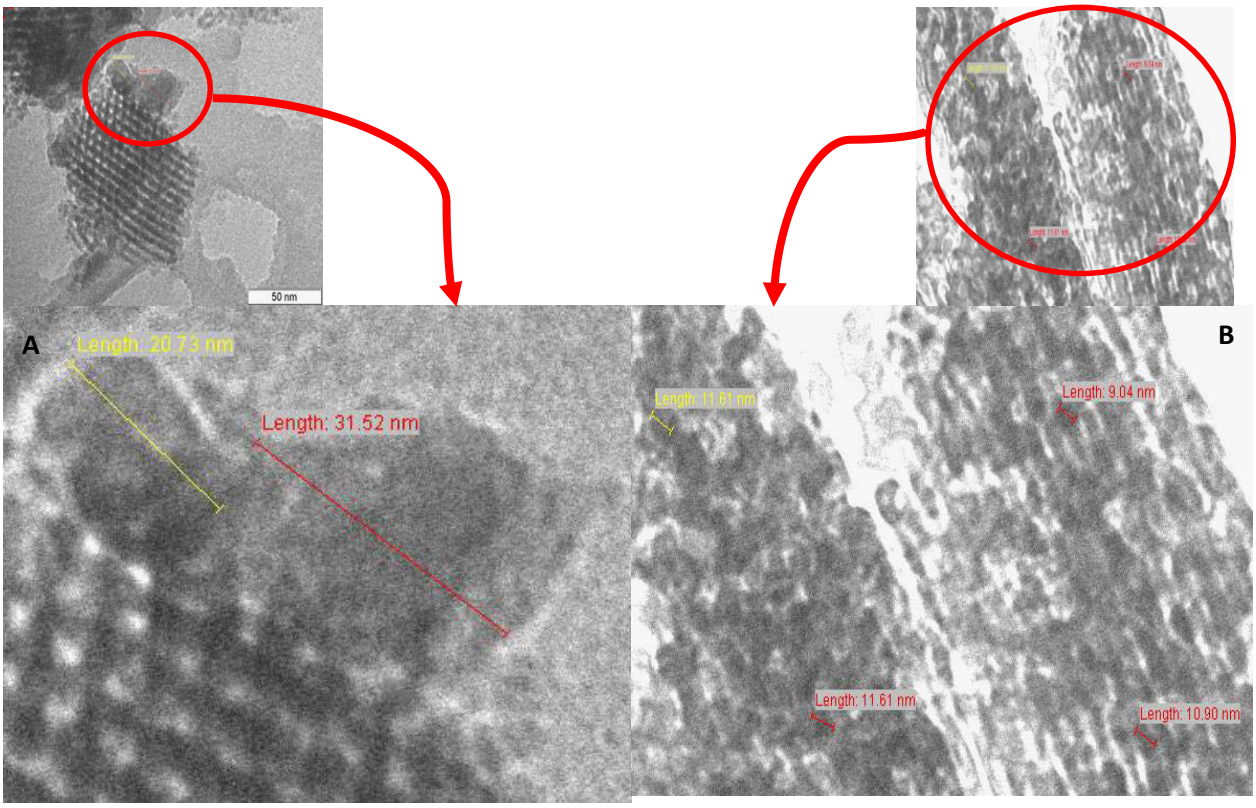

Figure 3.5 Metal oxide particle size measurements of (A) 9W and (B) 9D catalysts.

3.1.8 Scanning Electron Microscopy

SEM-EDX and line scan analyses of the catalyst were carried out for the 9W catalyst shown in Figure 3.6. The morphology of the SBA-15 is similar to that reported [111, 112], with the manganese confirmed present as determined by EDX mapping. For the 9W catalyst, a line scan of the sample revealed that as the amount of silicon increased, so did the amount of manganese present, which suggests agglomeration for the metal oxide on the surface of the support. This was confirmed by EDX mapping which showed the large amount of manganese present on the surface of the support.

Looking at a point scan of the 9W catalyst in Figure 3.7 and Table 3.4, the average metal composition throughout the sample is relatively high when compared to silicon. Although this technique does not give us an absolute percentage of metal present, the relative composition for this catalyst also suggests agglomeration of the metal oxide on the surface of the support.

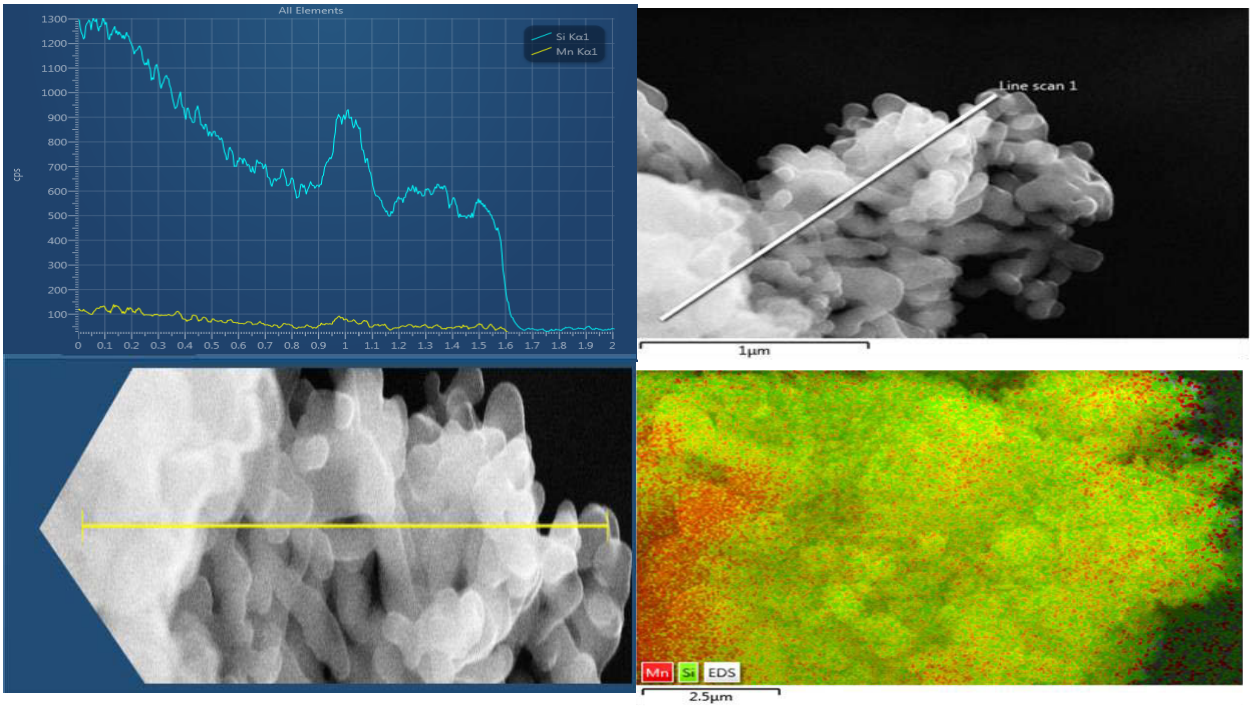

Figure 3.6 SEM-EDX and line scan of the 9W catalyst.

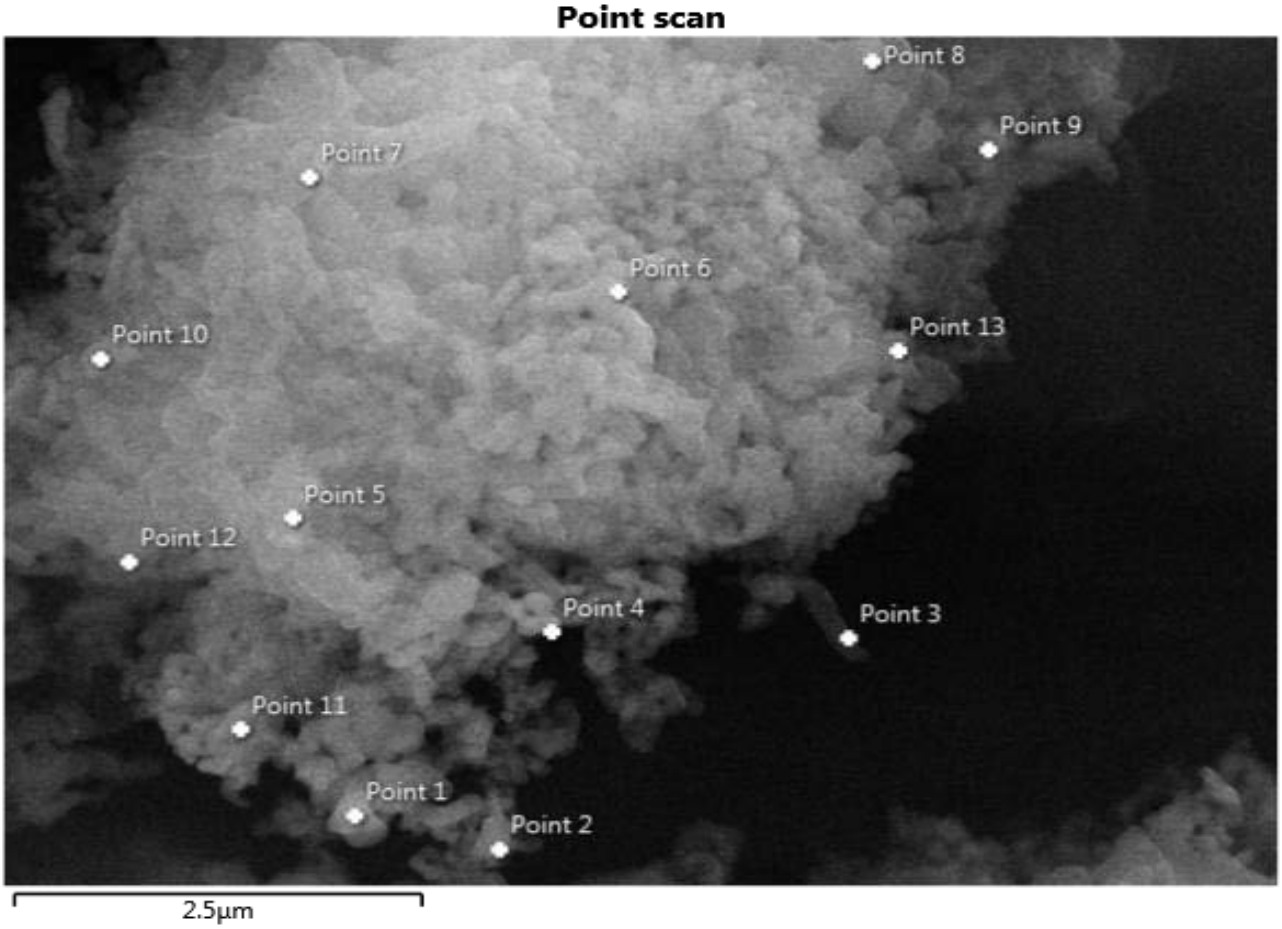

Figure 3.7 Point scan of the 9W catalyst.

Table 3.4 Relative metal composition of different points for 9W catalyst.

	Percentage Si / %	Percentage Mn / %
Point 1	63.99	36.01
Point 2	76.72	23.28
Point 3	78.90	21.10
Point 4	77.49	22.51
Point 5	71.82	28.18
Point 6	76.62	23.28
Point 7	66.99	33.01
Point 8	75.39	24.61
Point 9	75.06	24.94
Point 10	67.34	32.66
Point 11	65.22	34.78
Point 12	70.45	29.55
Point 13	80.18	19.82

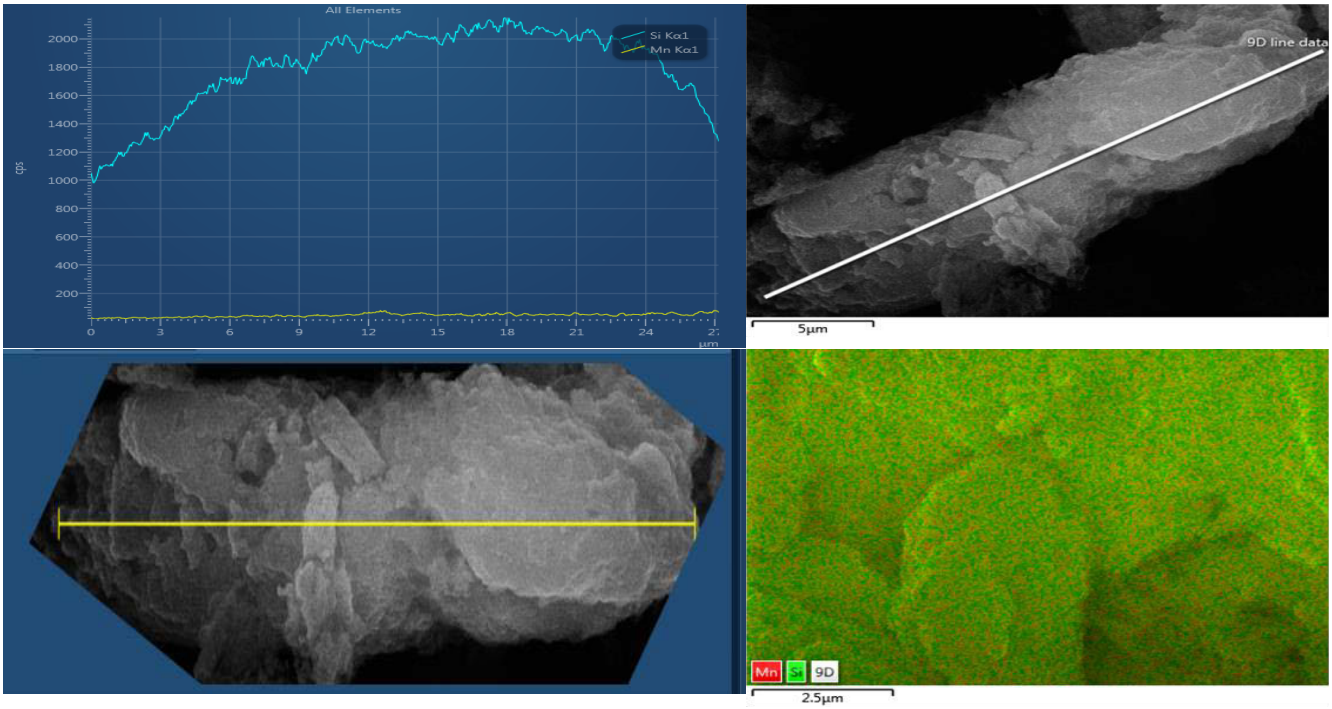

Figure 3.8 SEM-EDX and line scan of the 9D catalyst.

Both the line scan and EDX map of the 9D catalyst, shown in Figure 3.8, suggest that there is a homogeneous distribution of metal oxide particles throughout the SBA-15, indicating the metal oxide being evenly distributed in the pores of the support. A point scan also suggested the different position of the metal oxide, shown in Figure 3.9 and Table 3.5, with the average metal composition being much lower than the 9W catalyst, indicating an even distribution throughout the pores of support.

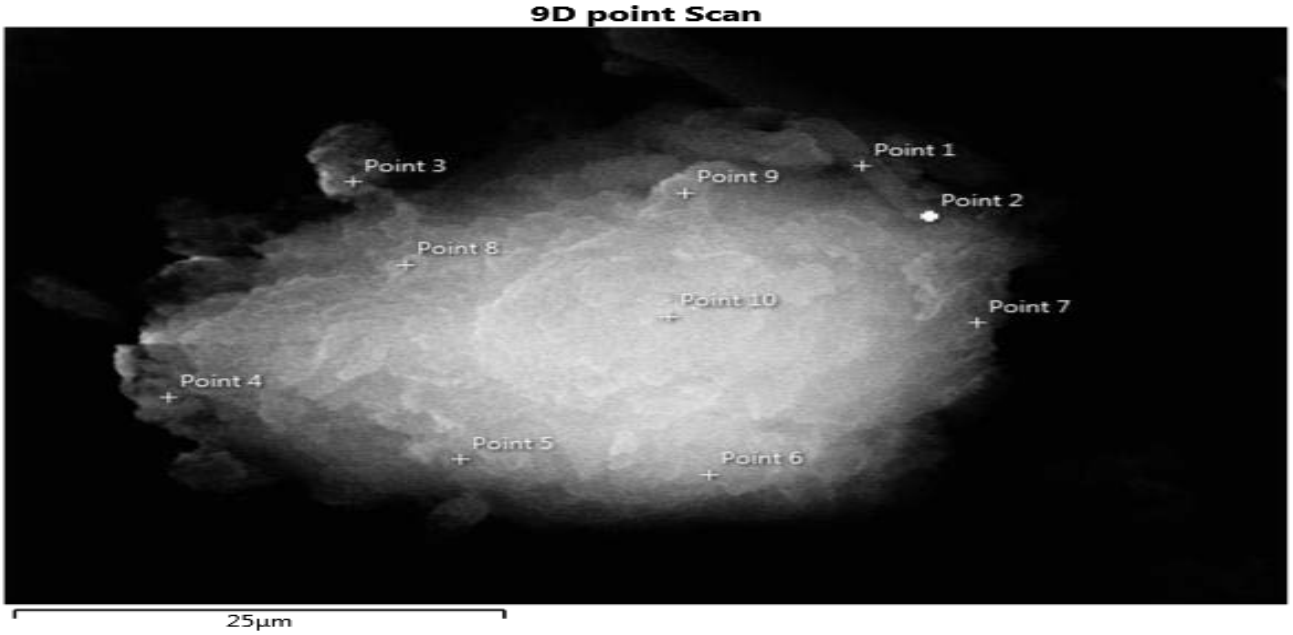

Figure 3.9 Point scan of the 9D catalyst.

Table 3.5 Relative metal composition of different points for 9D catalyst.

	Percentage Si / %	Percentage Mn / %
Point 1	95.35	4.65
Point 2	95.19	4.81
Point 3	94.38	5.62
Point 4	93.75	6.25
Point 5	96.03	6.97
Point 6	95.68	4.22
Point 7	92.67	7.33
Point 8	95.44	4.56
Point 9	95.40	4.60
Point 10	96.18	3.72

3.1.9 Temperature programmed analysis (TPR and TPO)

Temperature programmed analyses were carried out in the form of TPR and TPO for the 9W and 9D catalysts. For the 9W catalyst (Figure 3.10), TPR was carried out followed by TPO. Similarly, for the 9D catalyst (Figure 3.11), TPR was followed by TPO, however, an additional TPR experiment was done after oxidation. For both catalysts, it can be seen that the catalyst can be reduced and reoxidised easily to form MnO and Mn_3O_4. The additional reduction of the 9D catalyst also shows the reduction can still take place more than once in the pores of the support. This suggests that these phases can be established with varying reduction and oxidation environments during a catalytic reaction. The reduction peak of the 9D catalyst is higher than that of the 9W catalyst which is likely because of the metal oxide being in the pores and a higher temperature is thus required for this reduction. Once the catalyst is reduced, the interaction between the pores of the support and the metal oxide isn't as strong as the interaction between the metal oxide and the support surface. This is why, since there is a smaller particle size of the metal oxide for the 9D catalyst, lower temperatures are required for the reoxidation of the 9D catalyst [114]. Wang *et al.* found reduction peaks in the same temperature range for a TPR analysis of Mn_3O_4 and attributed the 2 peaks to the reduction of firstly a two dimensional dispersed phased of Mn_3O_4 and secondly a three dimensional crystalline phase of Mn_3O_4 [98].

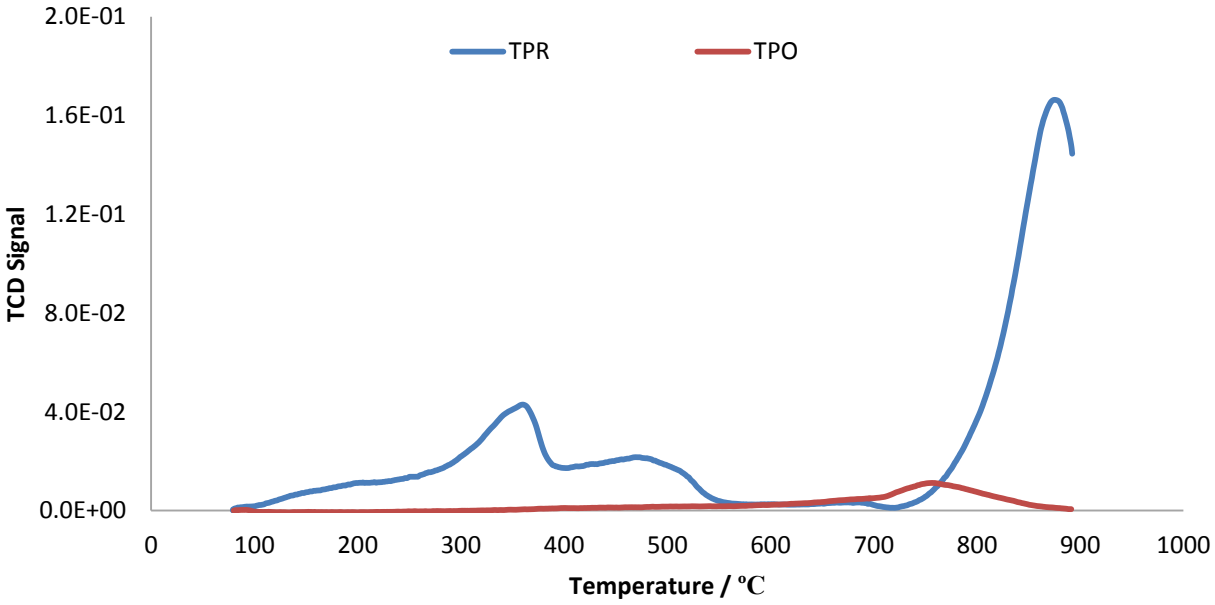

Figure 3.10 TPR-TPO of 9W catalyst.

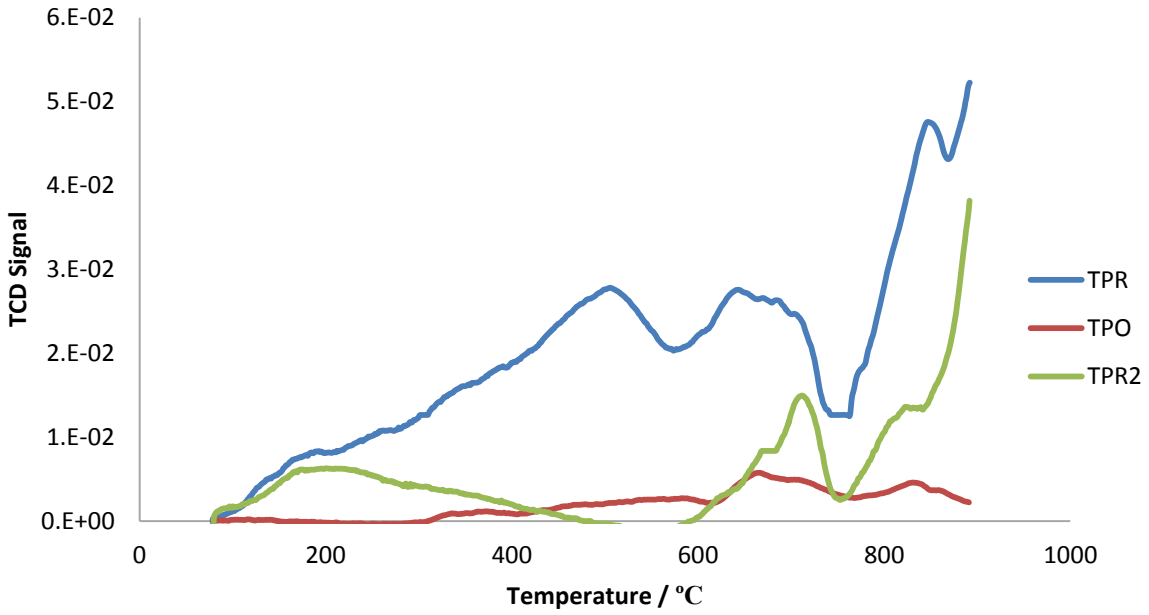

Figure 3.11 TPR-TPO-TPR of 9D catalyst.

3.1.10 Chemisorption analyses

Table 3.6 H_2/O_2 titration results for SBA-15, 2W and 2D catalysts at atmospheric pressure.

	Quantity of O_2 Chemisorbed / (mmol/g)
SBA-15	0.096
2W	0.119
2D	0.494

The method of hydrogen-oxygen titration was used to measure the amount of oxygen chemisorbed for the support and catalysts, with the results obtained summarized in Table 3.6. During a catalytic reaction, the metal in the catalyst is presumed to be reduced by the feed and re-oxidised by the air present. This method of hydrogen-oxygen titration was used to mimic the environment present in the reactor. By this technique, the catalyst was reduced under a constant flow of hydrogen, with MnO being the dominant phase present. The catalyst was then re-oxidised under oxygen and the amount of oxygen chemisorbed was measured. The amount of oxygen chemisorbed was lowest for the SBA-15, but increased with a

catalyst loaded at 2 wt% and was highest for the 2D catalyst. This is probably because the amount of oxygen chemisorbed is greater with metal oxide being present and the metal dispersion is greater for the 2D catalyst when compared to the 2W catalyst and this results in a higher amount of oxygen chemisorbed [34].

3.2 Spent catalyst characterisation

Once a reaction was complete, the catalyst was cooled in the reactor under a flow of nitrogen. At room temperature, the catalyst was unloaded from the reactor and characterisation was carried out on the used or spent catalyst. Due to the possibility of carbon deposits present on the surface of the catalysts, a full range of characterisation techniques could not be done on these samples since instrumentation used may be damaged if these deposits were to settle in them.

3.2.1 Inductively coupled plasma – optical emission spectroscopy analysis

ICP - OES analyses were carried out on the spent/used catalysts to determine whether the amount of metal present after the reaction was the same as before the reaction. A lower metal content may indicate metal leaching. However, for all catalysts, the amount of metal present in the catalyst remained unchanged after the reaction was carried out. If metal leaching did take place, a loss in catalyst activity would be expected, and perhaps selectivity.

3.2.2 BET studies

Table 3.7 summarizes the surface area, pore volume and pore diameter results for both the support and catalysts after the reaction. When comparing these results to those in Table 3.2, it is evident that both surface area and pore volumes are lower than those of the fresh samples for the support and all catalysts. This may be due to carbon deposits being present on the surface of the sample after the reaction. These carbon deposits, known as coke, have been known to hinder catalytic activity if too much is formed or a too high area of the surface is covered [114]. From these results, the greatest decrease in surface area was noted for the 9W, with a 16% decrease in surface area. There was no clear trend observed with the pore diameter values of the support and catalysts, which may indicate erratic coke formation on the catalysts after the reaction took place.

Table 3.7 Surface areas, pore volume and pore diameter for spent support and spent catalysts.

Catalyst	**SBA-15**	**2W**	**5W**	**9W**	**2D**	**5D**	**9D**
Surface Area / (m^2/g)	693	415	353	289	310	249	201
Pore Volume / (cm^3/g)	1.1	0.7	0.8	0.6	0.2	0.3	0.2
Pore Diameter / (nm)	15	10	14	10	12	11	9

3.2.3 Transmission Electron Microscopy analysis

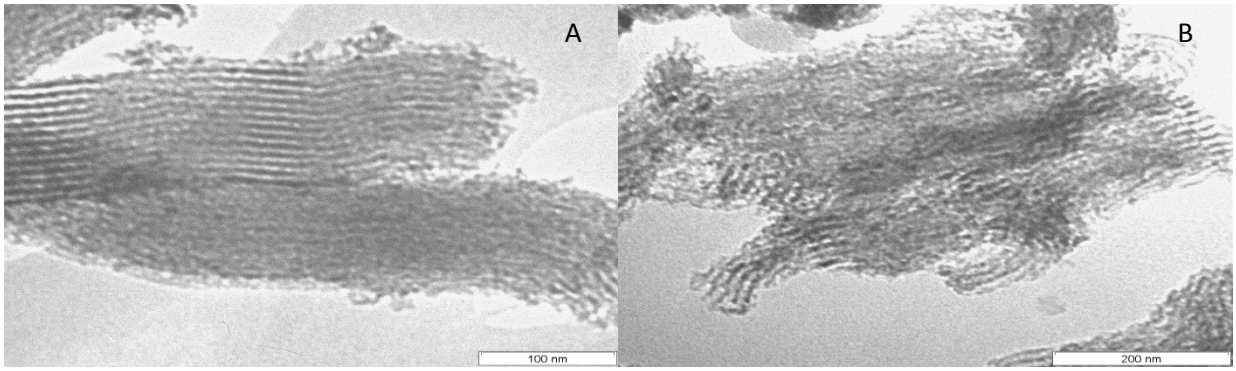

Figure 3.12 TEM images of spent catalyst (A) 9W catalyst and (B) 9D catalyst.

The TEM images obtained for both the 9W and 9D spent catalysts show that there is no significant structural change in both groups of catalysts after the reaction was carried out. For the 9W catalyst, the metal oxide particles can still be seen on the surface of the SBA-15 support and inside the pores of the support for the 9D catalyst. This indicates that the structure of the support and position of the metal oxide was still the same after the reaction was carried out. No particle growth was observed from the images in Figure 3.12 and carbon deposits were also not observed.

Chapter 4

Preliminary catalytic testing and determination of optimum reaction conditions

4.1 Investigation of non-catalytic activation of *n*-octane

Prior to catalytic testing, it was important to establish the extent of homogeneous gas phase reactions or non-catalytic reactions in the reactor system. All reactions were carried out as described in Chapter 2. In addition, the SBA-15 was tested to establish what contributions, if any, it made to the catalytic reactions. This was followed by the catalytic testing of the 2W catalyst to establish the working temperature range, particle pellet size, C:O ratio and GHSV to determine optimum catalytic performance [30].

The blank reaction was carried out in the reactor which was packed with carborundum powder granules to determine the effect of the diluent gas only and thereafter, the effect of the diluent and oxidant gas with changing temperature, for *n*-octane activation. The results obtained for both reactions are summarized in Figures 4.1 and 4.2.

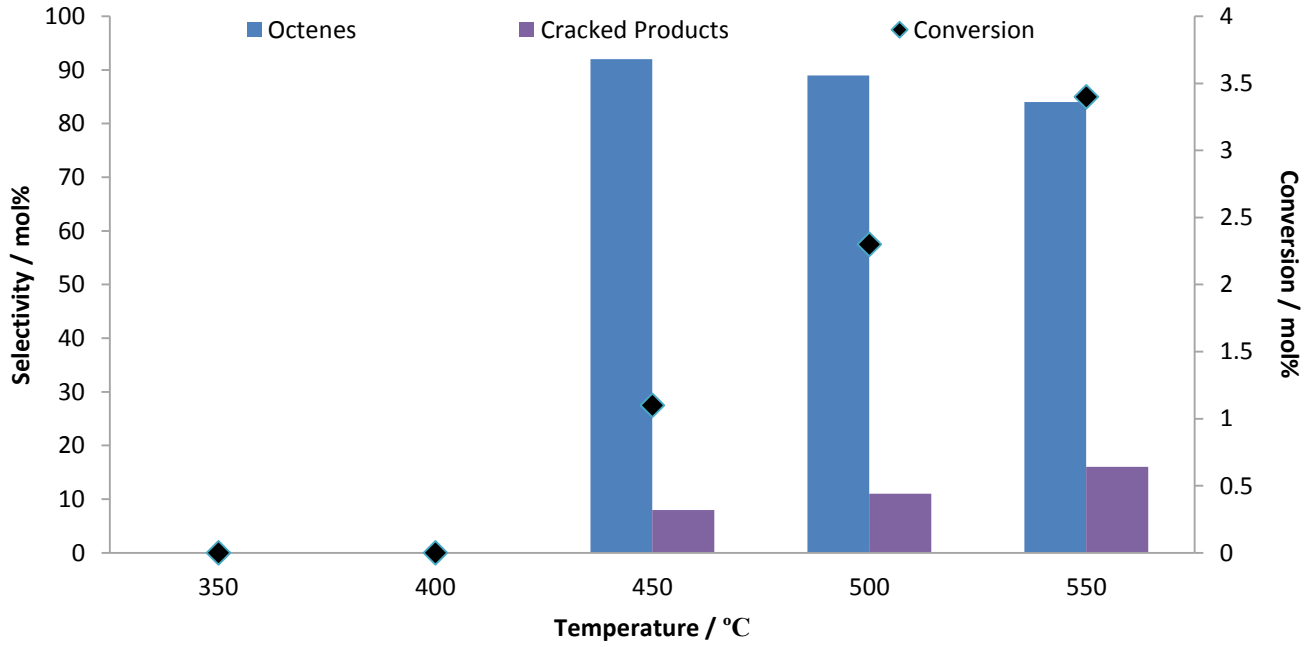

Figure 4.1 Effect of temperature on *n*-octane conversion and product selectivity in the carborundum packed reactor (N_2 gas, GHSV = 4000 h^{-1} and C:O = 8:0).

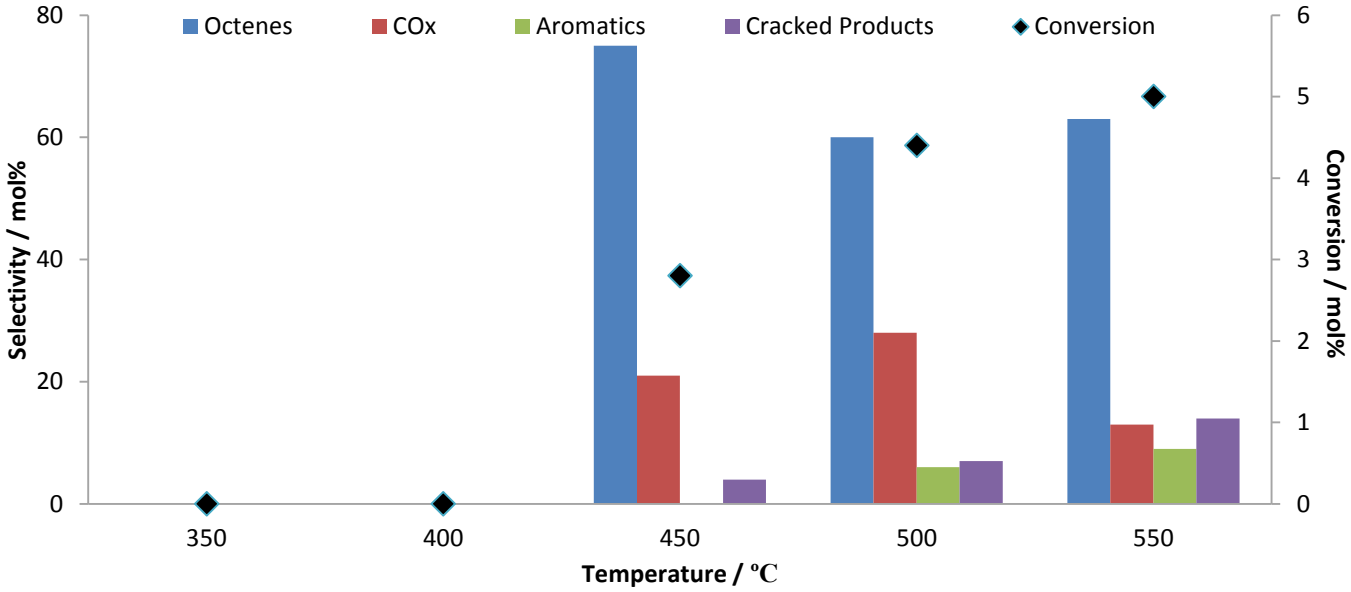

Figure 4.2 Effect of temperature on *n*-octane conversion and product selectivity in carborundum packed reactor (Air and N_2 gas, GHSV = 4000 h^{-1} and C:O = 8:2).

From Figure 4.1, it was observed that under anaerobic conditions, *n*-octane conversion was very low and only occurred from 450 °C to 550 °C. It varied from 1 % to 3 % and is likely due to thermal cracking and dehydrogenation. The primary products, octenes, form from the latter reaction [30]. Cracked products observed were methane, ethane, propane, butane, methanol and acetone. Methanol and acetone formed due to the presence of air in the reactor. These cracked products were not observed in a carborundum packed reactor with no air. These products were made in small quantities and were grouped together. Cracking may take place catalytically, as discussed in Chapter 1, or thermally. Thermal cracking takes place when large product molecules are broken down into smaller molecules at high temperatures via the formation of free radicals. These reactions occur easily with hydrocarbons, in particular long chain hydrocarbons, and the molecules are often broken down into shorter chain hydrocarbons [28].

Upon the introduction of oxygen in the system, again no conversion was observed until 450 °C. After 450 ºC, conversion increased with increasing temperature until a maximum conversion of 5% at 550 °C, as presented in Figure 4.2. The highest selectivity was observed toward the formation of octenes (75 % at 450 °C). The selectivity to octenes then decreased with increasing temperature and the selectivity towards cracked and aromatic products increased. This suggests that octenes are precursors to aromatic

and cracked products, as reported by Dasireddy *et al.* [30]. Carbon oxide selectivity varied with temperature.

4.2. Catalytic testing of the SBA-15 support

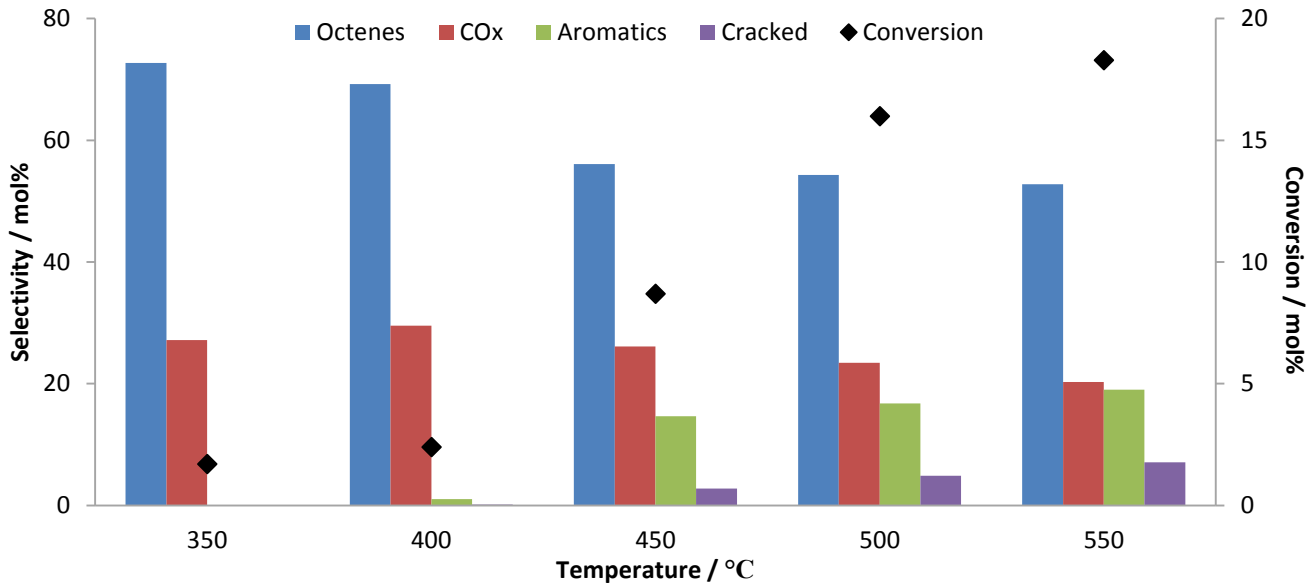

Figure 4.3 Effect of temperature on *n*-octane conversion and product selectivity over SBA-15 (GHSV = 4000 h^{-1}, C:O = 8:2 and pellet particle size = 600 - 1000 µm).

The SBA-15 support showed a considerable increase in conversion of *n*-octane, as shown in Figure 4.3, compared to the blank reaction. As expected, conversion increased with an increase in temperature. Octenes are the dominant products at all temperatures but their selectivity decreased with an increase in temperature. Carbon oxides are also prominent with selectivities varying between 20 and 30 % over the temperature range. As the temperature increased, formation of aromatic and cracked products was observed. This is accompanied by a decrease in selectivity toward octenes, which suggests that octenes are primary reaction products and aromatic and cracked products are formed from them. Aromatic product formation is higher compared to cracked product formation at all temperatures. The SBA-15 support, being silica based, is reported to have basic sites present [116], which speed up the desorption of the octenes from the catalytic surface once they are produced and hence results in the higher selectivity toward octenes [117].

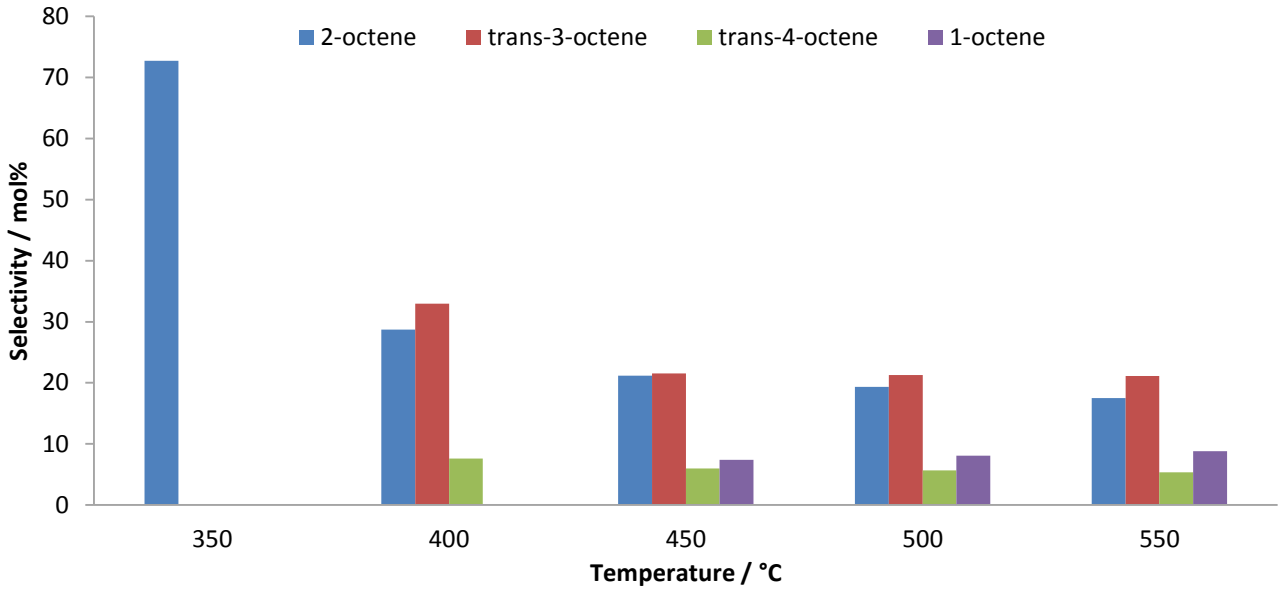

Figure 4.4 Selectivity of octene isomers as a function of temperature over SBA-15 (GHSV = 4000 h^{-1} and C:O = 8:2).

Figure 4.4 gives the distribution of the selectivity of various octene products. It can be observed that at 350 °C, the only octene formed is 2-octene. It is present as a mixture of cis- and trans-2-octene. As the temperature was increased, the selectivity towards 2-octene decreased and trans-3-octene became the dominant product from 400 ºC. The presence of the terminal octene was observed only from 450 ºC onwards and its selectivity showed a slight increase with temperature.

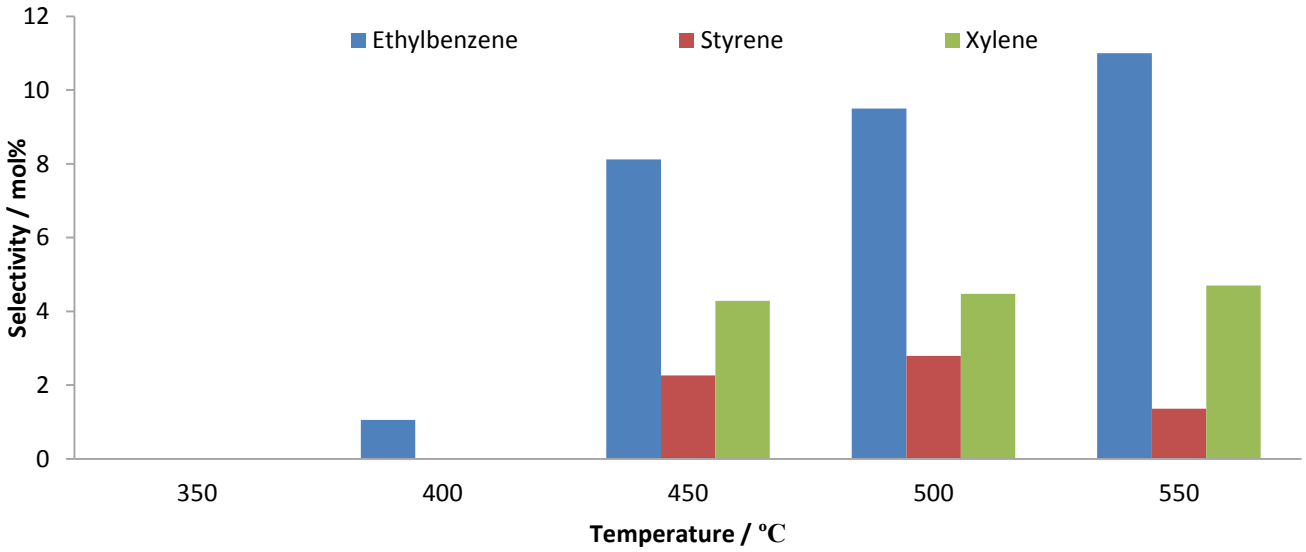

Figure 4.5 Aromatics selectivity as a function of temperature over SBA-15 (GHSV = 4000 h^{-1} and C:O = 8:2).

Ethylbenzene was the only aromatic product observed at 400 °C, as shown in Figure 4.5. Ethylbenzene was also the dominant aromatic product followed by xylene and then styrene at temperatures exceeding 400 ºC. Ortho-xylene was the only isomer of xylene observed. This is because of the C2-C7 cyclisation that occurs, resulting in the ortho-isomer forming. Due to the *n*-octane isomer being linear, this is the only possible isomer of xylene that could have formed during the reaction. If the molecule was branched, other isomers could form, but there was no evidence of isomerisation taking place. Ethylbenzene formed from a C1-C6 cyclisation, which further oxidatively dehydrogenated to form styrene.

4.3. Catalytic testing of the 2W catalyst

The 2W catalyst contains 2 wt% manganese oxide on the outer walls of the SBA-15 support. The catalytic data can be seen in Figure 4.6 and was obtained at a GHSV of 4000 h^{-1} and C:O of 8:2.

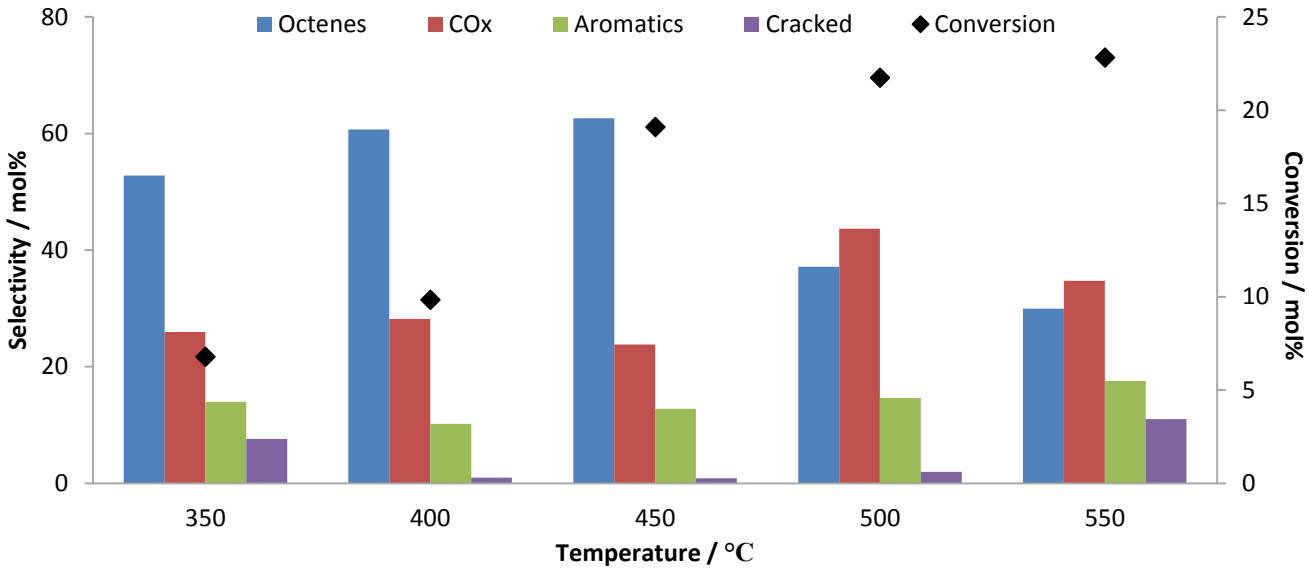

Figure 4.6 Conversion of *n*-octane and selectivity to products as a function of temperature over the 2W catalyst (GHSV = 4000 h^{-1}, C:O = 8:2 and pellet particle size = 600 - 1000 µm).

The catalytic data shown in Figure 4.6 shows that conversion increases with an increase in temperature and the selectivity profile also varies with temperature. At temperatures exceeding 450 ºC, there is very little change in conversion. This can be due to the different phases present at different temperatures of the catalyst, as shown by the *in situ* XRD analysis in Chapter 3. The XRD analysis revealed that at lower reaction temperatures, Mn_3O_4 was the dominant phase of manganese present, while at higher temperatures it was reduced to MnO, with MnO being the dominant phase from 450 °C onwards. It is

expected that MnO is less reactive than Mn_3O_4 because MnO contains Mn^{2+} whereas Mn_3O_4 has a mixture of oxidation states, namely Mn^{3+} and Mn^{2+}. Mn^{3+} is less stable than Mn^{2+}, hence phases containing a mixture of Mn^{3+} and Mn^{2+} will be more reactive than phases containing Mn^{2+}. Tang *et al.* [107] synthesized Mn/SBA-15 catalysts for the epoxidation of trans-stilbene and found that manganese oxides containing a mixture of the 2+ and 3+ oxidation states showed improved activity and superior selectivity toward desired products.

In terms of selectivity, the most selective product group was octenes until 450 °C, with the second most selective products being CO_x. From 450 °C onwards, this was reversed and CO_x became the most selective products, with the octenes being the second most selective products. This gives an indication that the introduction of the metal oxide onto SBA-15 promotes combustion reactions at higher temperatures. The selectivity toward aromatics varied throughout the temperature range. At 350 °C cracked product selectivity was 7.6%, but then decreased to 1% at 400 °C. It then gradually increases with increasing temperature, with a maximum selectivity of 11% at 550 °C. The increase in this selectivity at the highest temperature of the analysis could be due to thermal cracking of the products taking place. The selectivity towards aromatic products is higher than that of cracked products because the aromatisation reaction is favoured by the active sites of the catalyst which are easily accessible on the surface of the support and once they are formed, they are stable. From the trends in Figure 4.7, trans-2-octene was the dominant product, followed by trans-3-octene, whilst 1- octene and trans-4-octene selectivities vary and are significantly lower.

When comparing the 2W catalytic data in Figure 4.6 to the SBA-15 catalytic data in Figure 4.3, there is an increase in the conversion when the metal is present on the support as compared to the support alone, which was expected since the metal oxide enhances the catalytic activity when compared to the support only [30]. The selectivity profiles between SBA-15 and the 2W catalyst also vary throughout the temperature range. At 350 °C and 400 °C the selectivities toward aromatics are 14 and 10 % and to cracked products, 8 and 1% respectively. With the SBA-15, at those temperatures, only little or no selectivity towards the aromatics and cracked products was observed. The products with the highest selectivity are octenes until 450 °C but at higher temperatures the carbon oxides are the most selective products for the 2W catalyst, as opposed to the SBA-15 which has octenes as the most selective product throughout the temperature range. The selectivity toward aromatics and cracked products are similar at 500 and 550 °C for both the SBA-15 and the 2W catalyst, suggesting they may be produced on the

support at these temperatures. When looking at the product distribution of the octenes in Figure 4.7, all four octene isomers are present at all temperatures, unlike with SBA-15 however, trans-2-octene is the dominant isomer at all temperatures for this catalyst. Octenes selectivity decreases with increasing temperature for the SBA-15 (Figure 4.3), while for the 2W catalyst (Figure 4.6), octenes selectivity increases till 450 ºC and thereafter decreases with an increase in temperature. This trend in *n*-octane conversion and product selectivity indicates that the presence of metal oxide on the support does provide enhanced conversion and a varied selectivity profile as opposed to the support alone. This is most likely due to the interaction of the support and the metal oxide with the oxygen in the reactor and the effect each has in activating the oxygen. This will be looked at in more detail in section 4.3.1.3.

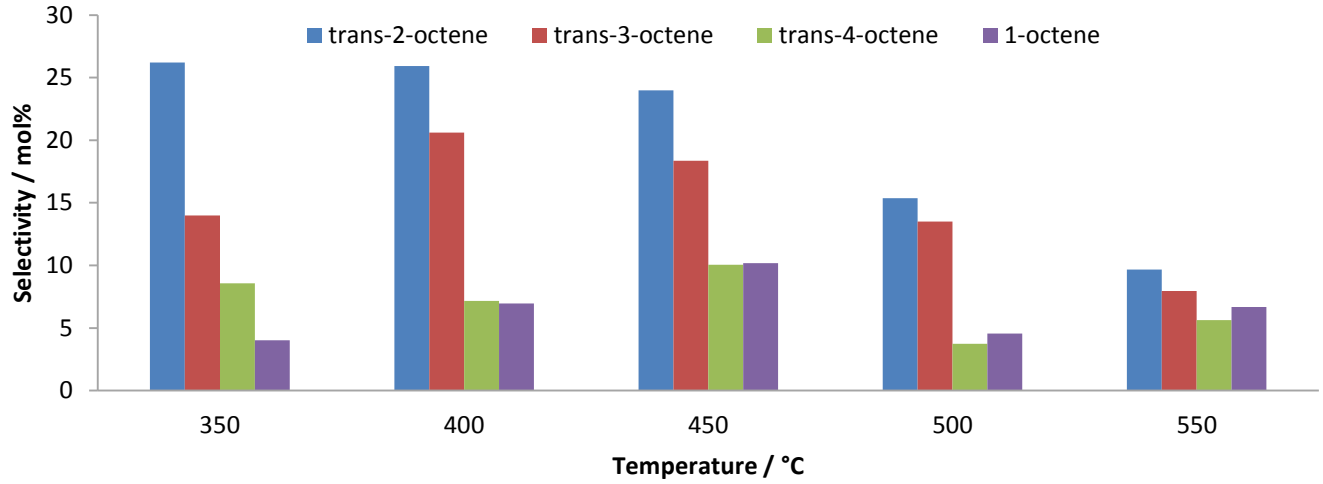

Figure 4.7 Selectivity of octene isomers as a function of temperature over the 2W catalyst (GHSV = 4000 h^{-1} and C:O = 8:2).

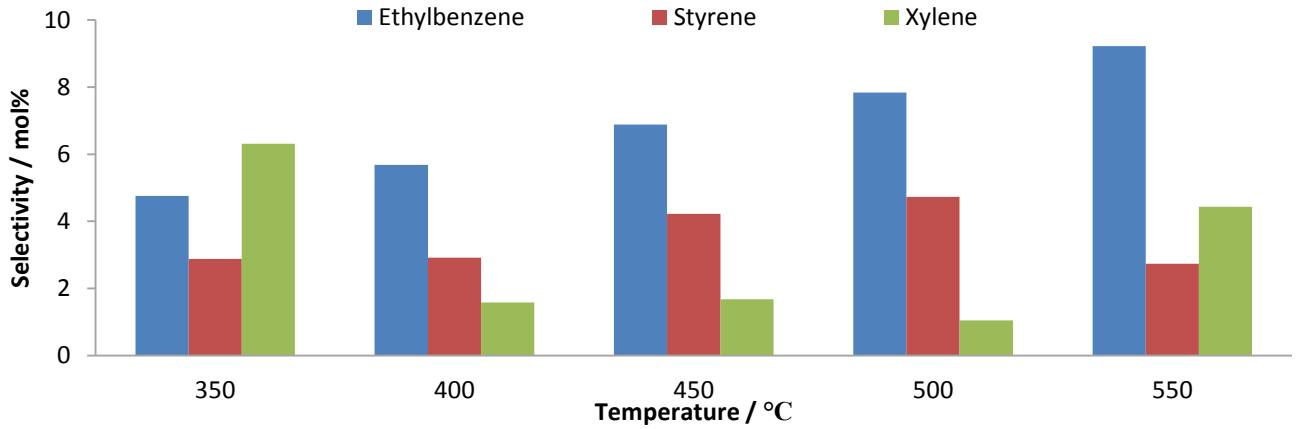

Figure 4.8 Aromatics selectivity as a function of temperature over the 2W catalyst (GHSV = 4000 h^{-1} and C:O = 8:2).

The selectivity towards aromatic products are shown in Figure 4.8 for the 2W catalyst, where ethylbenzene and xylene were observed to form at 350 and 400 °C. These products are not present at these temperatures for the SBA-15 alone. From 400 °C, ethylbenzene was the dominant aromatic produced, followed by styrene and then xylene. This is in contrast to the SBA-15, where xylene selectivity is higher than that of styrene (Figure 4.5).

4.3.1 Determination of optimum reaction conditions

Once an initial idea of catalytic activity was obtained, optimisation of reaction conditions were carried out using the 2W catalyst. Due to the low weight loading of the metal and it being present on the surface of the support, changes in catalytic activity due to varying reaction parameters may be more pronounced with this catalyst. The factors that were investigated included pellet particle size, carbon to oxygen ratio and gas hourly space velocity.

4.3.1.1 The role of pellet particle size

Catalyst particle size was varied in order to determine whether activity of the catalyst was affected by internal diffusion within the catalyst bed itself. For this experiment, a particle size of 300 – 600 μm was used in contrast to the 600 – 1000 μm used previously, while all other reaction parameters were kept constant. By using smaller pellets, more channels or pathways were created inside the catalyst bed to promote inter-particle diffusion. The increase in the number of these internal pathways can lead to varying catalytic activity if the reaction was controlled by mass transfer as a result of internal diffusion of the feed within the catalyst bed [118]. The results obtained are shown in Table 4.1

Table 4.1 Conversion of *n*-octane and selectivities to products for 300 – 600 μm pellets.

Temperature / °C	**350**	**400**	**450**	**500**	**550**
Conversion / mol %	6.8	9.7	19.1	21.6	22.9
Product	**Selectivity / mol%**				
Octenes	51.1	58.1	63.4	38.5	32.0
Aromatics	14.1	11.7	11.9	16.2	18.1
Cracked Products	7.8	1.5	1.2	3.2	11.3
CO_x	27.0	28.7	23.5	42.1	38.6

Analysing the results of the catalysis shown in Table 4.1, the conversion values are within 1% and the selectivity values within 5% of those of the higher pellet size. It can be said that the lower pellet size does not result in a change in catalytic activity. This means that internal diffusion does not affect the catalytic system and the system probably has no kinetic limitations within the catalyst bed itself. It might be controlled by the rate at which the *n*-octane adsorbs and product desorbs from the catalyst surface rather than by internal diffusion [118]. Pellet sizes of 600 – 1000 µm were chosen for catalytic testing as the larger pellets ran a lower risk of back-pressure developing in the reactor.

4.3.1.2 The influence of varying space velocities

The space velocity was investigated to establish what influence this would have on the rates as well as on selectivity. To explore the function of GHSV for the system, GHSV's of 2000 h^{-1} and 6000 h^{-1} were looked at, at all 5 temperatures of interest as with the 4000 h^{-1} run. Also, GHSV's of 8000 h^{-1} and 10000 h^{-1} were studied at 450 ºC. The carbon to oxygen ratio was kept constant throughout these experiments at C:O = 8:2.

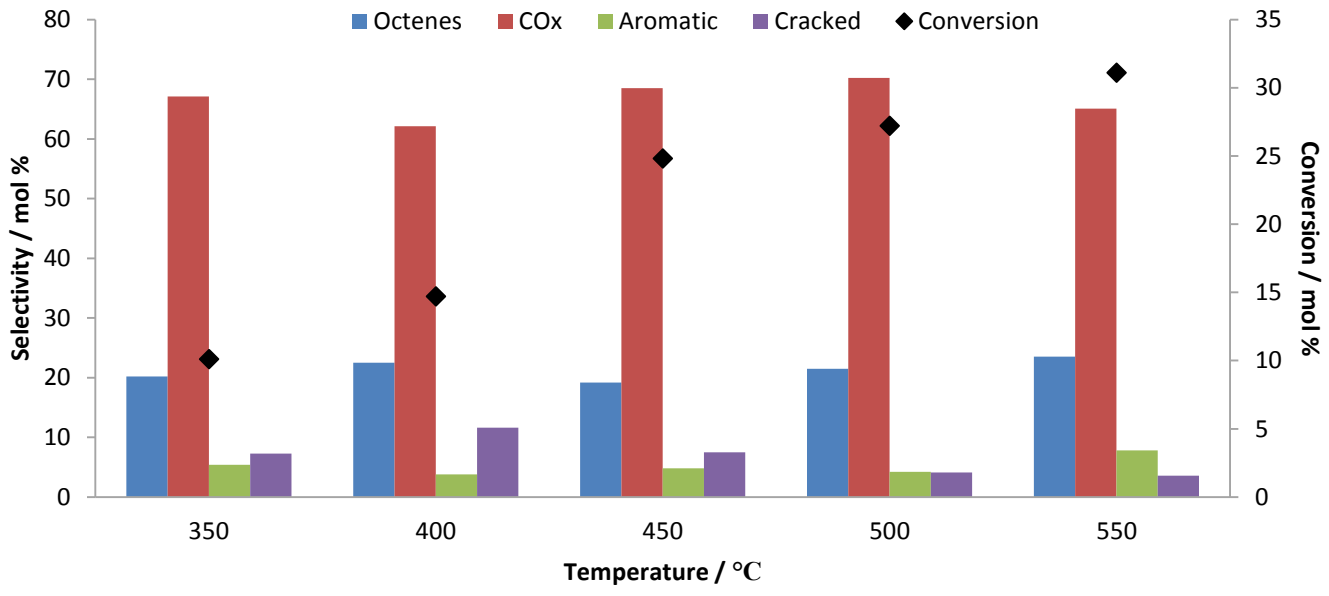

Figure 4.9 Conversion of *n*-octane and selectivity to products at different temperatures over the 2W catalyst (GHSV = 2000 h^{-1} and C:O = 8:2).

Figure 4.9 displays the conversion and selectivity profile for a GHSV of 2000 h^{-1}. Conversions of *n*-octane ranged from a minimum of 10 % at 350 ºC to a maximum of 31 % at 550 ºC. The dominant product group at all temperatures is CO_x, with a maximum selectivity of 70 % at 500 ºC. The product group with the second highest selectivity is octenes, followed by cracked products and then aromatics. Aromatic and cracked product formation varies with temperature.

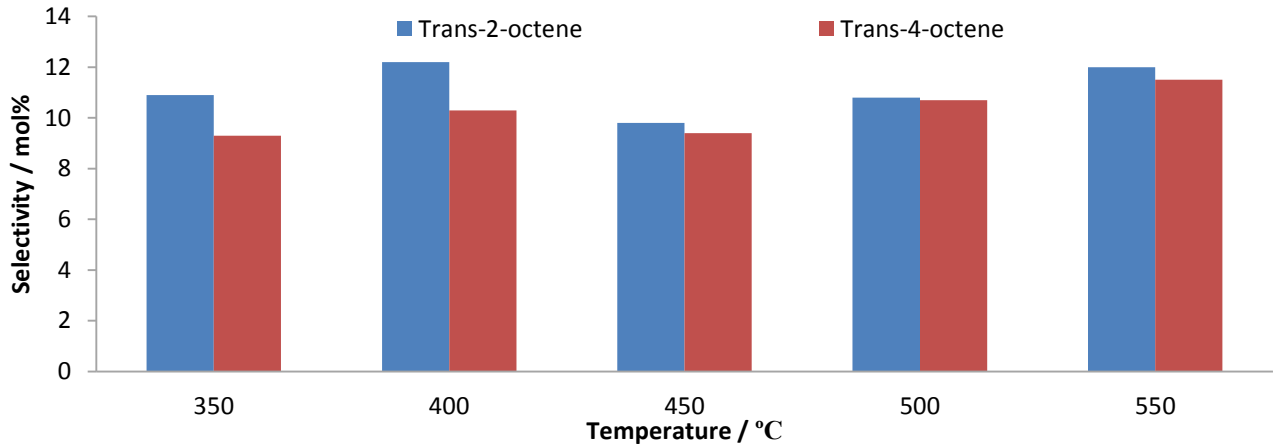

Figure 4.10 Selectivity towards octene isomers at different temperatures over the 2W catalyst (GHSV = 2000 h^{-1} and C:O = 8:2).

Of the octene isomers present in the product mixture, only trans-2-octene and trans-4-octene were observed to form, with trans-2-octene being the most selective isomer throughout the temperature range. The varying selectivities of the 2 and 4 isomers with increasing temperature are shown in Figure 4.10.

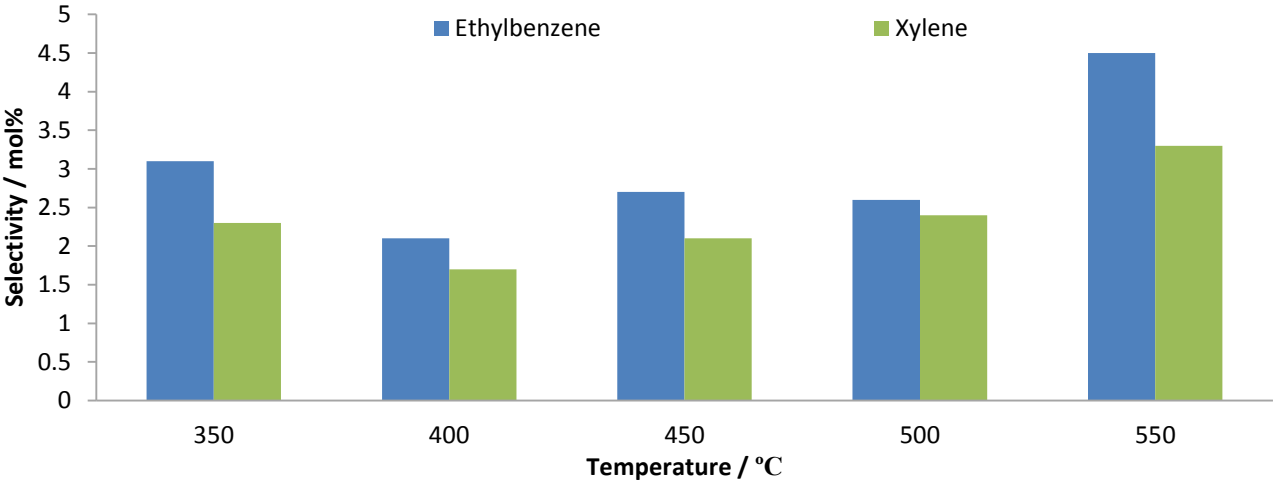

Figure 4.11 Aromatics selectivity at different temperatures over the 2W catalyst (GHSV = 2000 h^{-1} and C:O = 8:2.

Ethylbenzene and xylene are the only 2 aromatic products formed at this space velocity, as seen in Figure 4.11, with ethylbenzene being the most selective aromatic product at all temperatures. Styrene was not observed, suggesting decomposition of styrene with the higher contact time, as it is known that the monomer of styrene is not stable [28].

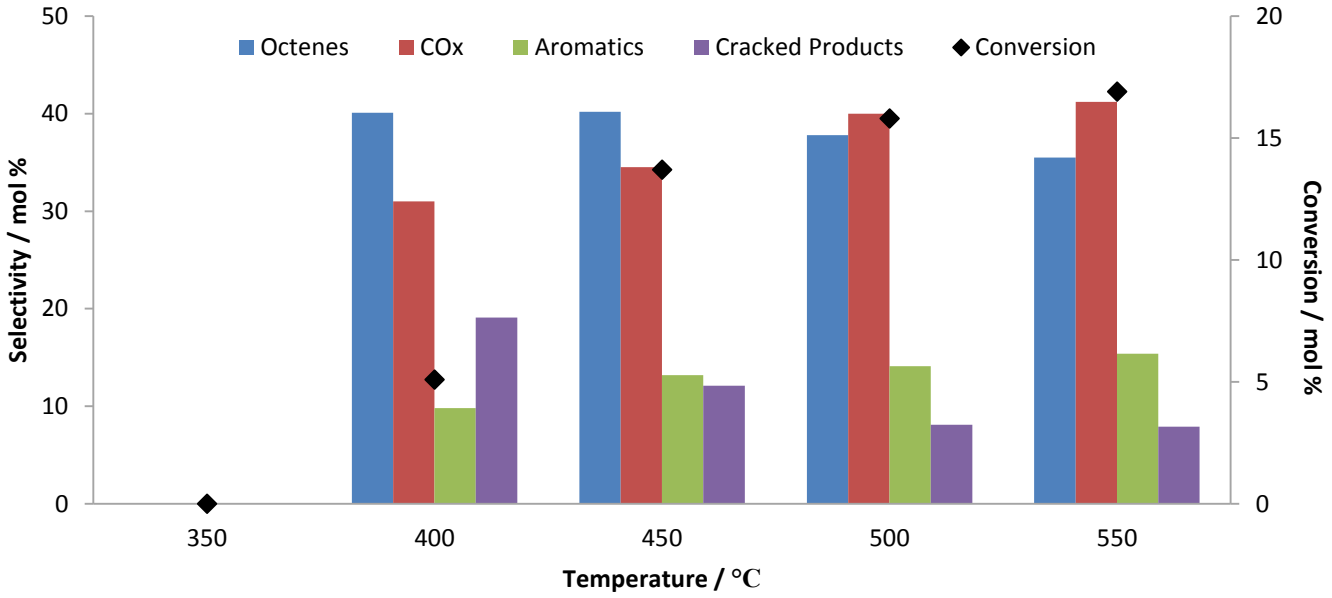

Figure 4.12 Conversion of *n*-octane and selectivity to products at different temperatures over the 2W catalyst (GHSV = 6000 h^{-1} and C:O = 8:2).

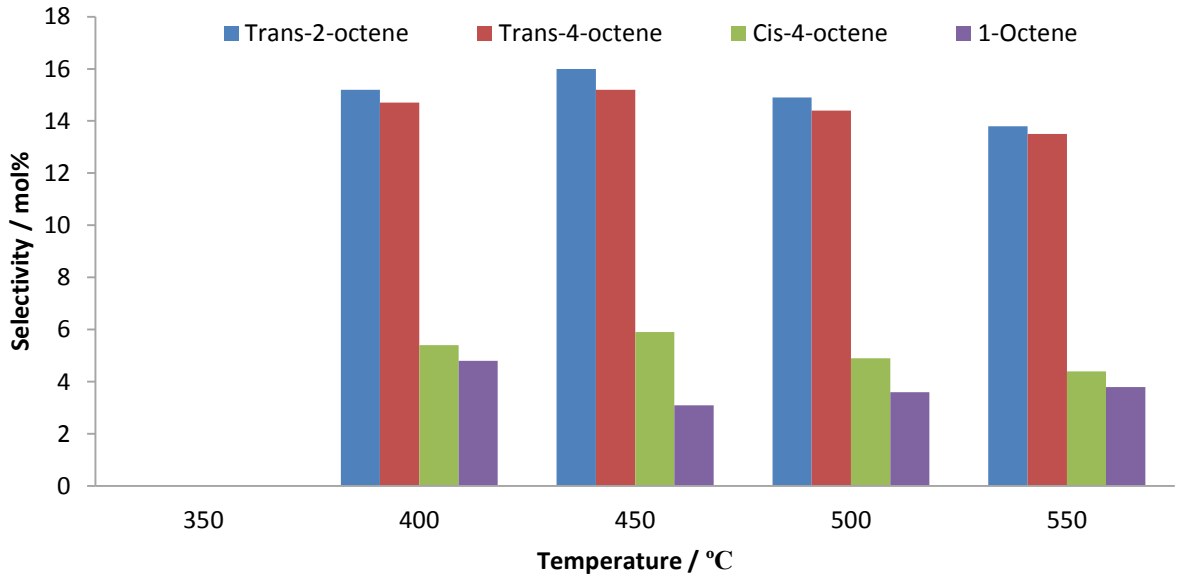

Figure 4.13 Selectivity towards octene isomers at different temperatures over the 2W catalyst (GHSV = 6000 h^{-1} and C:O = 8:2).

A GHSV of 6000 h^{-1} was investigated and the results are summarized in Figure 4.12 to Figure 4.14. At this GHSV, conversion of *n*-octane begins from 400 ºC at 5 % and reaches a maximum of 17 % at 550 ºC. In terms of product selectivity, at 400 and 450 ºC, the product group with the highest selectivity is octenes, followed by CO_x products. This is reversed at the higher temperatures, with CO_x products having the highest selectivity at 500 and 550 ºC and octenes being the second most selective product group.

In terms of aromatic and cracked products, they are the third and 4th most selective product groups. Cracked product formation is higher than aromatic product formation at 400 ºC, but from 450 ºC onwards, aromatic product formation is higher than that of cracked product formation. Selectivity toward aromatic products increased and selectivity toward cracked products decreased with temperature (Figure 4.12).

Trans-2-octene is the dominant octene isomer formed at all temperatures, followed by trans-4-octene, cis-4-octene and lastly 1-octene (Figure 4.13). Ethylbenzene is the aromatic product with the highest selectivity, followed by xylene and lastly styrene (Figure 4.14).

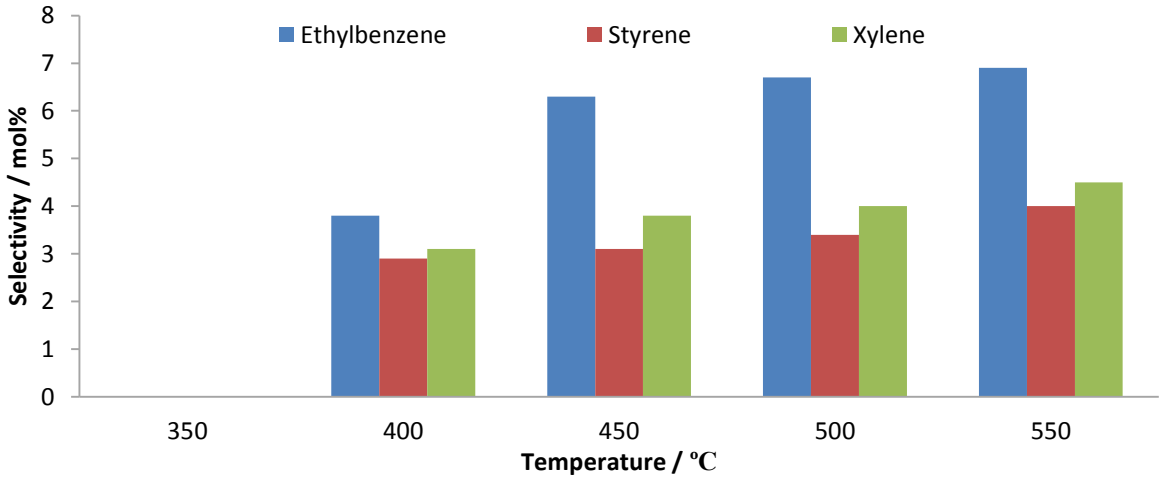

Figure 4.14 Aromatics selectivity at different temperatures over the 2W catalyst (GHSV = 6000 h^{-1} and C:O = 8:2).

The conversion values of the 8000 h^{-1} and 10000 h^{-1} runs are 9% and 4%, respectively, as shown in Figure 4.15. The octenes and aromatics selectivities are shown in Figures 4.15 and 4.16 respectively for these GHSVs. At both these GHSVs, the dominant product group are octenes, followed by CO_x

products. Aromatic products have the 3rd highest selectivity, with cracked products being the least selective of the major product groups. At both GHSVs, trans-2-octene is the octene isomer with the highest selectivity, followed by trans-4-octene, cis-4-octene and 1-octene respectively. Styrene is the only aromatic compound observed at these higher GHSVs.

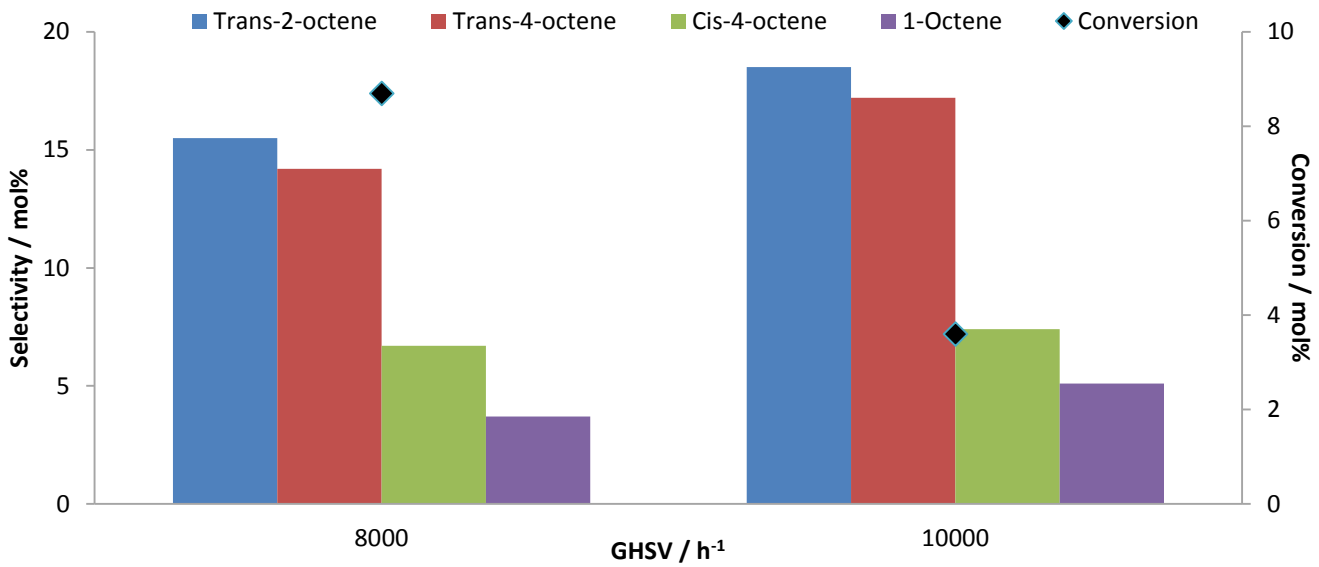

Figure 4.15 Conversion of *n*-octane and selectivity of octene isomers over the 2W catalyst (Temperature = 450 ºC and C:O = 8:2 at 8000 h^{-1} and 10000 h^{-1} GHSV).

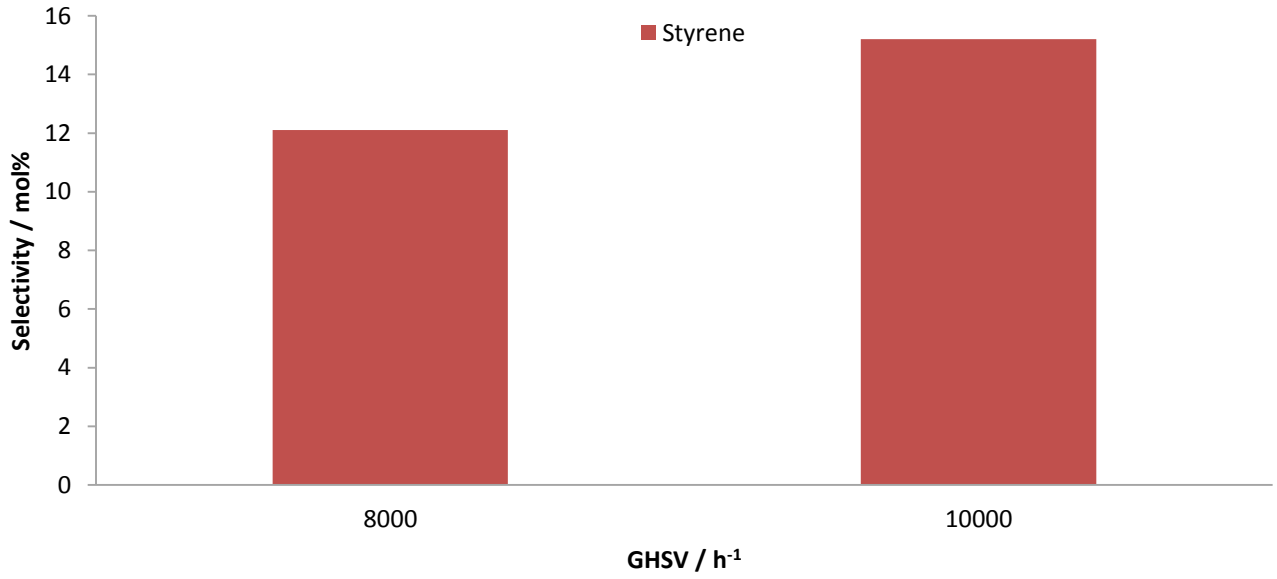

Figure 4.16 Aromatics selectivity over the 2W catalyst (Temperature = 450 ºC and C:O = 8:2 at 8000 h^{-1} and 10000 h^{-1} GHSV).

Figure 4.17 shows a comparison of all five GHSV's and the conversion of *n*-octane decreases with increasing GHSV. This is because with increasing GHSV, there is a shorter residence or contact time between the feed and the catalyst, resulting in a lower conversion of the feed. This is the reason that highest conversion was noted for the lowest GHSV (25% for 2000 h^{-1}) and lowest conversion was observed for the highest GHSV (4% at 10000 h^{-1}). This trend can be observed clearly in Figure 4.17 and the comparison of conversion with contact times can be seen in Table 4.2. Contact time was calculated from the inverse of GHSV.

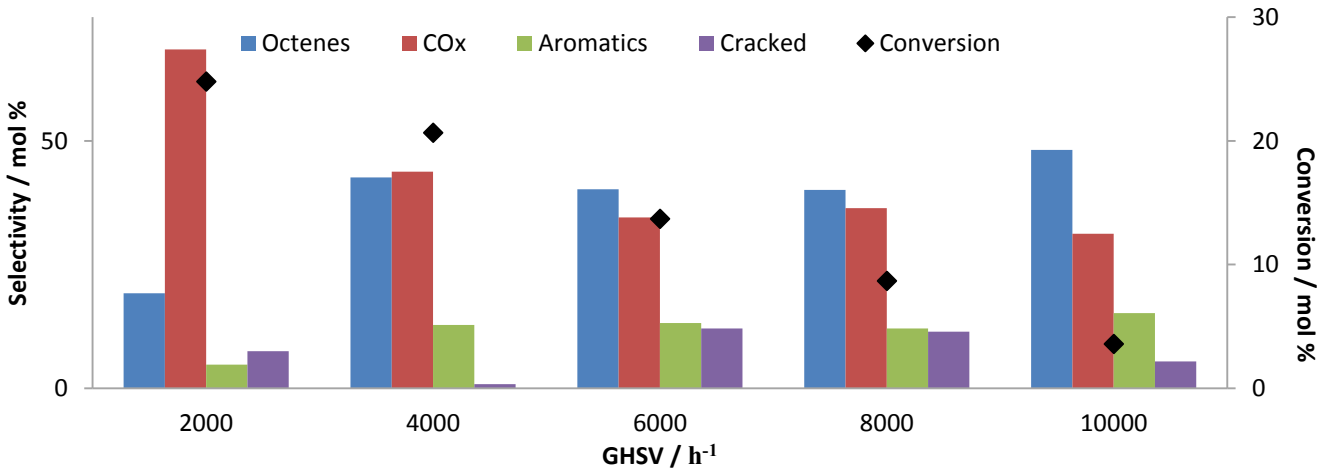

Figure 4.17 Conversion of *n*-octane and selectivity to products with varying GHSV over the 2W catalyst (Temperature = 450 ºC and C:O = 8:2).

Table 4.2 Conversion of *n*-octane, selectivities toward desired products and contact time of this feed with varying GHSV's at 450 °C.

GHSV/h^{-1}	Contact time/s	Conversion/mol%	Selectivity towards desired products/mol%
2000	1.8	25	26.7
4000	0.9	21	75.3
6000	0.6	14	53.4
8000	0.45	9	52.2
10000	0.36	4	63.4

There is a change in product selectivity as the contact time increases. Increased contact time means there is a greater chance of secondary oxidation taking place [29]. This implies that primary reaction products will decrease with contact time and secondary oxidation products increase. Looking at the data in Figure

4.17 and Table 4.2, desired products selectivity (octenes and aromatics) increased with decreasing contact time and all other product groups' selectivities decreased. CO_x selectivity was the highest with the highest contact time as they are the final oxidation product and formation would be favoured with increased contact time. Cracked product formation was higher than that of aromatic product formation with the highest contact time, but with a contact time of 0.9s or lower, cracked product formation is higher than aromatic product formation.

The desired products shown in Table 4.2 for the reaction are octenes and aromatic products and the individual isomers for each of these products groups vary with the contact time. Trans-2-octene is the octene isomer with the highest selectivity at all contact times and that of ethylbenzene is highest for the aromatics. As contact time decreases, the other octene isomers, namely trans-4-octene, cis-4-octene and 1-octene, begin to form and styrene formation was also observed. Not all octene isomers were observed at all the GHSVs investigated as once formed, they may subsequently cyclize or decompose depending on the reaction conditions. The selectivity towards aromatics increased, while the selectivity towards cracked and carbon oxides decreased with decreased contact time. This suggests competitive reaction pathways from octenes to form these products and this behaviour was observed with decreasing contact time. Due to these competitive pathways, individual reaction schemes cannot be identified with this information alone. Thus the data was compared with the results obtained from varying the carbon to oxygen ratio in order to propose an overall reaction mechanism for this system as discussed later on in this chapter.

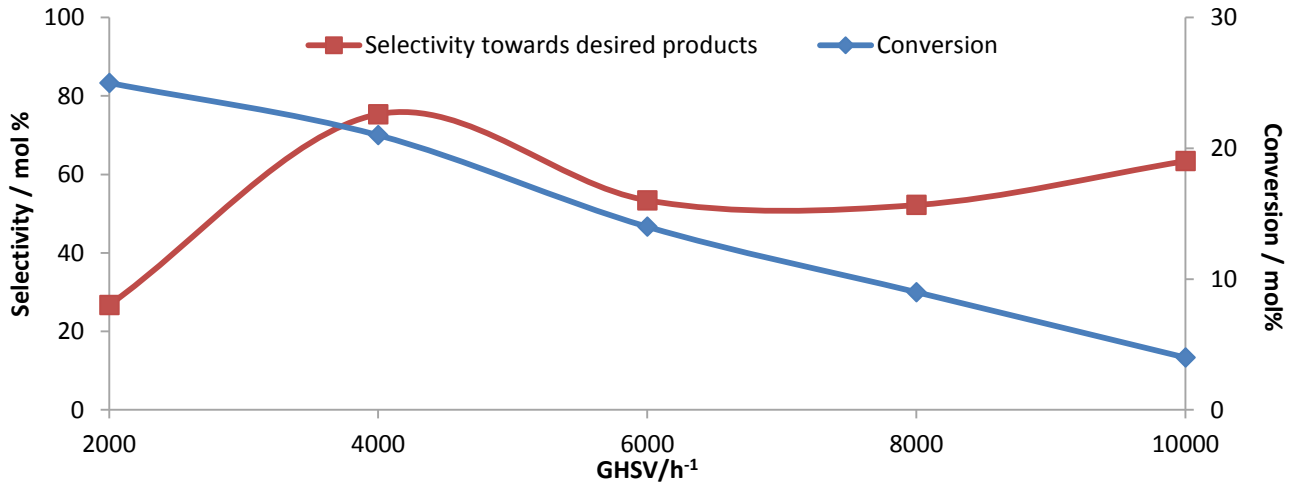

Figure 4.18 Conversion of *n*-octane and selectivities toward desired products with varied GHSV's at 450 ºC.

Based on the behaviour of the catalyst with respect to space velocity, as shown in Figure 4.18, the conversion of *n*-octane and selectivity toward desired products was noted to be ideal at a GHSV of 4000 h^{-1} and this was deemed the optimum GHSV for the catalysts being tested. This was based on the higher conversion at 4000 h^{-1} when comparing higher GHSVs, except for 2000 h^{-1}.However, a higher selectivity toward desired products was observed at 4000 h^{-1} as compared to 2000 h^{-1} and hence all subsequent catalytic work thus was carried out at a GHSV of 4000 h^{-1}.

4.3.1.3 The effect of changing carbon to oxygen ratio

To determine the influence of carbon to oxygen ratio, the carbon to oxygen ratios were varied from 8:0 to 8:4 while all other reaction parameters were kept constant. These atomic ratios represent the number of carbon atoms present for a reaction, which is based on the amount of *n*-octane, and compared to the number of oxygen atoms present. These ratios were chosen to firstly investigate the catalytic activity under anaerobic conditions (C:O = 8:0), and then going on to higher ratios, for instance where there is one oxygen molecule for every molecule of *n*-octane present (C:O = 8:2) and lastly, a rich oxidative environment was looked at, where two oxygen molecules were present for every molecule of *n*-octane (C:O = 8:4). Firstly, oxygen deficient conditions were looked at and before the 2W catalyst was tested, SBA-15 was tested to find out the influence of the support under anaerobic conditions, and the results are shown in Figure 4.19.

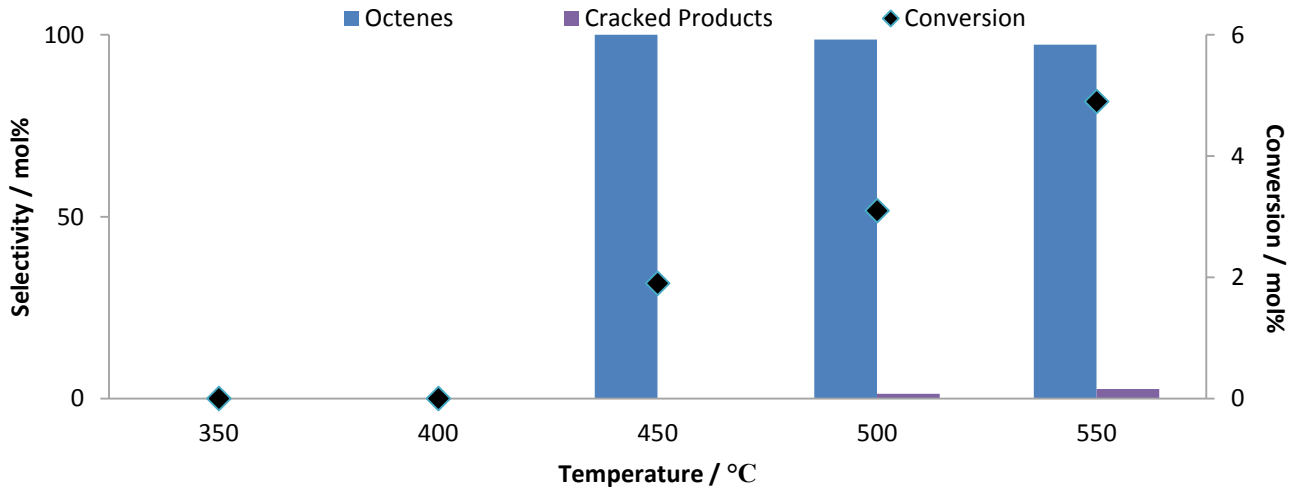

Figure 4.19 Conversion of *n*-octane and selectivity towards products as a function of temperature over the SBA-15 (GHSV = 4000 h^{-1} and C:O = 8:0).

SBA-15 showed conversion of *n*-octane from 450 ºC upwards and this increased with increasing temperature. Conversion ranged from 2 % at 450 ºC to 5 % at 550 ºC. These conversion values are slightly higher than the blank reactor conversions under the same conditions shown earlier (Figure 4.1), which indicates that they are in part a result of the support itself. Octenes were the dominant product groups at all temperatures, with close to 100 % selectivity at 450 ºC.

The selectivity toward octenes then decreased with increasing temperature as cracked products are formed at 500 and 550 ºC. The dominant octene isomers, shown in Figure 4.20, are trans-2-octene and trans-4 octene with trans-2-octene having the higher selectivity at all temperatures, with the highest being 51.2 % and 48.8 % respectively at 450 °C.

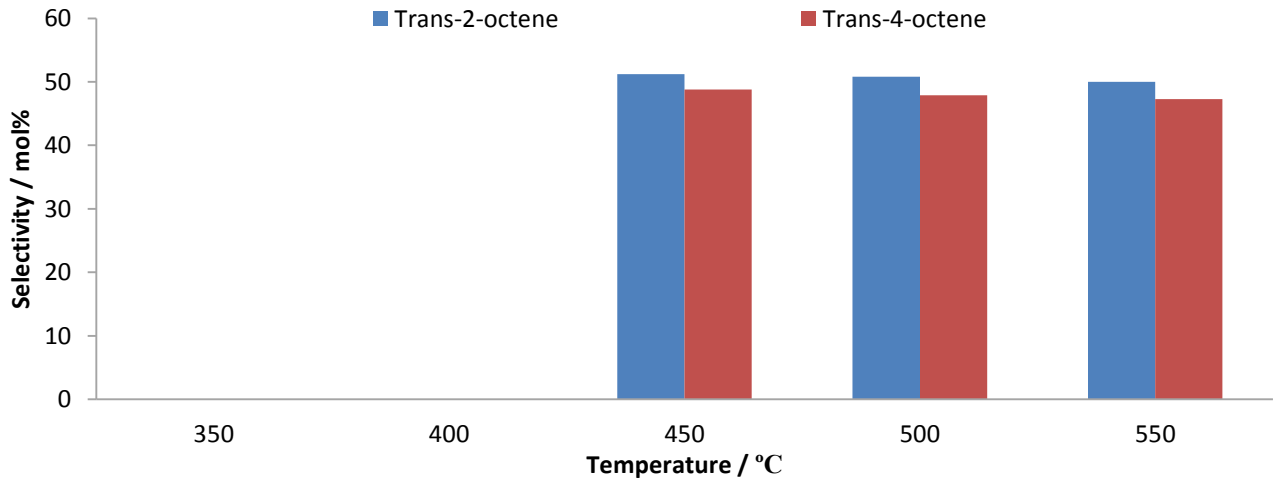

Figure 4.20 Selectivity of octene isomers as a function of temperature over the SBA-15 support (GHSV = 4000 h^{-1} and C:O = 8:0).

Steinke *et al.* [120] proposed a silica radical forming by breaking of Si-O bonds during the mechanical treatment of quartz. The silica radical may be forming on this SBA-15 support and is responsible for the formation of the octene isomers by the following reactions:

$$SiO\cdot + HC_8H_{17} \rightarrow SiOH + \cdot C_8H_{17}$$

$$SiO\cdot + \cdot C_8H_{17} \rightarrow SiOH + C_8H_{16}$$

Upon comparison of the results obtained from the SBA-15 tested at a C:O ratio of 8:2 to the results of the run in an anaerobic environment, there was a noticeable increase in conversion with the introduction of oxygen for the reaction. The product profile is also very different, as with no oxygen present the

primary products obtained are octenes and with an increase in oxygen content, secondary products such as carbon oxides, aromatic and cracked products begin to form. This suggests that under anaerobic conditions, the support favours the formation of octenes and once oxygen is introduced into the system, the octenes are oxidised to form secondary products. This oxidative dehydrogenation reaction is possible due to the hydroxyl species present on the surface of the SBA-15 support [76]. Optimisation of C:O ratios was then carried out with the 2W catalyst, with C:O = 8:0 being looked at first and then the ratios with higher oxygen content following in order.

The conversion of *n*-octane for the 2W catalyst tested under anaerobic conditions ranged from 1 % at 400 ºC to a maximum of 6 % at 550 ºC, as shown in Figure 4.21. These conversion values are higher than those of the blank reactor (Figure 4.1) and the SBA-15 (Figure 4.19) support tested under the same conditions. This indicates that the higher catalytic activity is a direct result of the catalyst, namely 2 wt% manganese oxide supported on SBA-15 and not from the blank reactor and support only. Throughout the temperature range, octenes are the dominant products of the reaction, with cracked products being second most selective, but having a very low selectivity when compared to octenes. Aromatic products only formed at 550ºC. The octene isomers noted were trans-2-octene and trans-4-octene, with trans-2-octene having a higher selectivity at all temperatures as seen in Figure 4.22. Ethylbenzene was the only aromatic product observed and only at 550ºC.

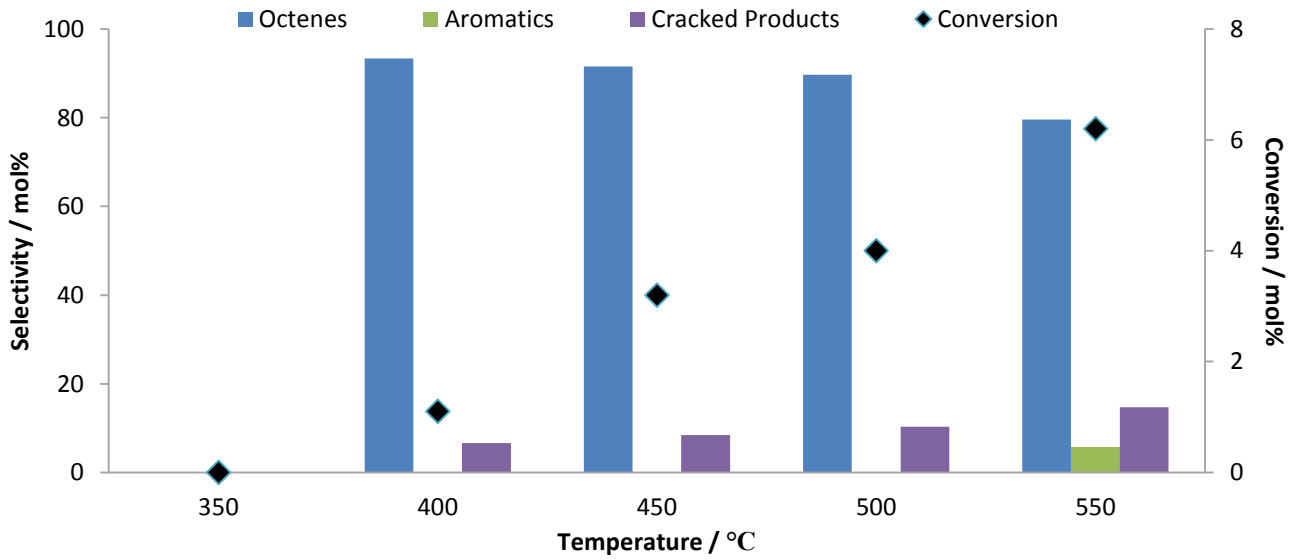

Figure 4.21 Conversion of *n*-octane and selectivity towards products as a function of temperature over the 2W (GHSV = 4000 h^{-1} GHSV and C:O = 8:0).

Comparing the selectivity profile of the 2W catalyst with that of SBA-15 under anaerobic conditions, both catalyst and support gave octenes as the major product group, with trans-2-octene and trans-4-octene being formed. There is minimal cracked product formation for both the support and the catalyst but the noted difference was that the catalyst was active from 400 ºC and ethylbenzene began to form at 550 ºC.

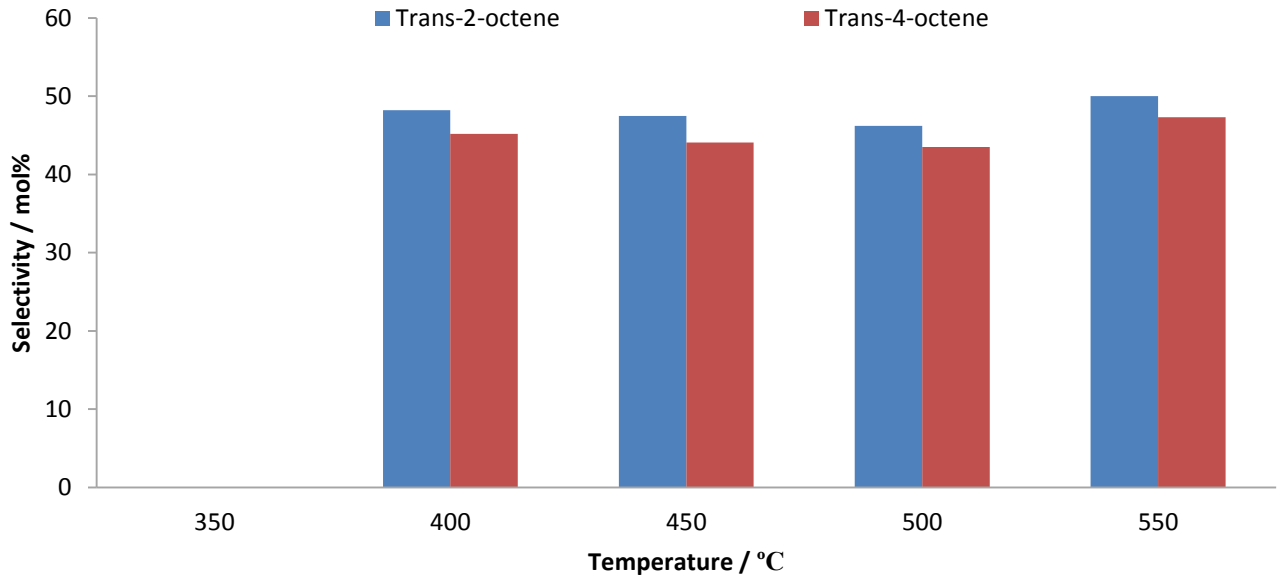

Figure 4.22 Selectivity of octene isomers as a function of temperature over the 2W catalyst (GHSV = 4000 h^{-1} GHSV and C:O = 8:0).

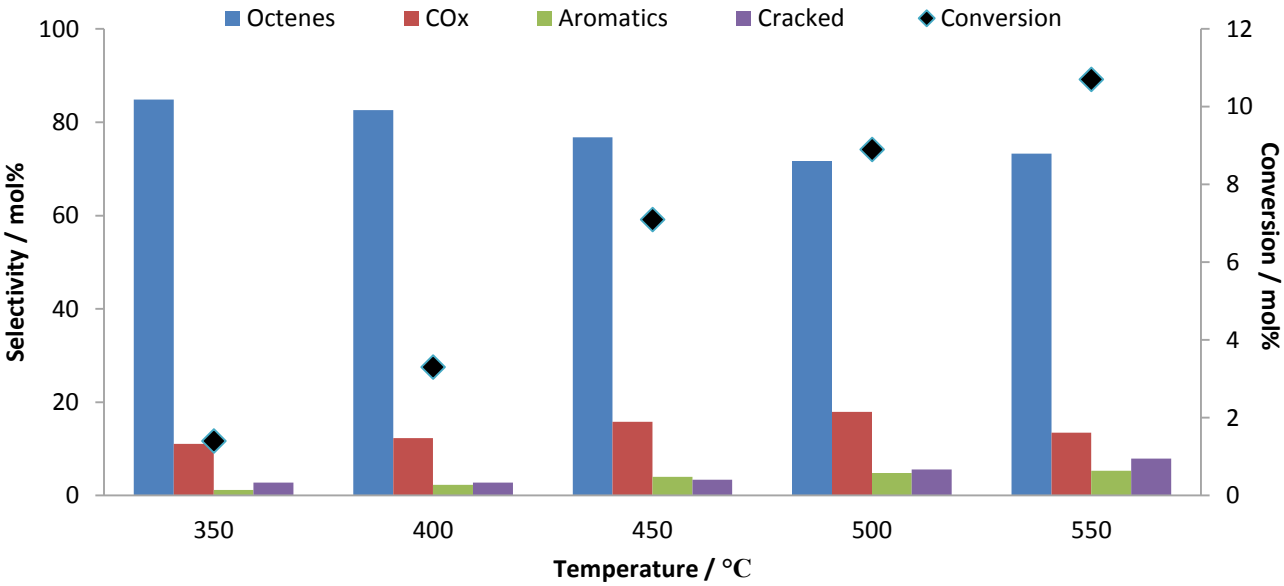

Figure 4.23 Conversion of *n*-octane and selectivity towards products as a function of temperature over the 2W catalyst (GHSV = 4000 h^{-1} and C:O = 8:1).

The enhanced conversion and higher selectivity toward aromatics of the 2W catalyst was also noted when comparing the results of the 2W catalyst (Figure 4.6) and SBA-15 support (Figure 4.3) at a C:O ratio of 8:2. The role of manganese oxide for this system was assessed by comparing the results of all the C:O ratios analyzed.

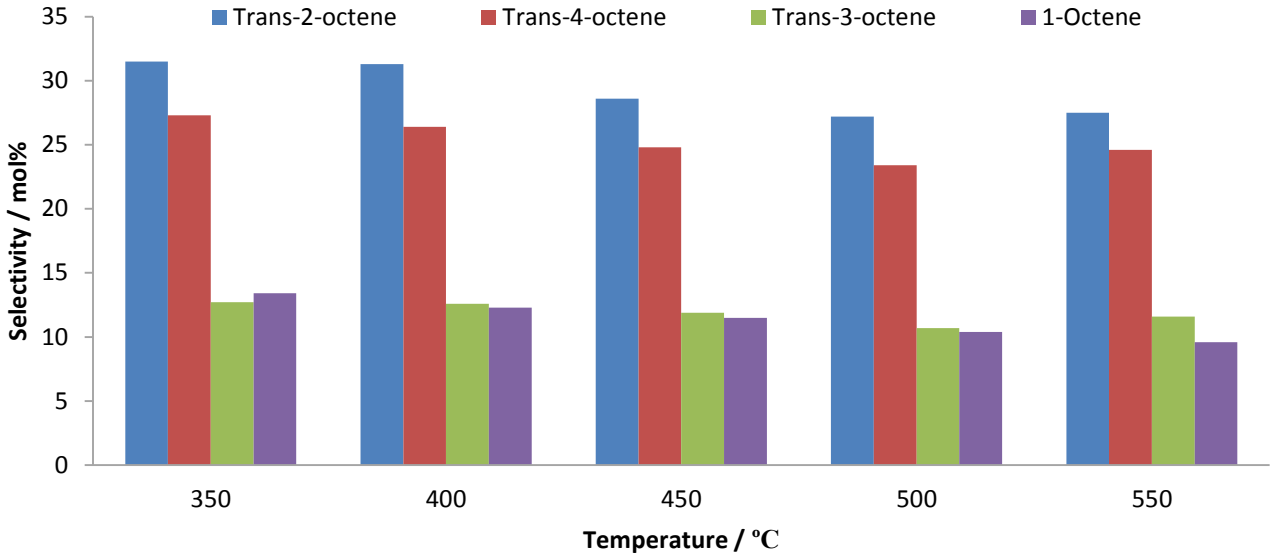

Figure 4.24 Selectivity of octene isomers as a function of temperature over the 2W catalyst (GHSV = 4000 h^{-1} and C:O = 8:1).

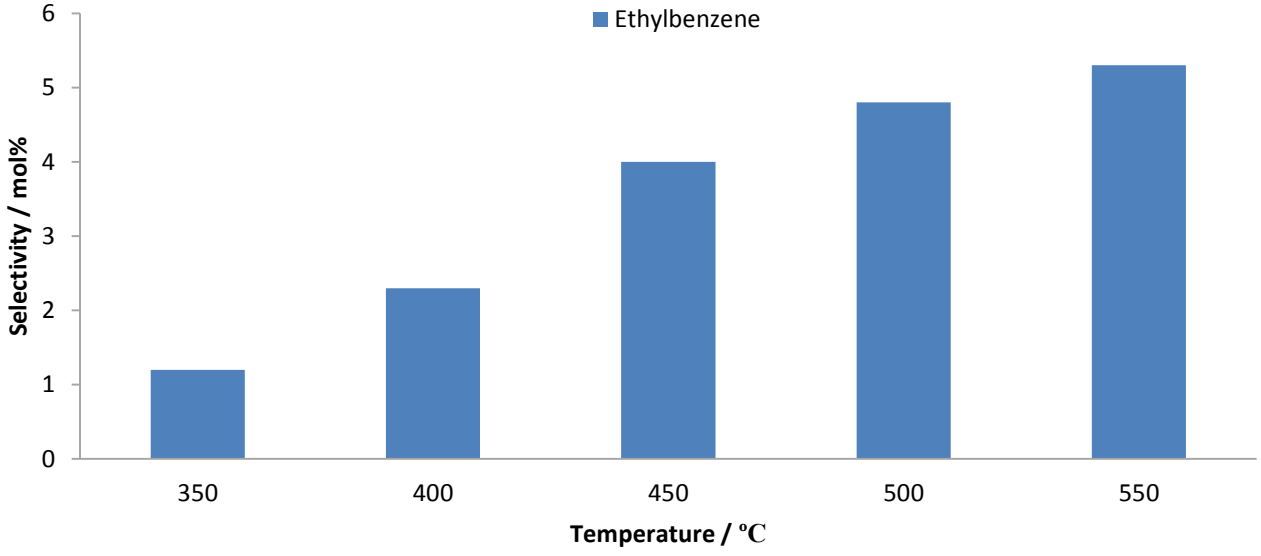

Figure 4.25 Ethylbenzene as a function of temperature over the 2W catalyst (GHSV = 4000 h^{-1} and C:O = 8:1).

The results for a C:O ratio of 8:1 are shown in Figure 4.23 and show that conversion of *n*-octane increases as a function of temperature, ranging from 1-11 % within the temperature range. The dominant products formed from the reaction are octenes, with a maximum selectivity of 85 % at 350 °C. The product group with the second highest selectivity is carbon oxides, followed by cracked and aromatic products. For this reaction, the selectivity towards octene decreases with temperature as selectivity towards all other product groups increase.

The dominant octene isomers are trans-2-octene and trans-4-octene respectively, followed by varying amounts of 1-octene and trans-3-octene shown in Figure 4.24. Ethylbenzene was the only aromatic compound found for the reaction and its selectivity increases with increasing temperature as shown in Figure 4.25.

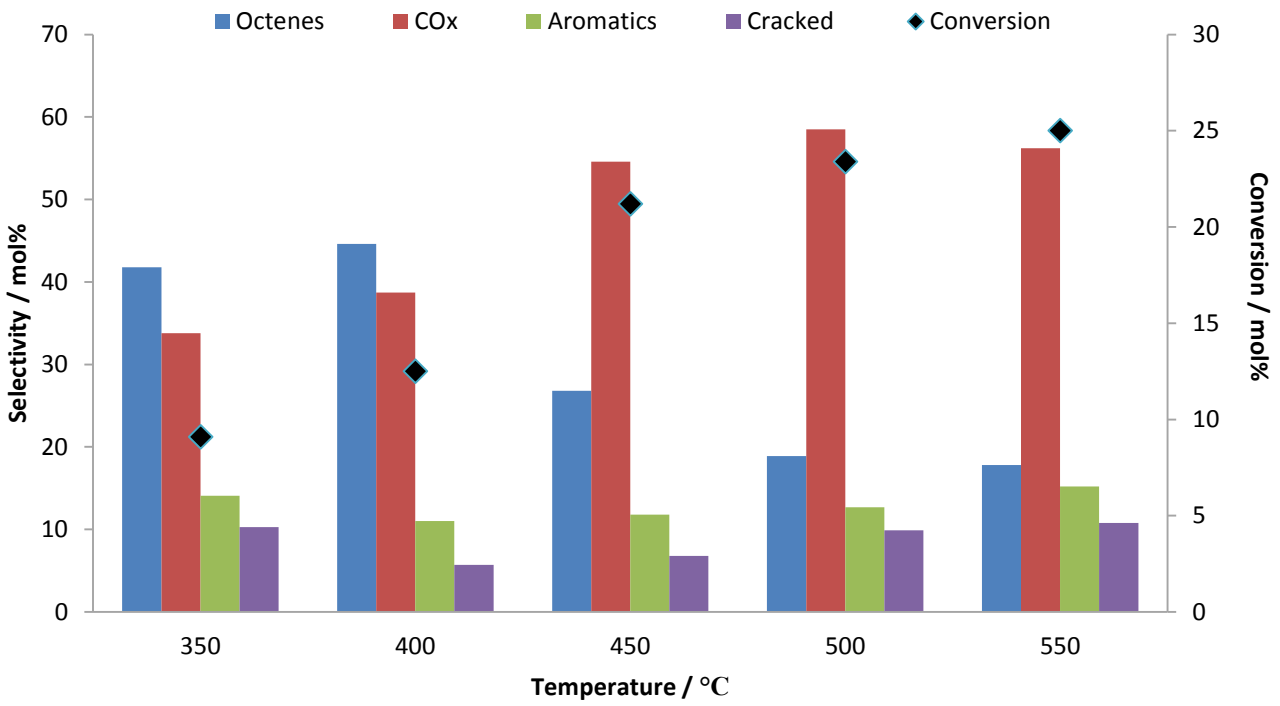

Figure 4.26 Conversion of *n*-octane and selectivity towards products as a function of temperature over the 2W catalyst (GHSV = 4000 h^{-1} and C:O = 8:3).

The results for a carbon to oxygen ratio of 8:3 are shown in Figure 4.26.The conversion of *n*-octane ranges from 9to 25% and increases with increasing temperature. The dominant products are octenes at 350 and 400 °C, with carbon oxides being the second most selective product group. This is reversed from 450 °C onwards, with carbon oxide selectivity being much higher than that of any other product

group. Aromatic and cracked product selectivities vary with temperature, while aromatic product selectivity is higher than cracked product selectivity at all temperatures.

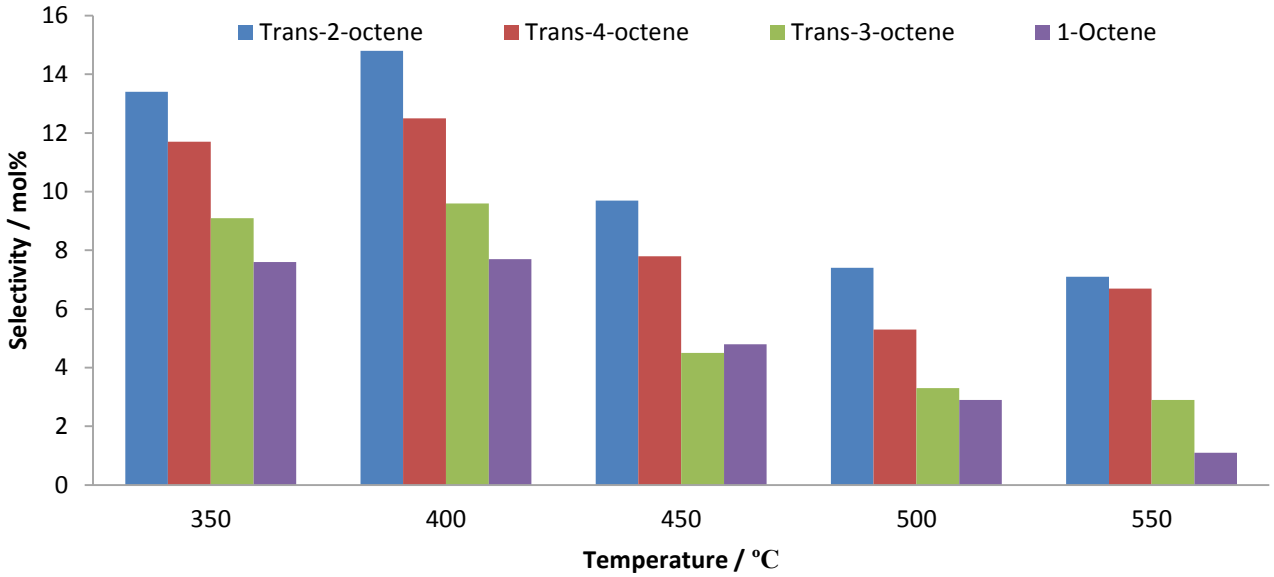

Figure 4.27 Selectivity of octene isomers as a function of temperature over the 2W catalyst (GHSV = 4000 h^{-1} and C:O = 8:3).

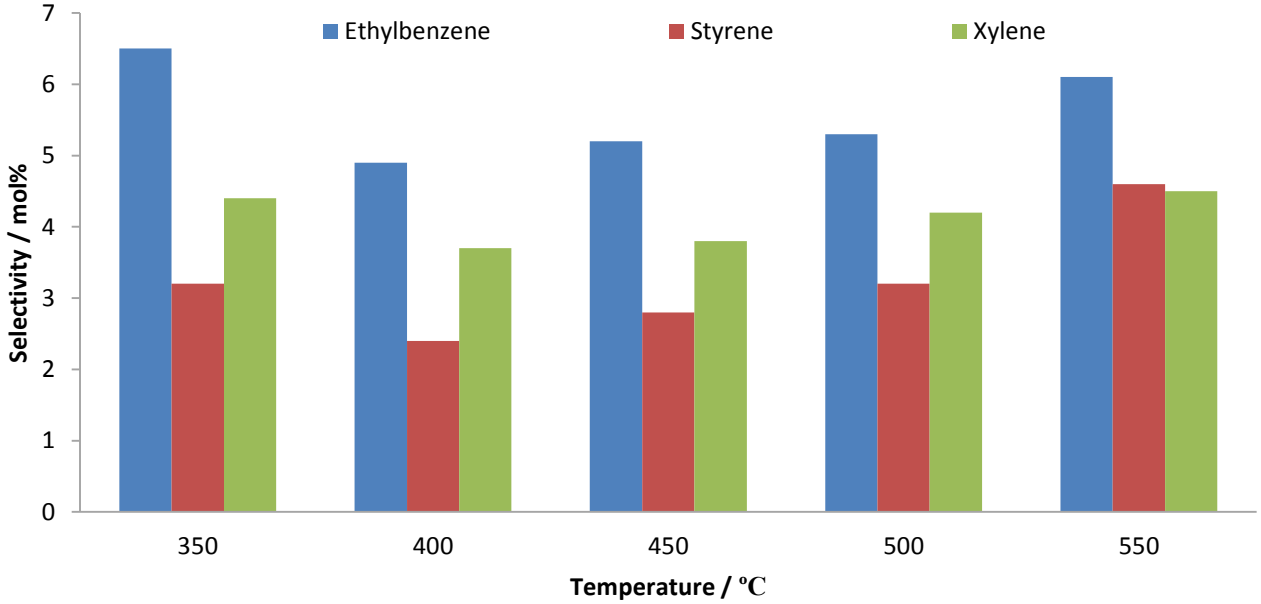

Figure 4.28 Aromatics selectivity as a function of temperature over the 2W catalyst (GHSV = 4000 h^{-1} and C:O = 8:3).

Figure 4.27 shows that the octene isomer with the highest selectivity when using a carbon to oxygen ratio of 8:3 was trans-2-octene, followed by trans-4-octene. Selectivity toward the formation of trans-3-octene and 1-octene decreased from 400 °C onwards. Figure 4.28 shows that the aromatics formed were ethylbenzene, styrene and xylene, with ethylbenzene being the most selective product of the aromatics at all temperatures.

The most oxygen rich feed ratio, shown in Figure 4.29, has conversion of *n*-octane ranged from 12 to 27 % from 350 °C to 550 °C respectively. The dominant product group of the reaction is carbon oxides at all temperatures. The second most dominant product group is octenes until 500 °C, followed by cracked and aromatic products. However, at 550 °C octenes have the lowest selectivity. At this temperature cracked products have the second highest selectivity, followed by aromatic products. As seen with all other carbon to oxygen ratios, selectivity toward octenes formation decreases and selectivity toward all other product groups increases with temperature.

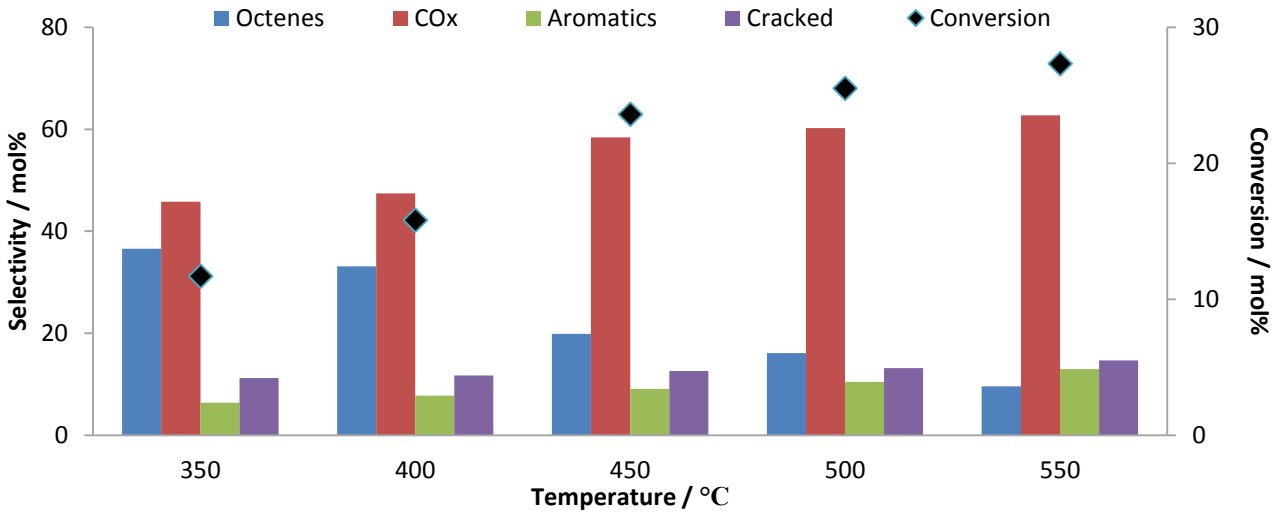

Figure 4.29 Conversion of *n*-octane and selectivity of products as a function of temperature over the 2W catalyst (GHSV = 4000 h^{-1} and C:O = 8:4).

Figure 4.30 shows the octene isomers formed and trans-2-octene has the highest selectivity, followed by trans-4-octene at all temperatures except 500 °C, at which trans-3-octene had the second highest selectivity. Selectivity towards 1-octene and trans-3-octene varied with temperature. Ethylbenzene was the dominant aromatic product formed at all temperatures, with xylene being the second most dominant product formed, followed by styrene as seen in Figure 4.31.

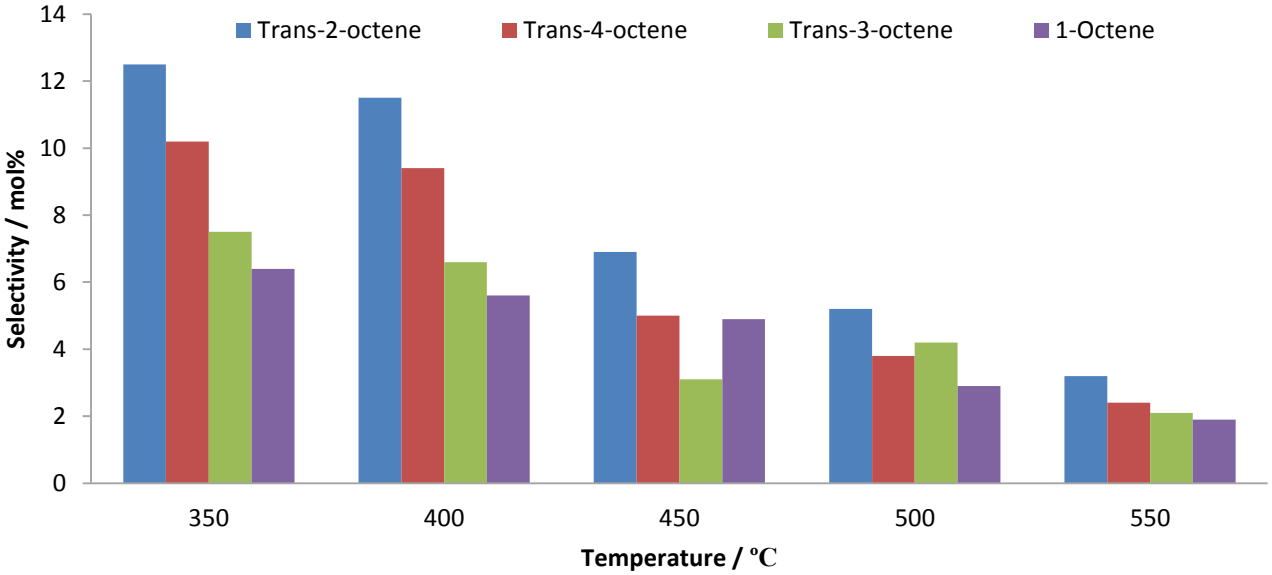

Figure 4.30 Selectivity of octene isomers as a function of temperature over the 2W catalyst (GHSV = 4000 h^{-1} and C:O = 8:4).

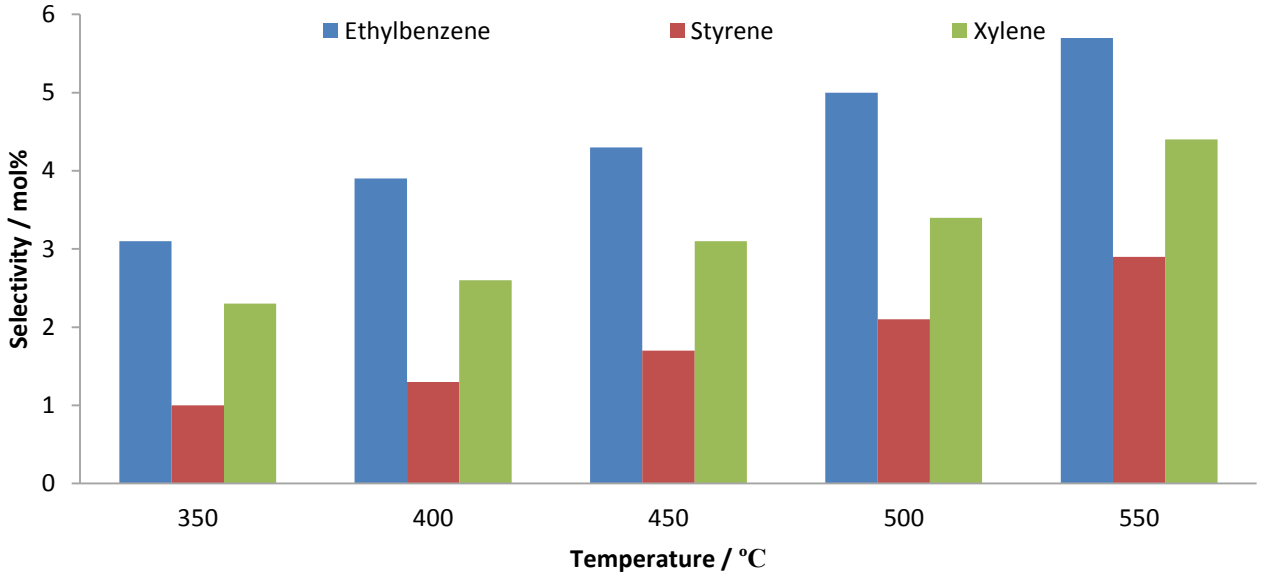

Figure 4.31 Aromatics selectivity as a function of temperature over the 2W catalyst (GHSV = 4000 h^{-1} and C:O = 8:4).

Comparing the results obtained for the 2W catalyst carried out at the various C:O ratios, the conversion of *n*-octane was observed to increase with increasing oxygen content at all temperatures. This indicates that the conversion of *n*-octane increases as the amount of oxygen present in the system increases. Table 4.3 summarises the conversion of *n*-octane and selectivities toward desired products at all of the carbon

to oxygen ratios analysed at 450 ºC. It is clear from the results obtained that as the oxygen content increases, the reaction becomes less selective.

Table 4.3 Conversion of *n*-octane and selectivity toward octenes and aromatics of the 2W catalyst with varying carbon to oxygen ratios at 450 °C.

C:O ratio	Conversion/mol%	Octenes selectivity /mol%	Aromatics selectivity /mol%
8:0	3.2	91.6	-
8:1	7.1	76.8	4.0
8:2	19.1	62.6	12.8
8:3	21.2	26.8	11.8
8:4	23.6	19.9	9.1

At a C:O ratio of 8:0, olefin selectivity was the highest, albeit at the lowest conversion. It is proposed that in absence of oxygen in the feed, lattice oxygen is being stripped from the catalyst to oxidatively dehydrogenate the *n*-octane to octene. After almost complete reduction of the catalyst, olefins are produced by dehydrogenation. These octenes are then oxidatively dehydrogenated by the same lattice oxygen to form aromatic products, via a dehydrocyclisation reaction which is the most likely reaction pathway as reported previously [30, 121]. Cracking products are formed from the *n*-octane and octene molecules and selectivities varied with oxygen ratios. Carbon oxides are the final oxidation products and were also formed via combustion of the octane and octene molecules. This is noted by increasing selectivity to this product group with increasing oxygen content. Burch and Crabb [122] stated that the olefin is more likely to combust than the paraffin, implying that carbon oxides may form more easily from the octene isomers rather than the octane molecule. Since there is no clear decrease in octenes selectivity and a corresponding increase in selectivity to a single product group with varying oxygen content, concurrent reaction pathways may be taking place for this system from the *n*-octane molecule. These octene isomers may also break down to cracked products or undergo further oxidation themselves to form CO_x products.

The conversion results imply that conversion of *n*-octane is favoured when there are one or more oxygen molecules present for every octane molecule, meaning carbon to oxygen ratios of 8:2 or higher. This can be explained by the Mars and van Krevelen mechanism [118, 119]. The oxygen atoms present in the manganese oxide were removed and are responsible for the formation of oxidation products from the *n*-octane molecule. Firstly, the *n*-octane is a known reducing agent [9, 30] and the manganese oxide can

undergo a phase change under this reducing environment. The oxygen thus removed from the metal oxide lattice can then be used to oxidatively dehydrogenate the molecule to form an octene isomer.

$$Mn_3O_4 + C_8H_{18} \rightarrow 3MnO + C_8H_{16} + H_2O$$

The oxygen in the feed to the reactor system was then used to replenish the oxygen atoms in the metal oxide.

$$3MnO + 0.5O_2 \rightarrow Mn_3O_4$$

Once the Mn_3O_4 phase is formed again, it can then be reduced and the oxygen removed can take part in more reactions. This is a continuous cycle that takes place during the reaction. One molecule of *n*-octane was used to reduce the catalyst and produce one molecule of water and the octene molecule. Following this,one molecule of oxygen gas was needed to replenish the 2 vacant oxygen atom sites of the metal oxide and re-oxidise it. This is why there is a significant increase in conversion of *n*-octane at C:O = 8:2, because surface oxygen increases and there is enough oxygen present to replenish those stripped from the metal oxide. At C:O = 8:0 and C:O = 8:1, the rate of lattice oxygen replacement low in C:O = 8:1 or did not occur at C:O = 8:0, hence the lower conversion and high selectivity toward octenes and lower selectivity toward secondary reaction products. At higher ratios, namely C:O = 8:3 and C:O = 8:4, there was an excess of oxygen present and this results in some of it being used for combustion, likely due to it being physisorbed on the metal oxide surface [34], resulting in the high selectivity toward carbon oxides.

Since oxygen from the metal oxide in the catalyst was used for the reaction, this reaction follows the Mars and van Krevelen mechanism. The present of small amounts of water in the product mixture of the reaction also supports the notion of this mechanism taking place. With greater oxygen content, there are more oxygen atoms present to replenish the lattice oxygen removed from the manganese oxide phase. This will increase the rate of re-oxidation in a Mars and van Krevelen cycle. This is why desired products are obtained in high yields at a carbon to oxygen ratio of 8:2. At lower ratios, the rate of re-oxidation is low and at higher ratios, the excess of oxygen on the surface leads to oxygen being used to promote combustion reactions and resulted in the high CO_x selectivity. A Mars and van Krevelen cycle showing the formation of primary products and reduction followed by re-oxidation of the manganese phases are shown in Figure 4.32.

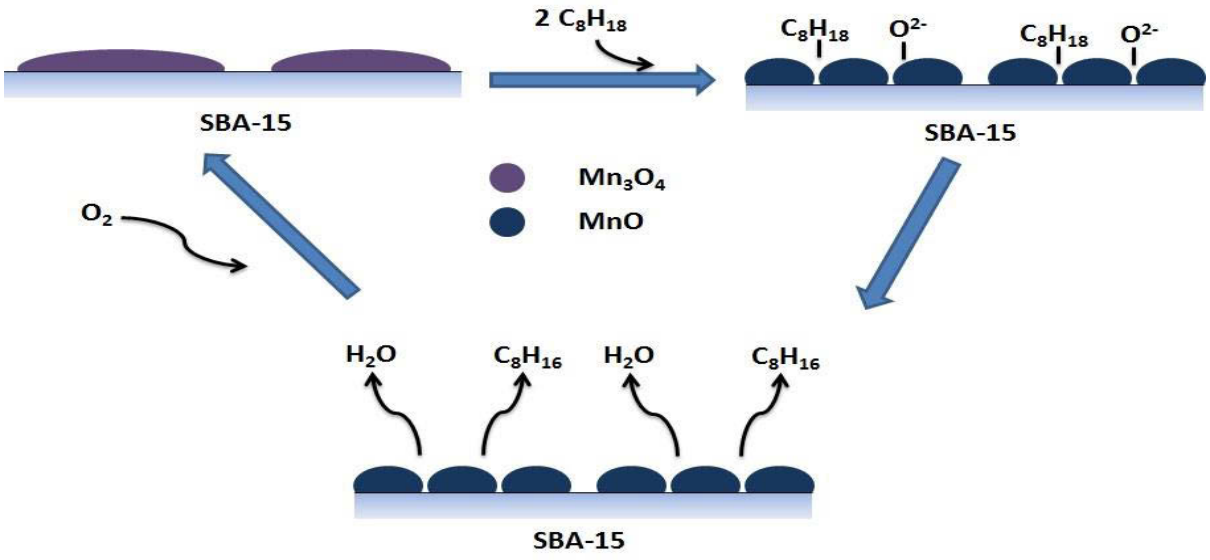

Figure 4.32 Mars and van Krevelen cycle of metal oxide phases and formation of primary product.

Upon comparison of the octene isomers formed individually, trans-2-octene is the dominant octene isomer formed at all carbon to oxygen ratios, followed by trans-4-octene except at C:O = 8:2, where trans-3-octene is the second most abundant octene isomer, with 1-octene selectivity varying. Comparing the previous results from the support only with the results obtained from varying GHSV, there was also the formation of cis-4-octene and cis-2-octene. These octenes were converted to other reaction products via simultaneous and most likely competitive reaction mechanisms and that is likely the reason why their selectivities vary with changing reaction parameters.

Formation of octenes from *n*-octane depends on the position and orientation of the double bond. It is well noted that double bond position towards the end of the chain is favoured, but is less stable and hence reacts more easily to form secondary products. Also, "trans" isomers of octenes are more stable than "cis" isomers [27, 28, 121]. This reasoning can be used to explain the varying selectivity of the octene isomers noted with varying oxygen content and GHSV's.

It is likely that trans-2-octene has the highest rate of formation because it is the most thermodynamically favoured. This means that it can be formed easily from *n*-octane and is relatively stable once it is formed. 1-Octene may form but it is less stable since the position of the double bond is between C1 and C2. This implies that formation of other octenes may be favoured. Trans-3-octene and trans-4-octene selectivity

is favoured due to the relative thermodynamic stability based on the position of the double bond away from the end of the carbon chain. Cis-2-octene and cis-4-octene isomers are not as stable as trans-isomers and hence these products are not consistently formed or react quickly once they are formed [27, 28]. In summary, the selectivity of the octene isomers depend on the position and orientation of the double bond which determines both the rate of formation and the relative stability once they are formed.

Ethylbenzene is the dominant aromatic compound formed at all C:O ratios. From C:O = 8:2 to C:O = 8:4, styrene and xylene begin to form. The likely mechanism of ethylbenzene formation would be via C1 to C6 cyclisation from 1-octene [29, 30]. This may be the case for this system because at C:O = 8:1, ethylbenzene formed at 550ºC while no 1-octene was seen. This could be because as 1-octene formed, it was directly converted to ethylbenzene under these specific reaction conditions. As the oxygen content is increased at the 8:2 ratio, both 1-octene and ethylbenzene selectivity increased with temperature and when compared to C:O = 8:1. This indicates more 1-octene is formed with the increase in oxygen content, more of it is available for ethylbenzene formation. With C:O = 8:3 and 8:4, 1-octene selectivity decreases but ethylbenzene selectivity increases as a function of temperature. This is again suggests that 1-octene is a precursor to ethylbenzene.

For ratios of C:O = 8:2 to 8:4, styrene was observed to form via the dehydrogenation of ethylbenzene. At lower oxygen content, ethylbenzene forms but its subsequent conversion to styrene was not observed likely due to the low amounts of ethylbenzene that formed. However, as *n*-octane conversion increases by virtue of increasing oxygen content in the feed, the rate of formation of ethylbenzene increases and its subsequent oxidative dehydrogenation to styrene occurs.

Xylene is likely to form from C2 and C7 cyclisation of an octene molecule. Precursors for xylene may be any of the other octene isomers except 1-octene, since cyclisation is favoured by non-terminal double bonds [28]. In general, ethylbenzene and xylene selectivity increases with increasing oxygen content, which suggests that it is likely formed due to the O^{2-} species from the manganese oxide present in the catalyst.

The O^{2-} species has been reported to be most likely responsible for the formation of octenes as well as the dehydrocyclisation of octenes to aromatic products [118]. Certain octene isomers that formed are responsible for the formation of specific aromatic compounds, depending on which carbon atoms

cyclise. This can be evaluated by looking at individual product formation at the different carbon to oxygen ratios.

A carbon to oxygen ratio of 8:2 showed best selectivities toward the desired products such as octenes and aromatics. The conversion was also reasonable, hence, this ratio was used to test the other catalysts prepared.

4.3.2 Experiments to determine catalyst stability

A time-on-stream analysis of the 2W catalyst was done for 48 hours at 450 °C with a GHSV of 4000 h^{-1} and a carbon to oxygen ratio of 8:2.

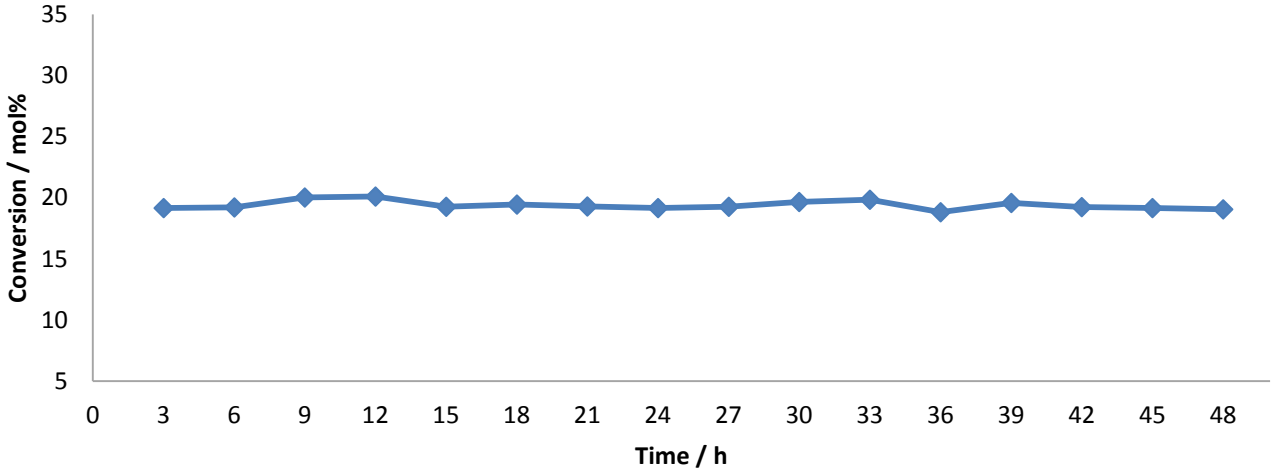

Figure 4.33 Effect of time with the conversion of *n*-octane over 2W catalyst (Temperature = 450 ºC, GHSV = 4000 h^{-1} and C: O = 8:2).

The catalyst remained stable for 48 hours as shown in Figure 4.33, as it showed no significant change in conversion of *n*-octane or selectivity toward desired products. The conversion of *n*-octane and selectivity toward products of interest are in a standard deviation range of 1 % for all the runs and the values are shown in Table 4.4.

Following the time-on-stream analysis, the catalyst was put through a recycle test and the results are shown in Figure 4.34. This is where the catalyst is tested from 350 – 550 °C in 50 °C increments and then once it has reached the maximum temperature, the catalyst is cooled to each of the temperatures in question and the products of the reaction are analysed. This experiment was used to determine

thecyclability of the catalyst, and for the 2W catalyst, it was found that that catalyst could be recycled. The results from the experiment are shown in Figure 4.33 and they are comparable to the results for

Table 4.4 Conversion of *n*-octane and selectivities for time-on-stream analysis.

Conversion / mol %	19.4
Product	**Selectivity / mol%**
Octenes	60.4
Aromatics	13.2
Cracked Products	1.9
CO_x	24.4

the 2Wcatalyst shown previously as both the conversion values are within 1% and all product selectivities are similar at all temperatures. Using the results of the time-on-stream analysis and the recycle test, it can be concluded that the catalyst is stable for 48 hours and is cyclable.

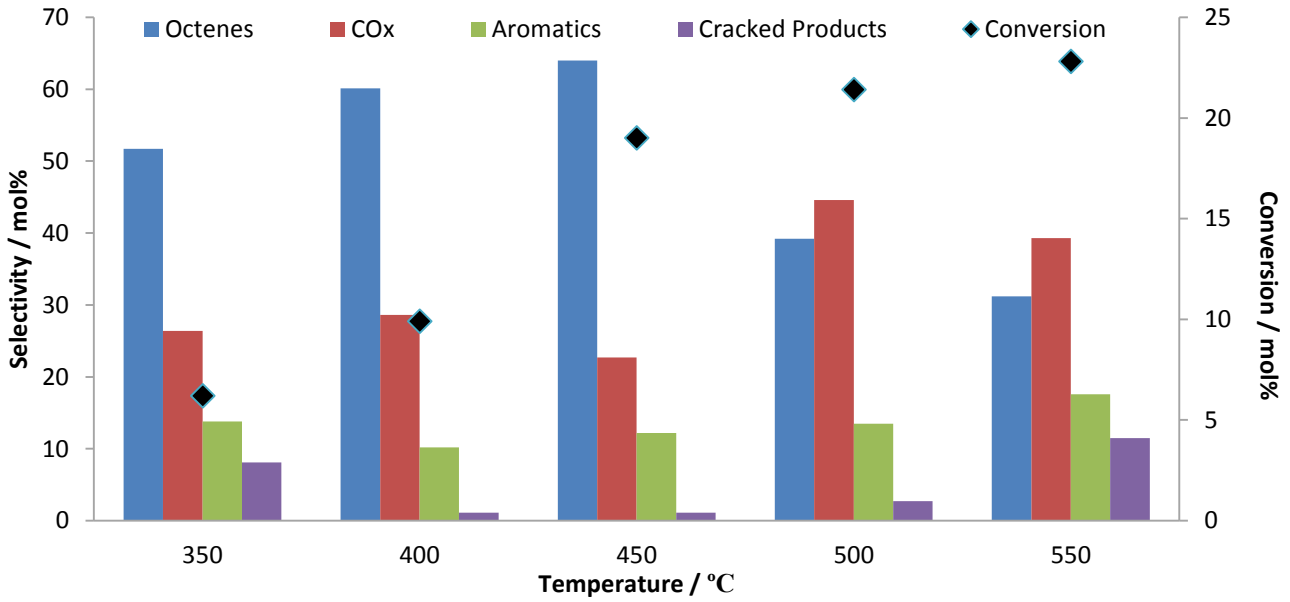

Figure 4.34 Conversion of *n*-octane and selectivity towards products over the 2W catalyst for recycle test (GHSV = 4000 h^{-1} and C:O = 8:2).

4.4 Proposed reaction pathway

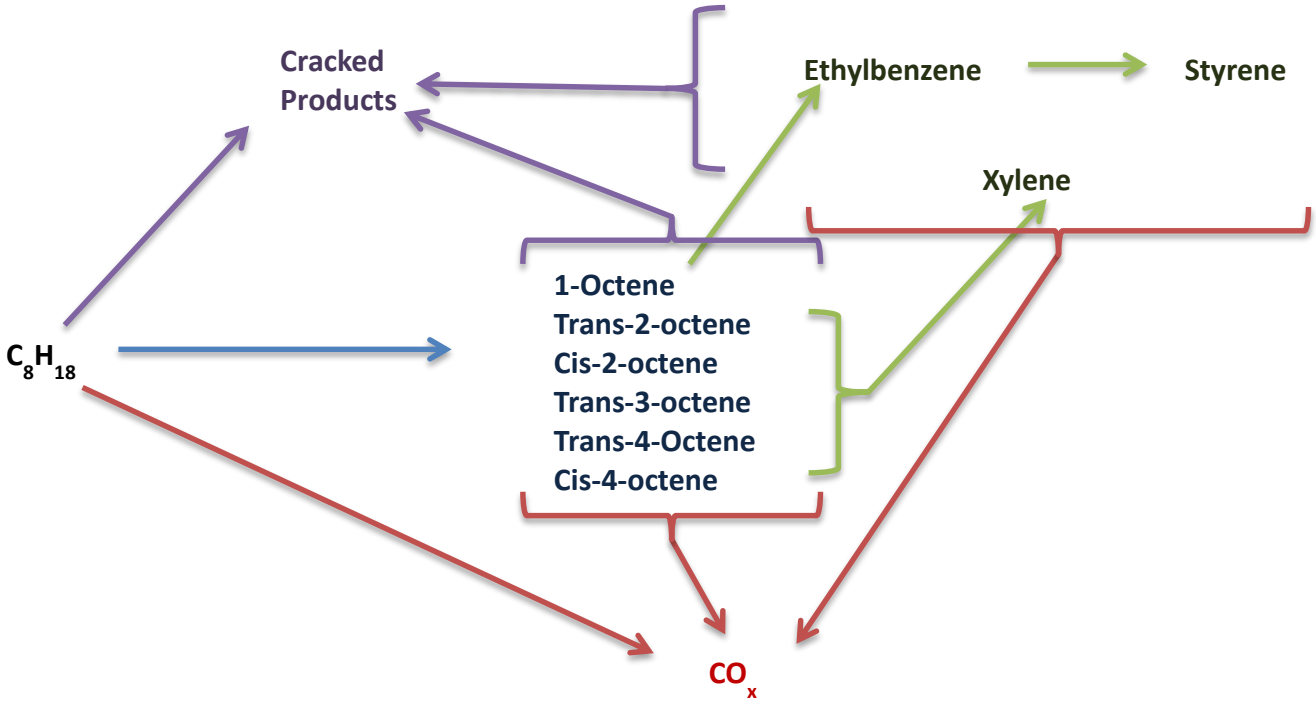

Figure 4.35 Scheme of individual product formation.

The individual reaction pathways for each of the products obtained from the reactions were evaluated based on the results obtained and from previous research in the field [29, 30 , 123], as shown in Figure 4.35. The primary products from the oxidative dehydrogenation of *n*-octane were octene isomers. The isomers that formed were 1-octene, trans-2-octene, cis-2-octene, trans-3-octene, trans-4-octene and cis-4-octene. The *n*-octane molecule was also simultaneously converted to carbon oxides and cracked products. Both the octene isomers and aromatic compounds reacted further to form carbon oxides and cracked products, with the reaction of octene isomers to form carbon oxides having a higher rate than the reaction of *n*-octane to form carbon oxides [122]. 1-Octene underwent a C1-C6 cyclisation to form ethylbenzene, which reacted further to form styrene. All other octene isomers underwent a C2-C7 cyclisation to form xylene.

Chapter 5

The role of active metal loading and position in support

In the previous chapter, the optimisation of catalytic reaction conditions was discussed and to some extent, the influence these changes in conditions have on catalytic performance. The conditions that showed the highest conversion coupled with high selectivity to desired products were identified. Optimisation was done using the 2W catalyst and the optimised reaction conditions were subsequently used to test the different catalyst to determine the role the active metal loading played as well as the position of the active metal, i.e. whether it was located deep in the pores or closer to the surface of the SBA-15 support.

5.1 Catalytic results of catalysts prepared by wet impregnation (2W, 5W and 9W catalysts)

To determine the effect of weight loading of metal oxide on the surface of the SBA-15 support, the 5W and 9W catalysts were tested and their results were compared to those of the 2W catalyst.

5.1.1 Catalytic results of the 5W catalyst

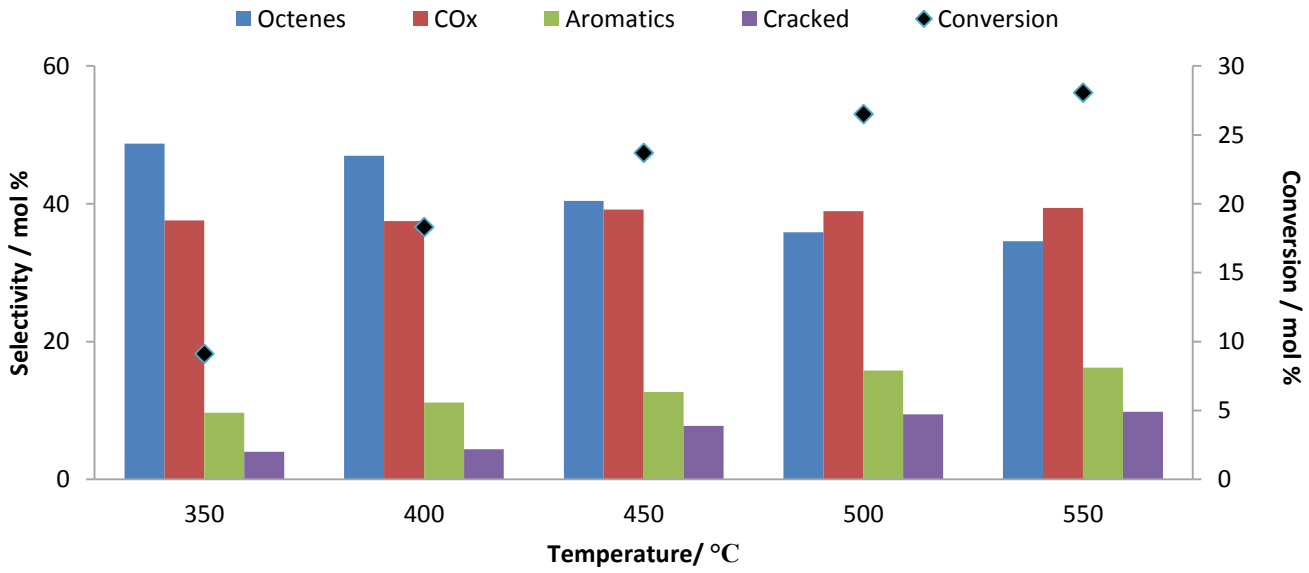

Figure 5.1 Conversion of *n*-octane and selectivity towards products as a function of temperature over the 5W catalyst (GHSV = 4000 h^{-1} and C:O = 8:2).

For the 5W catalyst, conversion was observed to increase with increasing temperature, as shown in Figure 5.1. Conversion of *n*-octane ranged from 9 % - 28 % within the temperature range. The dominant product groups observed were octenes, aromatics, carbon oxides and cracked products (Figure 5.1). The product group with the highest selectivity was octenes until 450 °C, with carbon oxides having the second highest selectivity. At 500 and 550 °C, however, carbon oxides had the highest selectivity with octenes being the second most selective product group. The other product groups obtained were aromatic and cracked products, with aromatic products having a higher selectivity than cracked products at all temperatures. Both aromatic and cracked product selectivities were observed to increase with increasing temperature with a corresponding decrease in octenes selectivity.

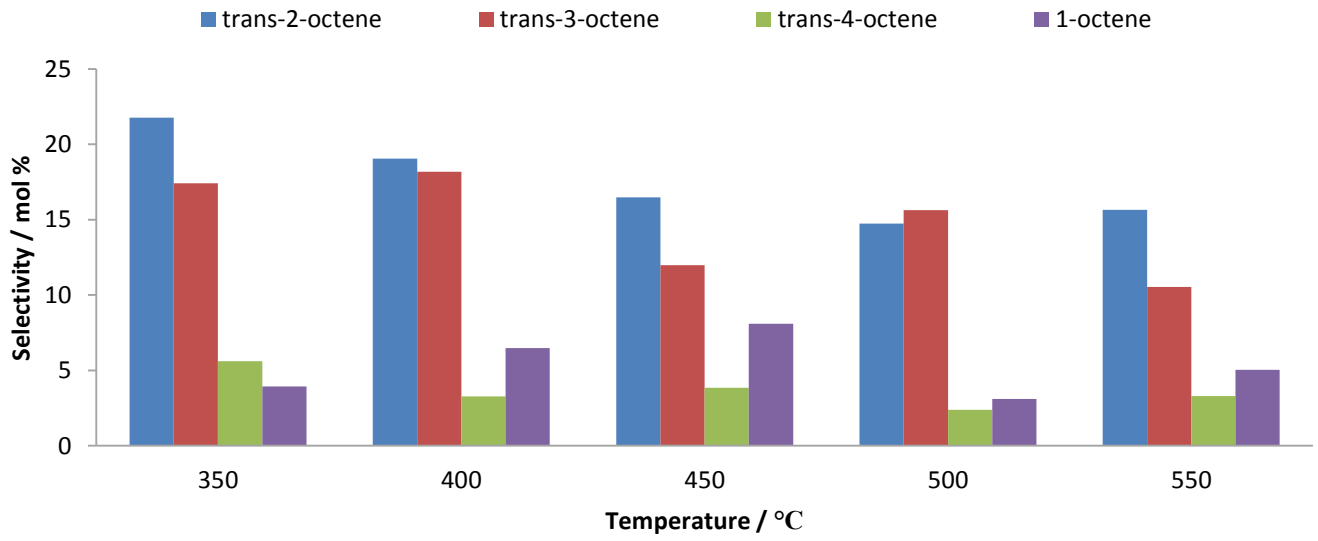

Figure 5.2 Octenes selectivity as a function of temperature over the 5W catalyst (GHSV = 4000 h^{-1} and C:O = 8:2).

Upon analysis of the octene selectivity over the 5W catalyst in Figure 5.2, trans-2-octene was the dominant product obtained from 350 °C – 450 °C and again at 550 °C. The second most dominant product at these temperatures was trans-3-octene. At 500 °C, this is reversed, with trans-3-octene having a slightly higher selectivity than trans-2-octene, however the values are still close to each other and the difference is likely within the range of experimental error. Throughout the temperature profile, there are varying selectivities of trans-4-octene and 1-octene. Trans-4-octene showed lower selectivity than 1-octene from 400 °C onwards. Upon comparison of the aromatics selectivity in, Figure 5.3, the aromatic product with the highest selectivity was ethylbenzene at all temperatures. This is followed by styrene and xylene, which showed the lowest selectivity. From 350 – 450 °C, the selectivity toward trans-2-

octene and trans-3-octene was observed to decrease as shown in Figure 5.2. Subsequently, an increase in selectivity towards xylene was observed, suggesting a C2-C7 cyclisation of these octene isomers to form xylene. Also, at these temperatures, 1-octene selectivity increased with a decrease in the two dominant octene isomers. Ethylbenzene and styrene selectivity also increased as 1-octene selectivity increased at these temperatures, with ethylbenzene likely being formed from 1-octene via C1-C6 cyclisation and subsequently dehydrogenated to form styrene. Dasireddy *et al.* [123] observed the same trend with 1-octene and ethylbenzene selectivities for *n*-octane activation using hydroxyapatite catalysts. At 500 and 550 °C, aromatic selectivity increased with temperature which was also noted for the 2W catalyst at these temperatures and reaction conditions.

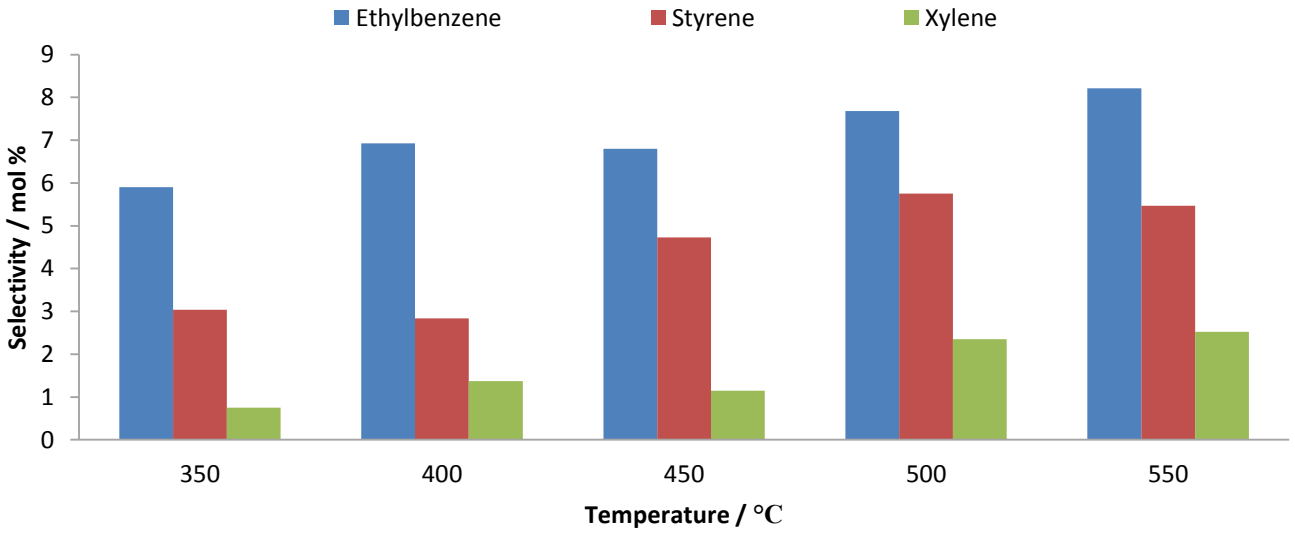

Figure 5.3 Aromatics selectivity as a function of temperature over the 5W catalyst (GHSV = 4000 h^{-1} and C:O = 8:2).

5.1.2 Catalytic results of the 9W catalyst

The results for the catalytic testing of the 9W catalyst are shown in Figure 5.4. For this catalyst, conversion increased with temperature which ranged from 14 % at 350 °C to 37 % at 550 °C. The selectivity of the 9W catalyst showed that octenes were the dominant products throughout the temperature range. The second most selective products were the CO_x group, except at 500 °C, where aromatics became the second most selective product group. As temperature increased, the selectivity towards octenes decreased and the selectivity toward aromatics and cracked products increased. Also

for the 9W catalyst, aromatic product selectivity was higher than cracked product formation at all temperatures.

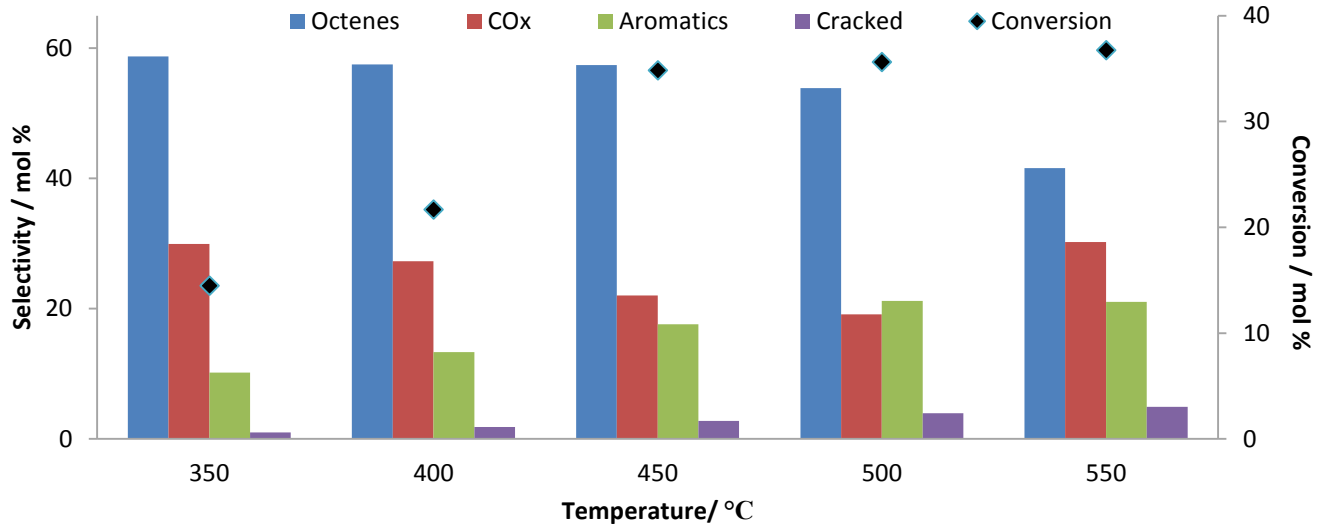

Figure 5.4 Conversion of *n*-octane and selectivity towards products as a function of temperature over the 9W catalyst (GHSV = 4000 h^{-1} and C:O = 8:2).

Figure 5.5 shows that trans-2-octene was the dominant octene isomer formed over the 9W catalyst. The second most dominant isomer was trans-3-octene, followed by varying amounts of trans-4-octene and 1-octene, likely due to the simultaneous reaction taking place to form these products. Ethylbenzene was the dominant aromatic isomer formed, followed by styrene and then xylene, as seen in

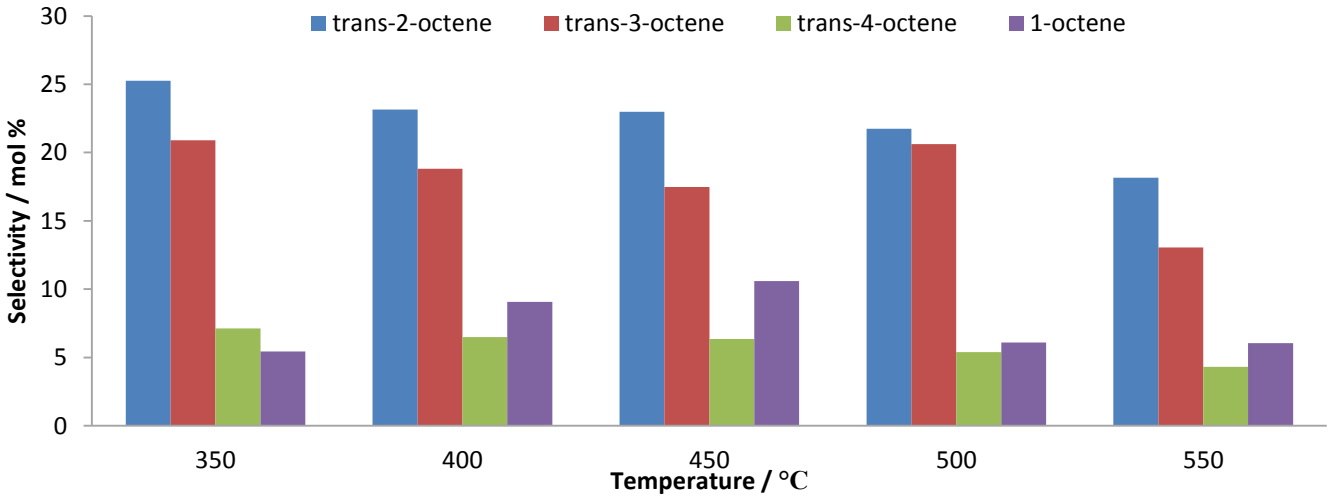

Figure 5.5 Octenes selectivity as a function of temperature over the 9W catalyst (GHSV = 4000 h^{-1} and C:O = 8:2).

Figure 5.6. Similarly to the 5W catalyst, throughout the temperature range, the selectivity of trans-2-octene and trans-3-octene decreased, whilst the selectivity to xylene increased. There was a slight decrease at 450°C, but it is less than 0.2% and can be viewed as negligible and within experimental error. At the lower three temperatures, 1-octene selectivity increased with the decrease in selectivity of the dominant two isomers and this was observed for all catalysts prepared by the wet impregnation technique. The selectivity towards ethylbenzene and styrene also increased at these temperatures, which is in agreement with the proposed reaction pathway.

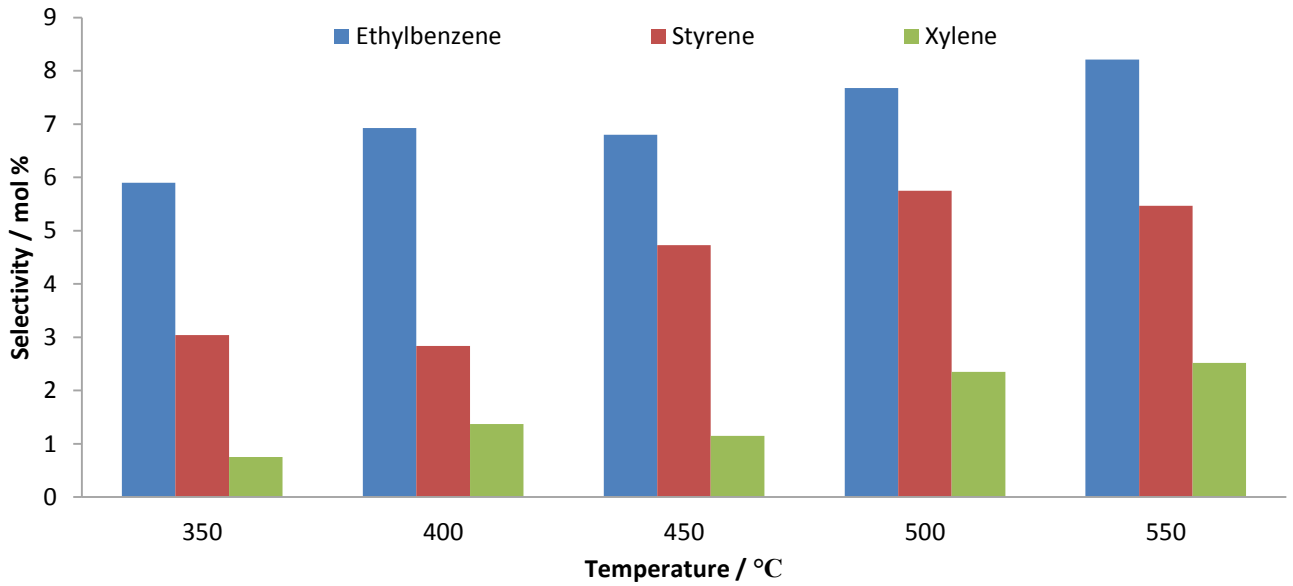

Figure 5.6 Aromatics selectivity as a function of temperature over the 9W catalyst (GHSV = 4000 h^{-1} and C:O = 8:2).

Upon comparison of the catalytic results obtained for the 2W, 5W and 9W catalysts, there were certain trends that were observed. These trends are shown in Figure 5.7 (A-E). Conversion of *n*-octane increased with increasing metal weight loading at all temperatures due to the higher surface area of the active metal oxide. With respect to selectivity, the selectivity toward octenes for the 9W catalyst was highest, followed by the 5W catalyst, but at 400 and 450 °C, the 2W catalyst is dominant. This trend was observed at all temperatures. The opposite was true for CO_x selectivity, where the 9W catalyst showed the lowest selectivity. This is suggestive of a higher rate of the oxidative dehydrogenation reactions as metal content is increased, likely due to the high concentration of lattice O_2. This reasoning is reinforced by the trends observed for the aromatics selectivity, with the 9W catalyst showing higher selectivity with increasing temperature when compared to catalysts with lower metal loading. Selectivity to cracked products was

lowest for the 9W catalyst, however at 400, 450 and 500 °C the 2W catalyst showed the lowest selectivity towards these products.

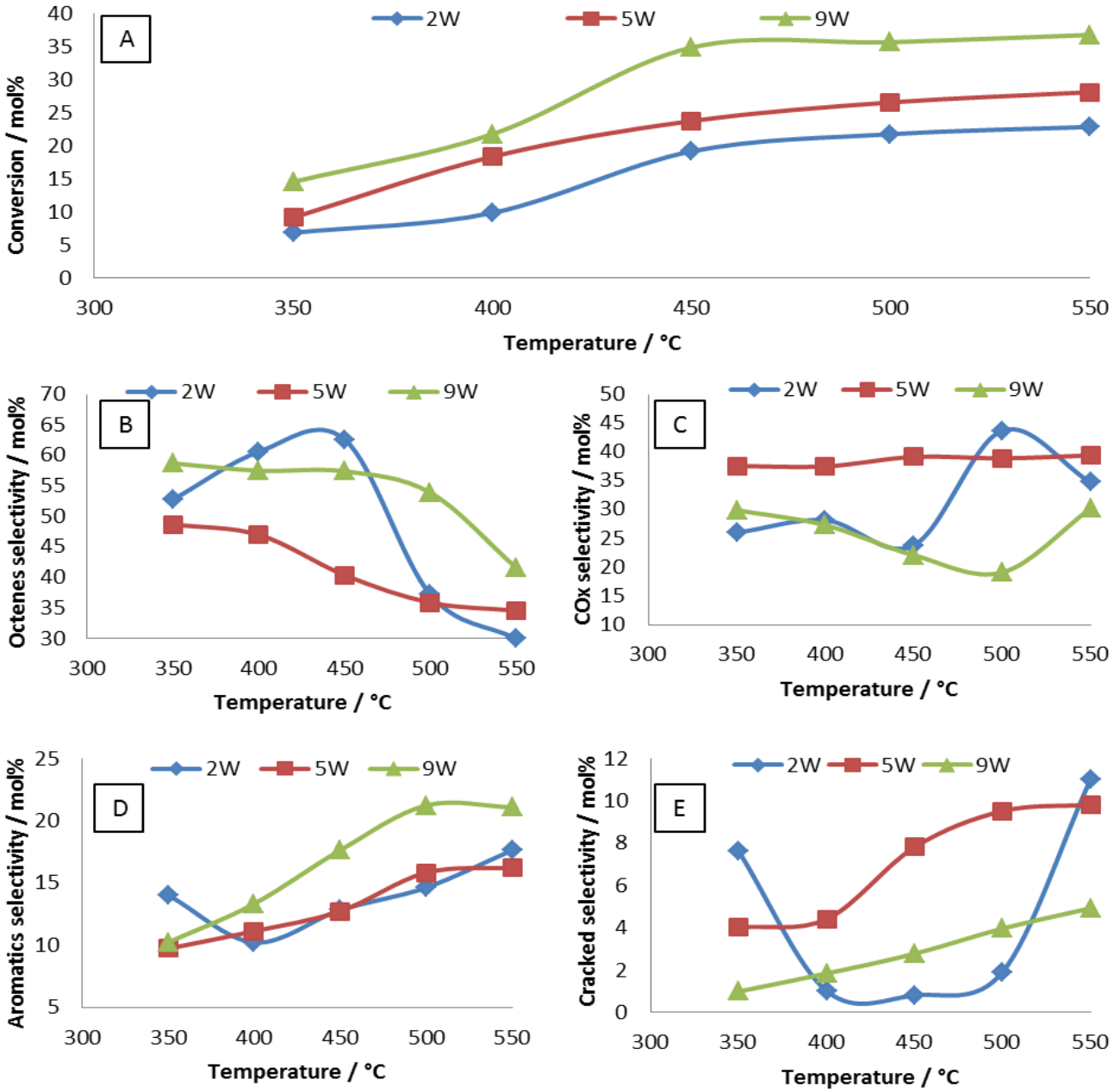

Figure 5.7 Conversion of *n*-octane and selectivity towards products as a function of temperature over catalysts prepared by wet impregnation (GHSV = 4000 h^{-1} and C:O = 8:2).

Aromatic and cracked products were formed by secondary oxidation of the primary products of the reaction, which were the octenes. These reactions follow the proposed reaction pathway, explained in Chapter 4. For all weight loadings and at most temperatures, trans-2-octene had the highest selectivity

when compared to the other octene isomers, followed by trans-3-octene.The selectivities in the production of trans-4-octene and 1-octene varied from catalyst to catalyst. For aromatic products, ethylbenzene was the dominant aromatic formed in the reactions, as it had the highest selectivity for all weight loadings. The aromatic product with the second highest selectivity is styrene, followed by xylene.

From the results obtained for catalysts prepared by wet impregnation, the 9W catalyst was found to be the better, as it provided the greatest conversion with a high selectivity toward octenes and aromatic products. Higher weight loading catalysts were not pursued as with very high weight loadings of the metal oxide, the mesoporous structure of the support may not remain after impregnation. This was reported by Laniecki and Wojtowski [124], as they found with high metal content for Ti/SBA-15 catalysts, there was a substantial loss in the textural characteristics of the support. Thus 9% manganese oxide the highest weight loading investigated.

5.2 Catalytic results of catalysts prepared by deposition precipitation (2D, 5D and 9D catalysts)

To investigate the influence of the location of the active site, the 2D, 5D and 9D catalysts which were prepared by deposition precipitation were studied and compared to the catalysts prepared by wet impregnation. These catalysts were tested under the optimum conditions that were established in the previous chapter.

5.2.1 Catalytic results of the 2D catalyst

For the catalytic behavior of the 2D catalyst, the results of which are shown in Figure 5.8, conversion increased with increasing temperature and ranged from 2 % at 350 °C to 19 % at 550 °C. The dominant products formed at all temperatures were carbon oxides, followed by octenes. Aromatic products began to form at 450 °C and were selectively formed with increasing temperature. The reason for the high CO_x formation over this catalyst was likely because the active site is located within the pores of the SBA-15 support and is not very accessible. This implies that once the olefins are formed, they spend more time in the pores of the support and are converted to carbon oxides. This is the more likely route of carbon oxide formation as olefins are more likely to combust than paraffins [122]. The combustion reaction may also be the reason why cracked products were not observed, as these cracked

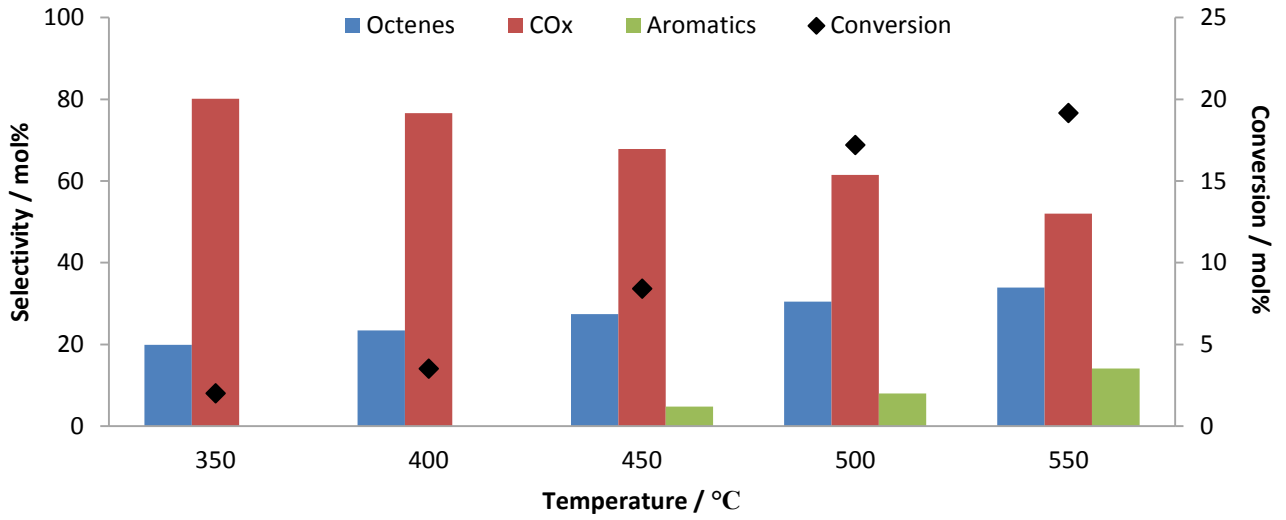

Figure 5.8 Conversion of *n*-octane and selectivity towards products as a function of temperature over 2D catalyst (GHSV = 4000 h^{-1} and C:O = 8:2).

products may directly combust to form carbon oxides. The low accessibility of the active site and low metal loading may be also the reason that the conversion of the 2D catalyst is only slightly higher than that of the SBA-15 support (Figure 4.3). CO_x selectivity decreases with increasing temperature, while octenes selectivity increased. This suggests a concurrent reaction pathway, which agrees with the proposed reaction pathway in Chapter 4.

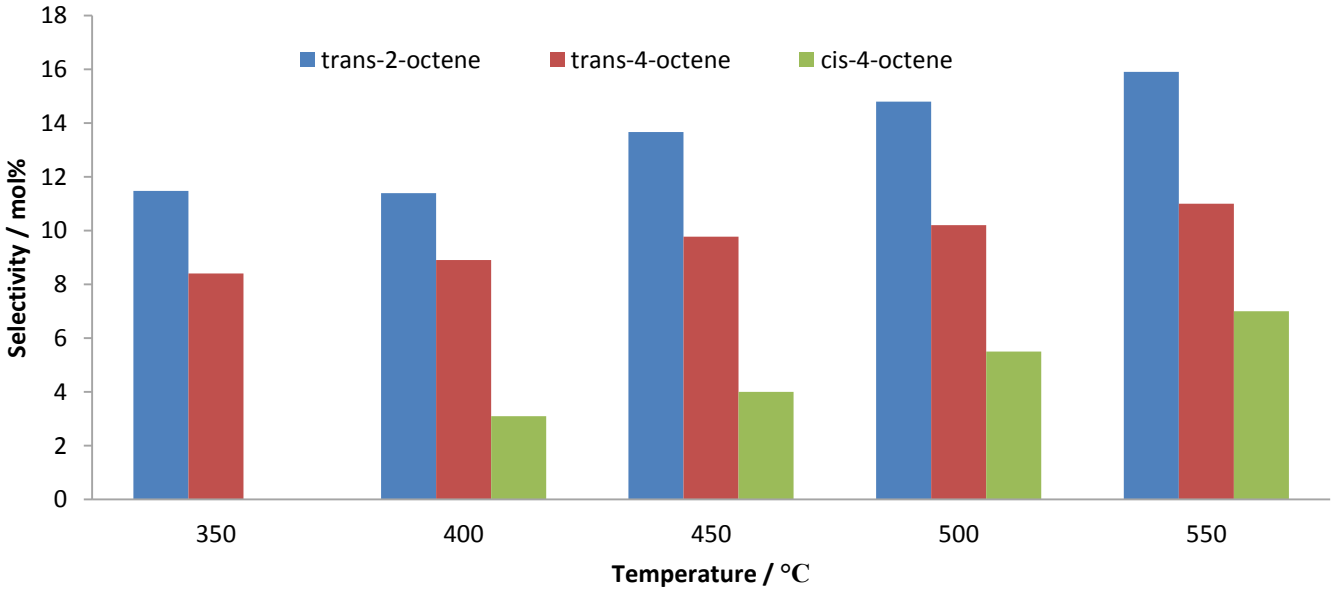

Figure 5.9 Octenes selectivity as a function of temperature over the 2D catalyst (GHSV = 4000 h^{-1} and C:O = 8:2).

In terms of octene selectivity over the 2D catalyst, shown in Figure 5.9, trans-2-octene was the dominant octene isomer at all temperatures, followed by trans-4-octene. Cis-4-octene began to form at 400 °C and it was selectivity lower than the other octene isomers and formed as temperature increased. It is, however, the least selective of the octene isomers. Ethylbenzene had the highest selectivity amongst the aromatic products, followed by xylene and then styrene, as shown in Figure 5.10. From 450 °C, all octene isomers increased in selectivity. At the same time, there was a corresponding increase in selectivity to xylene. This indicates that more octenes were formed at these temperatures and there was a greater amount available for the subsequent conversion to aromatic products. 1-Octene was not observed and this may be because as it formed, it underwent secondary reactions rapidly to form ethylbenzene and styrene [34, 47]. Aromatic product selectivity was low for this catalyst and this was examined further and is discussed with the results of the other catalysts prepared by deposition precipitation.

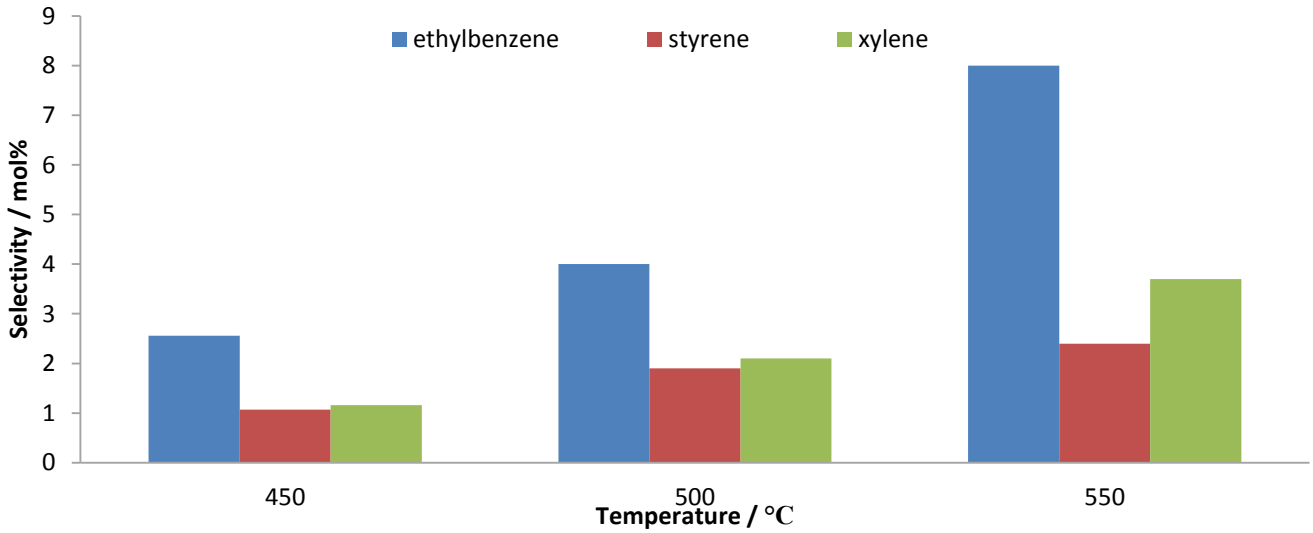

Figure 5.10 Aromatics selectivity as a function of temperature over the 2D catalyst (GHSV = 4000 h^{-1} and C:O = 8:2).

5.2.2 Catalytic results of the 5D catalyst

The catalytic results of the 5D catalyst are presented in Figure 5.11. The conversion and selectivity of *n*-octane over this catalyst varied with temperature and the conversion increased with increasing temperature, as expected. Conversion ranged from 4 % at 350 °C to 19 % at 550 °C. The product group with the highest selectivity throughout the temperature profile was the CO_x group, followed by octenes

and then cracked products. The products with the lowest selectivity were aromatics and they only began to form after 450 °C. With increasing temperature, octene product selectivity decreased and aromatic and cracked product selectivities increased, which is in agreement with the reaction pathway for this system. There was also a decrease in CO_x selectivity with increasing temperature which suggests that, as stable products form from octenes, less octenes combust to form CO_x.

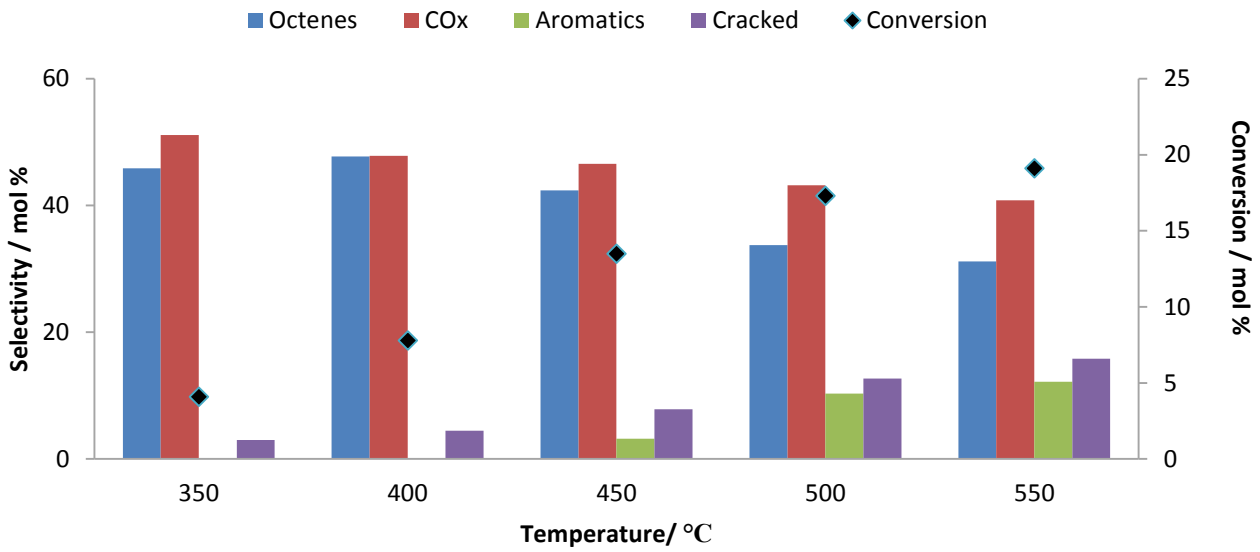

Figure 5.11 Conversion of *n*-octane and selectivity towards products as a function of temperature over the 5D catalyst (GHSV = 4000 h^{-1} and C:O = 8:2).

In terms of octenes selectivity shown in Figure 5.12, the order of selectivity was trans-2-octene > trans-3-octene > 1-octene > trans-4-octene. The most selective of the aromatic products was ethylbenzene at 450 °C, as it was the only aromatic compound present, shown in Figure 5.13. Styrene and xylene began to form only from 500°C, with xylene having higher selectivity than styrene at both temperatures.

Selectivities towards trans-2-octene and trans-3-octene were decreased while the selectivities toward 1-octene and trans-4-octene were varied. There was a decrease in selectivity of the formation of 1-octene from 400 – 450°C. This most likely occurred because it was aromatized to form ethylbenzene, which was found at 450 °C. The selectivity towards 1-octene was fairly constant from 450 – 550 °C, while the selectivities toward ethylbenzene and styrene increased with temperature. Xylene formed from 500 °C, with a corresponding decrease in selectivity toward trans-2-octene and trans-4-octene. This occurred via a C2-C7 cyclisation of the octene isomers.

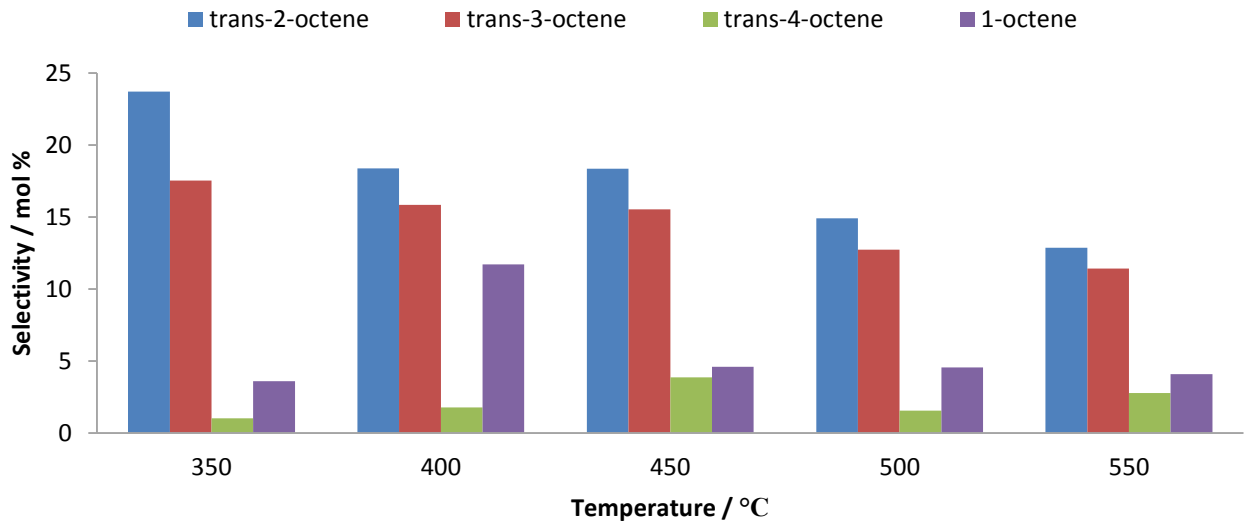

Figure 5.12 Octenes selectivity as a function of temperature over the 5D catalyst (GHSV = 4000 h^{-1} and C:O = 8:2).

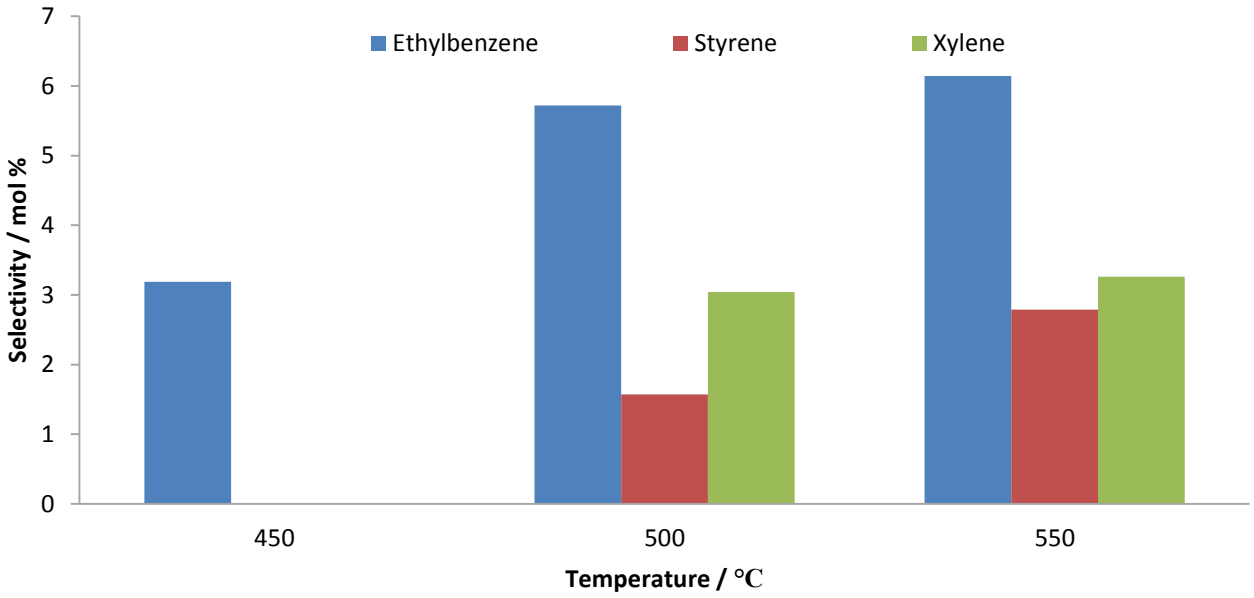

Figure 5.13 Aromatics selectivity as a function of temperature over the 5D catalyst (GHSV = 4000 h^{-1} and C:O = 8:2).

5.2.3 Catalytic results of the 9D catalyst

The conversion for the 9D catalyst, shown in Figure 5.14, increased with an increase in temperature and it ranged from 7 % at 350 °C to 20 % at 550 °C. Octenes were the dominant products throughout the temperature range and the second most selective product group was CO_x. Aromatic products

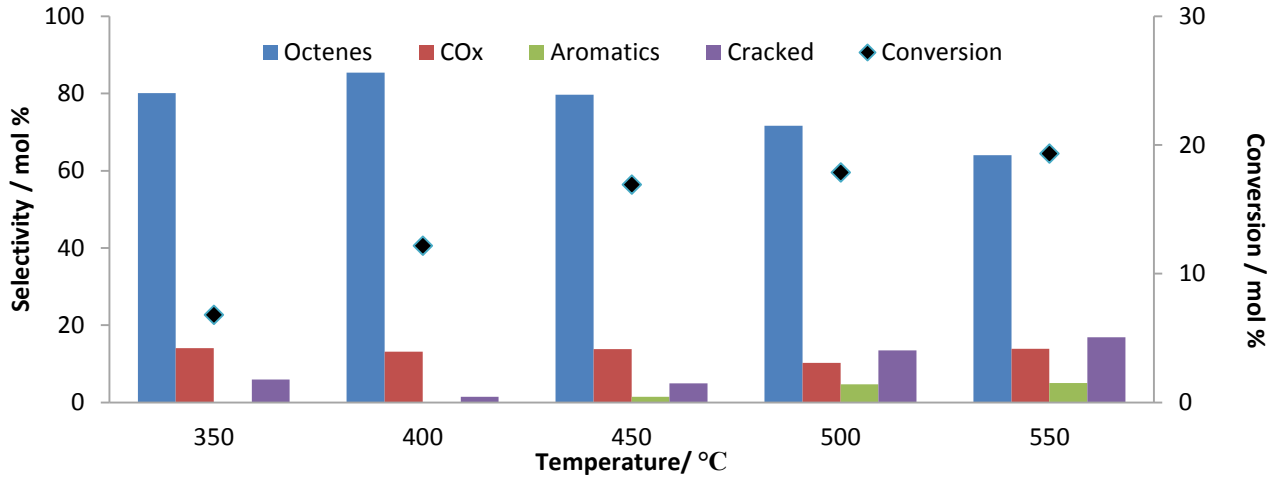

Figure 5.14 Conversion of *n*-octane and selectivity towards products as a function of temperature over the 9D catalyst (GHSV = 4000 h^{-1} and C:O = 8:2).

began to form from 450 °C and their selectivity increased with increasing temperature. Cracked products selectivities varied at all temperatures and these products had a higher selectivity than aromatic products at all temperatures. The reason for the higher octenes selectivity could be due to the change in accessibility of the active site associated with the higher weight loading.

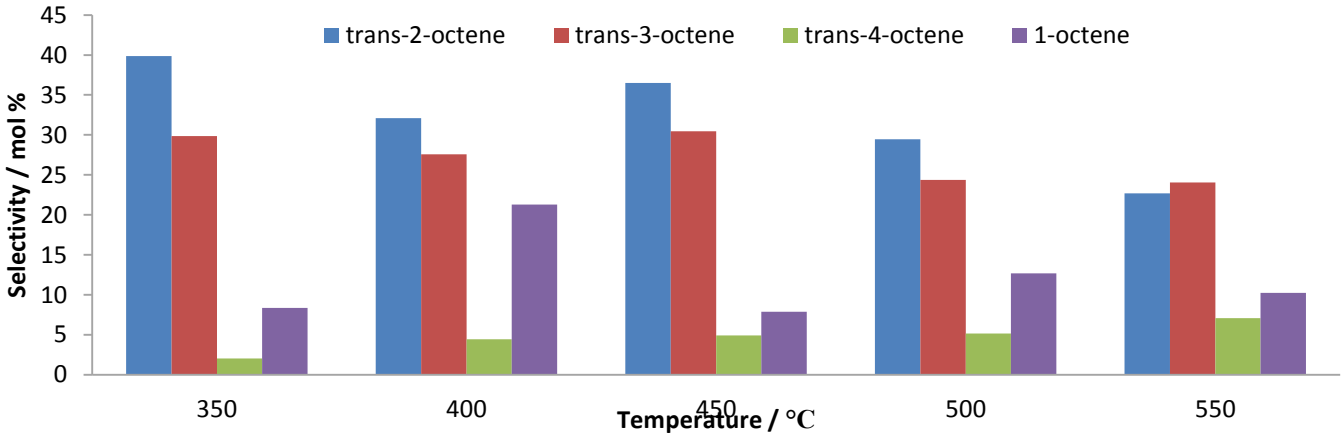

Figure 5.15 Octenes selectivity as a function of temperature over the 9D catalyst (GHSV = 4000 h^{-1} and C:O = 8:2).

The octenes selectivity for the 9D catalyst, shown in Figure 5.15, showed trans-2-octene as the dominant isomer from 350 – 500 °C, whereas trans-3-octene had the highest selectivity at 550°C. The octene isomer with the third highest selectivity is 1-octene, followed by trans-4-octene. Ethylbenzene was the only aromatic product that was found at 450 °C. At 500 and 550 °C, the other two aromatic compounds were also found, with xylene having the highest selectivity, followed by ethylbenzene and then styrene, seen in Figure 5.16.

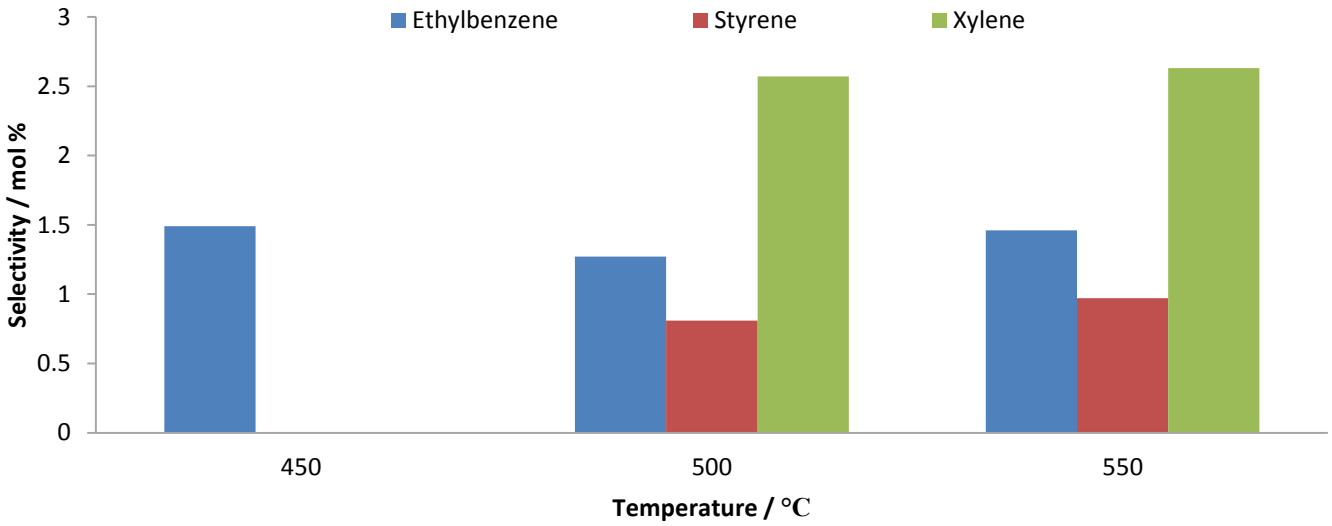

Figure 5.16 Aromatics selectivity as a function of temperature over the 9D catalyst (GHSV = 4000 h^{-1} and C:O = 8:2).

As was seen with all the other catalysts, the mixture of octenes is in agreement with the reaction pathway in the previous chapter. Similarly to the 5D catalyst, from 400 – 450 °C, there was a decrease in selectivity of 1-octene, while ethylbenzene and styrene formed at 450 °C, which will account for this decrease. The selectivity towards 1-octene varied from 450 – 550 °C, while the selectivity toward ethylbenzene and styrene increased with temperature. Xylene formed from 500°C onwards with a corresponding decrease in selectivity toward trans-2-octene and trans-4-octene.

A summary of the catalytic data obtained for the 2D, 5D and 9D catalyst is shown in Figure 5.17 (A-E). Conversion of *n*-octane increased with increasing weight loading due to the greater number of active sites present with higher weight loading. However, at higher temperatures, the conversions of all the catalysts prepared by deposition precipitation were similar and these conversions were comparable to

that of the SBA-15 support (Figure 4.3). This suggests that an increase in weight loading in the pores of the support had a greater effect on the selectivity of the catalyst than it did on the conversion. The selectivity profiles of all catalysts prepared by deposition precipitation varied with the weight loading. Selectivity toward octenes increased and selectivity towards CO_x decreased with increasing

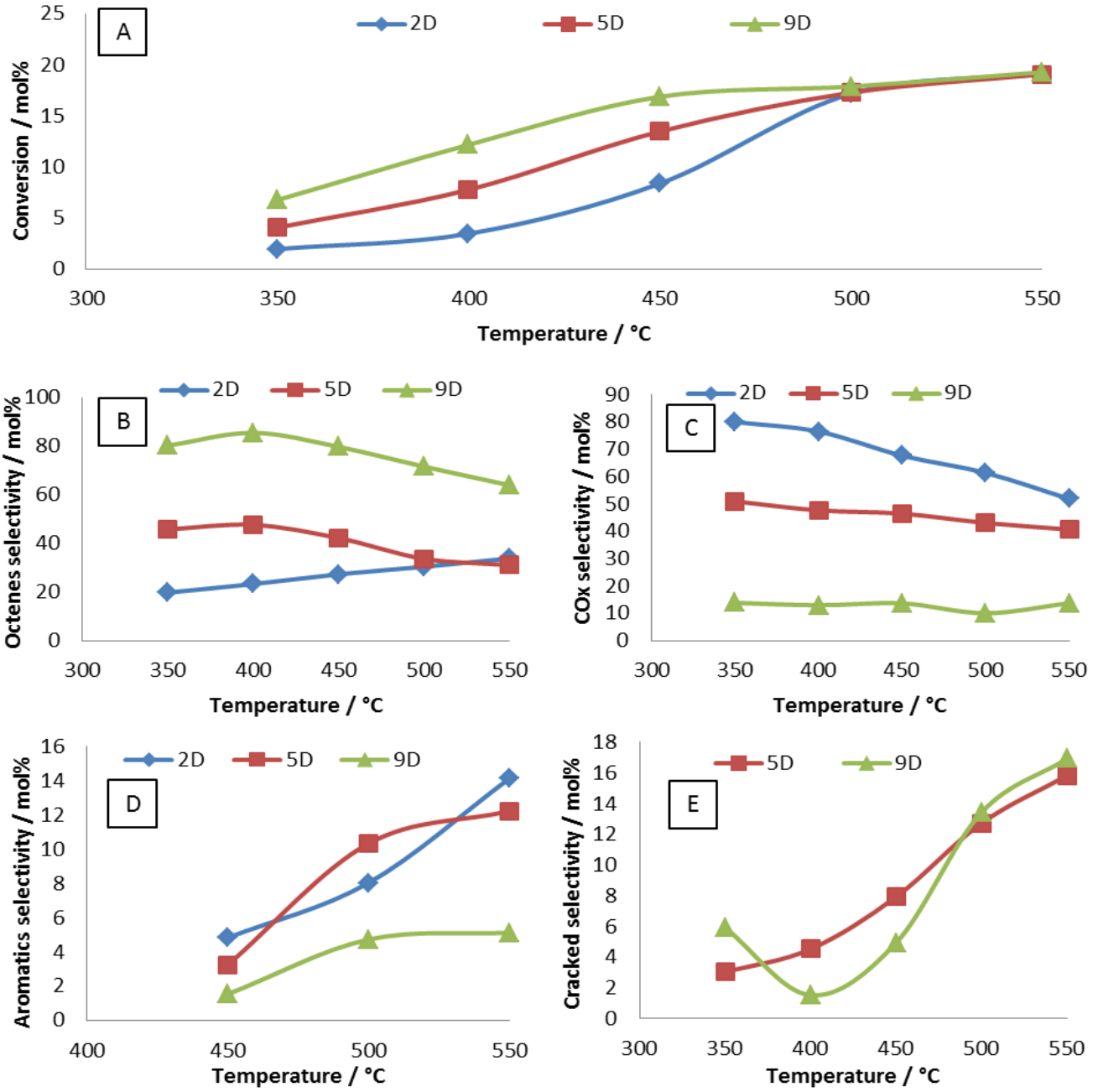

Figure 5.17 Conversion of *n*-octane and selectivity towards products as a function of temperature over catalysts prepared by deposition precipitation (GHSV = 4000 h^{-1} and C:O = 8:2).

weight loading of the metal oxide on the support. This is suspected to be due to the higher proportion of metal oxide being deposited on the outer walls of the SBA-15 support as the weight loading of metal oxide is increased from 2 to 9 wt%. Thus, for the 2D catalyst, the overall selectivity is governed by the metal oxide being predominantly in the pore. As the weight loading increases, the reactions on the outer walls of the support contribute more significantly and subsequently, there is a shift to a higher selectivity toward ODH products. The dominant octene isomer was trans-2-octene, and for the 2D and 5D catalysts ethylbenzene was the dominant aromatic isomer, whereas for the 9D catalyst, xylene is the dominant aromatic product from 500 °C onwards. The formation of octenes and aromatic products for all three catalysts was found to be in accordance with the proposed reaction pathway from Chapter 4.

Aromatic products began to form after 450 °C for all three catalysts and, also, cracked product formation was greater than aromatic product formation at all temperatures for all of the catalysts. A reason for the low aromatic product selectivity is possibly that the formation of aromatic products may be sterically hindered by the active site being present in the pores. The restricted access of the active site also hinders secondary reactions [89] of octenes towards aromatic products and perhaps favours the cracking reaction instead. This means more of the feed is available for thermal cracking of octenes rather than aromatic products being formed, which is likely the reason for the cracked product selectivity is higher than aromatic product selectivity for all catalysts prepared by deposition precipitation.

5.3 The effect of the position of the metal oxide

To determine the effect of the location of the metal oxide, that is, either on the outer walls or predominantly in the pores of the support, the catalytic activity of the catalysts prepared by wet impregnation and deposition precipitation were compared. The aim was to obtain a high conversion of *n*-octane towards the formation of octenes, the desired primary products of the reaction. Catalysts prepared by deposition precipitation showed clear differences with respect to how the metal was incorporated into the structure of the support when compared to catalysts prepared by wet impregnation. This was shown by various characterization techniques, as discussed in Chapter 3.

The shape of N_2 physisorption (Figure 3.3, A5 and A7) isotherms for catalysts prepared by wet impregnation were type IV hysteresis loops, which are indicative of mesopores. However, for catalysts prepared by deposition precipitation, the shapes of the isotherm changes, suggesting blockage of the

pores. Pore blockage was also observed from TEM for these catalysts (Figure 3.4 F-H). The blockage of the pores resulted in the octene isomers spending more time in the pores of the support and they were subsequently converted to carbon oxides and cracked products.

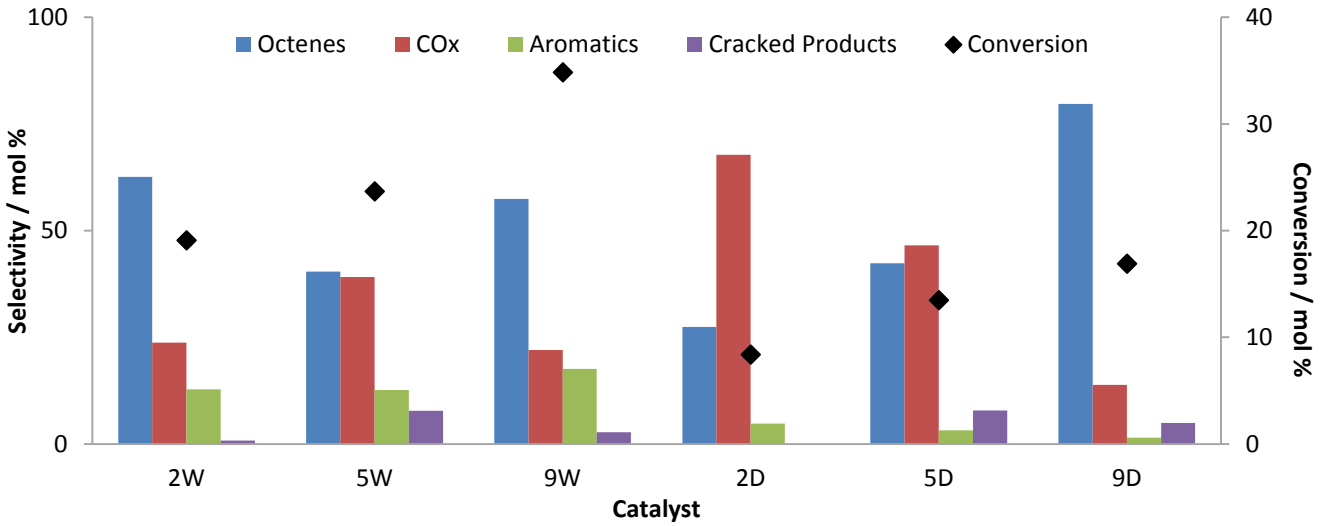

Figure 5.18 Conversion of *n*-octane and selectivity towards products for all catalysts (Temperature = 450 ºC, GHSV = 4000 h^{-1} and C:O = 8:2).

Comparing the results of the catalytic study of the two groups of catalysts; shown in Figure 5.18, it was observed that the conversion was lower at all weight loadings throughout the temperature range for the catalysts prepared by deposition precipitation as compared to those prepared by wet impregnation. Conversion increased with increasing weight loading for both groups of catalysts. This was due to the greater amount of lattice oxygen available to promote conversion of *n*-octane. The selectivity profiles were also different at all weight loadings. Octene selectivity increased and CO_x selectivity decreased with increasing weight loading for both groups of catalysts. Again, this is due to the increased availability of the lattice oxygen to form ODH products and prevent deep oxidation from occurring. Aromatic product selectivity was higher than cracked product selectivity for the catalysts with the metal oxide on the surface and the reverse was found for the catalysts with the metal oxide in the pores at all temperatures and at all weight loadings. This may be because there is steric hindrance limiting the formation of the aromatic compound inside the pore and the thermal cracking reaction is favoured over the aromatization reaction.

For the 2D and 5D catalysts, CO_x was found to be the major product at all temperatures. This may be because, as the olefins are formed over these catalysts, they spend more time in the pores due to the location of the metal oxide and are subsequently converted to carbon oxides, which is the more likely route for the formation of combustion products [122]. Dasireddy *et al.* [123] found that the O^- species was the species of oxygen responsible for secondary combustion of ODH products to form carbon oxides.

The catalysts with metal oxide on the surface have octenes are the major products at lower temperatures but at higher temperatures, CO_x is the dominant product. This was consistent with the assumption that lower weight loading catalysts have high CO_x selectivity and the metal oxide in the pores favours the combustion reaction taking place. However, for the 9 wt% catalysts, the catalyst with the metal oxide in the pores has higher selectivity toward octenes at all temperatures than the catalyst with the metal oxide on the surface. Since the conversions of both catalysts differ, selectivity profiles will need to be compared at isoconversion for the 9 wt% catalysts.

5.4 Product selectivity at isoconversion

Isoconversion profiles for the 9W and 9D catalysts were obtained at 400°C and at 12% *n*-octane conversion are shown in Figure 5.19. The selectivities toward octenes and CO_x products, which are shown in Figure 5.19, were within 1% of each other.This suggests that at a loading of 9 wt% and at the same conversion, the catalysts gave the same product selectivity whether the metal oxide is predominantly in the pores or on the outer walls of the SBA-15 support.

Upon comparison of all the catalysts, the 9D catalyst is the catalyst that does not fit the trend when comparing catalysts with the metal oxide in the pores and the ones with the metal oxide on the surface. This is because both the 2D and 5D catalysts showed higher CO_x selectivity and lower octene selectivity than the 2W and 5W catalysts respectively. However, for the 9D catalyst, the octenes selectivity was higher and CO_x selectivity was lower when compared to the 9W catalyst and the isoconversion results suggest that the catalysts behave in the same way. A reason for this could be that since the 9D catalyst has the highest weight loading, its dispersion of active metal sites may be providing a surface similar in character to that of the 9W catalyst

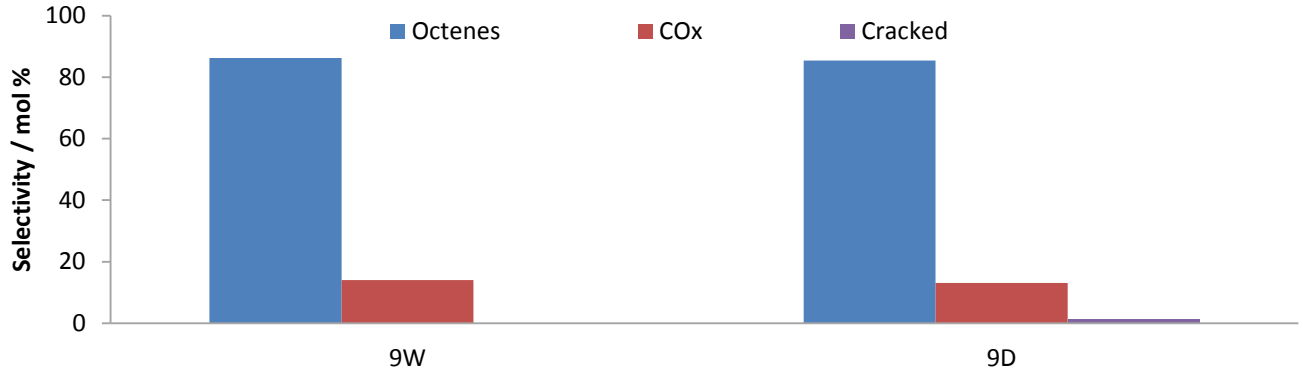

Figure 5.19 Isoconversion results of 9W and 9D catalysts catalyst at 12% conversion of *n*-octane and 400 °C.

The behavior of the 2W and 2D catalysts with respect to the selectivity at isoconversion, as observed in Figure 5.20, suggest a difference in the active surface characteristics of the two catalysts. Hence, when the catalysts particles are suspected to be predominantly in the pores as for the 2D system, the environment is conducive to secondary reactions of octene isomers, hence a high CO_x selectivity was observed. In contrast, for the 2W catalyst, which contains the catalyst particles on the outer walls of the support, desorption of olefinic products reduce their conversion to final oxidation products. The higher selectivity to aromatics over the 2W catalyst also suggests a lower propensity to form deep oxidation products over its surface.

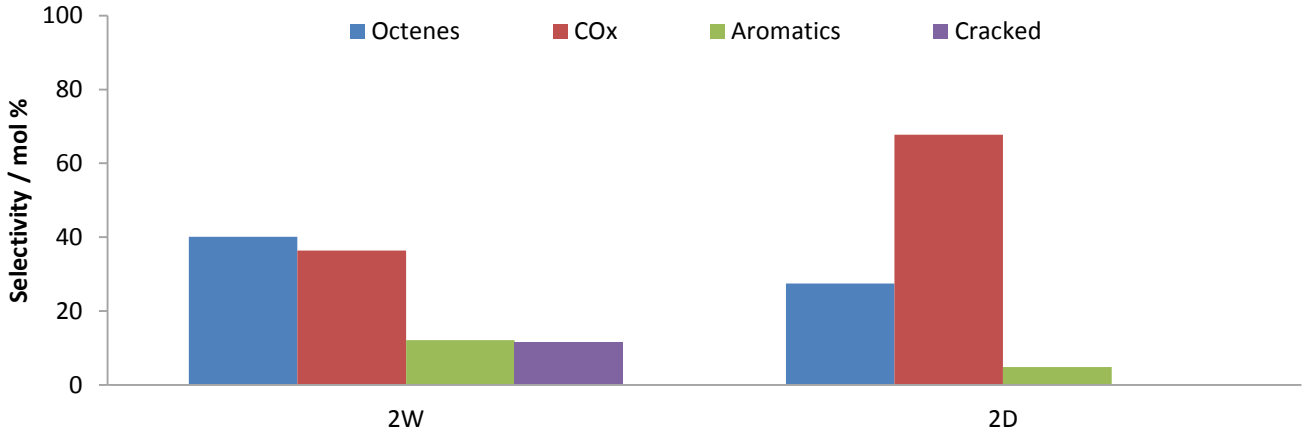

Figure 5.20 Isoconversion results of 2W and 2D catalysts catalyst at 8.5 % conversion of *n*-octane and 450 °C.

Chapter 6

Summary and Conclusion

Manganese oxide catalysts supported on SBA-15 were studied for the oxidative dehydrogenation of *n*-octane. SBA-15 was successfully synthesized via a hydrothermal treatment method that has been well reported [76, 112]. Two groups of catalysts were synthesised using wet impregnation and deposition precipitation, with manganese oxide weight loadings of 2, 5 and 9 wt% for both groups. Powder XRD confirmed the presence of Mn_3O_4 for both groups of catalysts at room temperature. The phase present at lower temperatures was found to be Mn_3O_4 and MnO was the dominant phase at higher temperatures as shown by the results of *insitu* XRD. Under reaction conditions, both Mn_3O_4 and MnO exist, however, the exact ratio was dependant on factors such as C:O ratio, temperature and contact time.Nitrogen physisorption revealed type IV hysteresis loops for the SBA-15 and for catalysts prepared by wet impregnation, indicating mesopores. However, for catalysts prepared by deposition precipitation, the shape of the isotherm changed, indicating pore blockage.

Surface areas and pore volumes for catalysts prepared by wet impregnation were higher than those for catalysts prepared by deposition precipitation at the same weight loading, indicating blockage of the pores.Electron microscopy showed the different position of the metal oxide clearly, with TEM showing the catalysts prepared by wet impregnation having metal oxide on the surface while the pores appeared to be blocked or filled with metal oxide particles for catalysts prepared by deposition precipitation. SEM - EDX showed the varying distribution of the metal throughout the support for the two groups of catalysts, confirming that the synthesis method impacted on the location of the metal.

Temperature programmed analyses in the form of TPR and TPO showed 2 distinct peaks for both the reduction of Mn_3O_4 to MnO and the re-oxidation of MnO to Mn_3O_4. These peaks were present for both groups of catalysts, but higher reduction and lower re-oxidation temperatures were required for the 9D catalyst when compared to the 9W catalyst. This is likely because of the metal oxide particles being predominantly in the pores for the 9D catalyst, as opposed to being mostly situated on the outer walls of the support for the 9W catalyst. Spent catalyst characterization revealed that no metal leaching took place and there were no major structural changes for both groups of catalysts. There was an indication of low amounts of coke present by the decrease in BET surface area for the spent catalysts.

Oxidative dehydrogenation reactions were carried out in a continuous flow fixed-bed microreactor system. The non-catalytic experiments showed a maximum contribution of 5% *n*-octane conversion. The reaction products observed were octene isomers, aromatic compounds, cracked products and carbon oxides. The SBA-15 support was found to be active for the oxidative dehydrogenation of *n*-octane. The 2W catalyst was tested and it showed enhanced activity when compared to the support. Based on optimization of reaction conditions using the 2W catalyst, the ideal reaction conditions were found to be at a particle pellet sizes of 600 – 1000 μm, a GHSV of 4000 h^{-1} and a carbon to oxygen 8:2. A time-on-stream experiment showed that the catalyst was stable for up to 48 hours and the catalyst was found to be cyclable. The catalytic results showed manganese oxide followed a Mars and van Krevelen reaction pathway, i.e the manganese oxide was reduced by *n*-octane and the reduced catalyst was thereafter oxidized by the oxygen present in feed. These results were then coupled with the characterization results to establish a proposed pathway for the formation of primary products of this reaction, namely octenes, as well as secondary and final oxidation products.

Upon comparison of the catalytic results of all catalysts prepared by wet impregnation, conversion of *n*-octane was found to increase with increasing metal loading. The formation of ODH reaction products was favoured by higher metal content due to the higher amount of lattice oxygen available. This is the reason the 9W catalyst showed the highest conversion and selectivity towards octene and aromatic compounds. The catalytic results of catalysts prepared by deposition precipitation indicated that the conversion of *n*-octane over these catalysts were low due to the restricted access to the metal oxide. For these catalysts, octenes formed but spent more time in the pores of the support and were consequently converted to carbon oxides. The weight loading of these catalysts controlled the proportion of metal oxide primarily in the pores to the amount present on the outer walls of the support. This proportion controlled the rate at which octenes were converted to carbon oxides. Aromatic product selectivity was low for catalysts prepared by deposition precipitation, likely due to steric hindrance in the pores of the support. Isoconversion experiments revealed that the surface characteristics of the 9D catalyst may be similar to the 9W catalyst since they have similar selectivity profiles at the same conversion. However, for the 2 wt% catalysts, the surfaces properties of these two catalysts were different and hence they provided two distinct selectivity profiles under isoconversion conditions.

Chapter 7

Summary and motivation for future work

The number of industrial coal-to-liquid, gas-to-liquid and petrochemical plants worldwide are increasing each year. With the rise in numbers of these plants, there is also a rise in the by-products manufactured, such as alkanes or paraffins [29]. Branched alkanes may be used in fuels due to their high octane numbers, but linear alkanes possess low octane numbers and find less use in fuels. This makes linear alkanes appealing for use as a feedstock for a large-scale industrial feedstock. Aromatic, oxygenated and olefinic compounds are well known industrial feedstocks for a number of different processes. With alkanes being precursors to these compounds and having a relatively lower value, it would be economically viable to substitute the more expensive feedstocks with their alkane precursors [30]. Thus, any process that is able to activate alkanes and convert them to value added products with a substantial yield would be of great interest industrially.

There has been extensive research carried out in paraffin activation, as discussed in Chapter 1. Also mentioned previously were the different methods of paraffin activation, namely cracking, dehydrogenation and oxidative dehydrogenation. Of these diverse routes of paraffin activation, oxidative dehydrogenation was deemed to be the best of the three methods for a research initiative. This was due to the low energy input required for the reaction and lower amount of coking when compared to the other methods of paraffin activation [36]. The major drawback to oxidative dehydrogenation is that side reactions are more apparent as compared to dehydrogenation. A typical example would be carbon oxide formation, which is very low or does not form with dehydrogenation [37]. However, this drawback has lead to an industrial demand for catalysts that can produce high selectivities toward desired products at reasonable conversions, while hindering the formation of unwanted side reactions such as carbon oxides. This has lead into many research endeavours into the oxidative dehydrogenation of paraffins to produce value added products.

Supported transition metal oxides have been widely reported to be used as heterogeneous catalysts for the oxidative dehydrogenation of paraffin molecules, as discussed in Chapter 1. Transition metals were chosen to be used as redox catalysts and manganese was the choice of transition metal due to its large number of stable oxidation states allowing easier manipulation of is redox potential, which allows for better performance as a redox catalyst [69]. The choice of support was SBA-15, a well ordered silica

based support. The desirable properties of SBA-15, such as high surface area, high thermal stability, well ordered mesoporous structure, open channels and relatively thick silica walls make it suitable for use as a catalyst support [78-80]. In order to obtain a selective catalyst for the oxidative dehydrogenation of a paraffin molecule, a basic principle of heterogeneous catalysis was looked at. This was the accessibility of the active site. By altering the accessibility of the active site, a catalyst can be tuned in terms of activity and selectivity. This was looked at using manganese oxide supported on SBA-15 catalysts.

The SBA-15 support was synthesized via a previously reported hydrothermal method [76, 112]. Wet impregnation and deposition precipitation were used to prepare two groups of catalysts, with each group containing 2, 5 and 9 wt% of manganese oxide. Powder XRD analyses of all catalysts showed that the dominant phase present was Mn_3O_4 at room temperature, indicated by the peaks at 2θ angles of 33 º, 37 º and 55 º corresponding to d-spacing values of 2.73, 2.42 and 1.67 Å respectively [113]. All catalysts also showed a large broad peak at lower 2θ values which can be attributed to the SBA-15 support. The redox behaviour of the catalyst was monitored using *in situ* XRD, and under reduction the dominant phase was found to be MnO, with complete reduction of the Mn_3O_4 phasing occurring at 450 °C. Nitrogen physisorption isotherms showed that the SBA-15 and catalysts prepared by wet impregnation showed type IV hysteresis loops, which indicate the presence of mesopores. However, for catalysts prepared by deposition precipitation, the relative quantity of nitrogen adsorbed is lower at the same metal loading when compared the catalysts prepared by wet impregnation. The shape of the isotherm also changes. This suggests that the pores are blocked for catalysts prepared by deposition precipitation.

Comparing the surface areas and pore volumes for the two groups of catalysts at the same weight loading, the catalysts prepared by deposition precipitation have lower values, again suggestive of pore blockage. TEM clearly showed the well ordered structure and hexagonal mesopores of the SBA-15. The support structure remains intact after wet impregnation (as seen from TEM images of the 2W, 5W and 9W catalysts) with the metal oxide being seen primarily on the surface of the support. However, with catalysts prepared by deposition precipitation, the pores of the supports appear to be blocked or filled with metal oxide particles (as seen from TEM images of the 2D, 5D and 9D catalysts). Metal oxide particle sizes were smaller for the D-series of catalysts than the W-series, which is likely the reason for the different location of the metal oxide with respect to the support. SEM-EDX mapping of the 9W catalyst showed large amounts of manganese present on the surface of the support, which was confirmed

by line and point scans of the sample. In contrast, for the 9D catalyst, EDX mapping, line and point scans indicated an even distribution of the metal oxide throughout the support. Temperature programmed analyses in the form of TPR and TPO revealed two peaks for both the 9W and 9D catalysts, for the reduction of Mn_3O_4 to MnO, with oxidation showing the reverse. The difference in reduction temperatures for the 9D and 9W catalysts was attributed to the difference in location of the metal oxide. Oxygen chemisorption analyses showed that the 2D catalyst had a higher amount of oxygen chemisorbed than the 2W catalyst, with SBA-15 chemisorbing the lowest when compared to the two catalysts. The difference in oxygen chemisorption amounts is due to the different metal dispersions for the two catalysts. There are further characterisation techniques that may provide additional insight in the properties of the catalyst. Cross-sectional SEM-EDX would provide a clear picture of the exact position of the metal oxide with respect to the support. Temperature programmed desorption and pulse chemisorption may also offer useful information on the acid/base properties of the catalyst.

Catalytic testing was carried out in a continuous flow fixed-bed reactor system and prior to testing, the non-catalytic contribution of this reaction was found to be minimal. The SBA-15 support and 2W catalyst were initially tested, with both being active for the oxidative dehydrogenation of *n*-octane. The reaction product groups obtained were octene isomers, aromatic compounds, cracked products and carbon oxides, with the first two product groups being desired reaction products. Although the support was found to be active, the introduction of metal oxide onto the support did provide enhanced catalytic activity and a diverse selectivity profile when compared to the catalytic results of the support. The dominant product group obtained over the support and 2W catalyst were octenes. The 2W catalyst was then used to optimise reactor conditions in terms of catalyst particle pellet size, GHSV and C:O ratio. Changes in reactor conditions were found to have a direct impact in the conversion of *n*-octane and the selectivity profile obtained over the 2W catalyst. The optimum reactor conditions were found to be at a GHSV of 4000 h^{-1} and a C:O ratio of 8:2, with a catalyst particle size of 600 – 1000 μm. These conditions were chosen based on conversion of *n*-octane and selectivities toward desired products. In addition to obtaining an optimum yield toward desired products, the analysis of results obtained from optimisation of reaction conditions, coupled with characterisation data, provided insight into the behaviour of the catalyst. The redox behaviour of the catalyst was established and the catalyst was found to follow a Mars and van Krevelen mechanism for the formation of primary products, which were octenes. Individual reaction pathways for each of the product obtained was also established.

All catalysts were then tested under optimum conditions and it was found that catalysts prepared by wet impregnation gave a higher conversion of *n*-octane than catalysts prepared by deposition precipitation at the same weight loading. This was likely due to the better accessibility of the active site for catalysts prepared by wet impregnation. However, the restricted access of the active site for catalysts prepared by deposition precipitation did lead the higher selectivities toward one product group, with the product group obtained being dependant on the weight loading. At lower weight loadings, the dominant product group was carbon oxides and at higher weight loadings, it was octenes. From both groups of catalysts, the 9 wt% catalysts were found the best weight loading based on conversion and selectivity toward desired products. An isoconversion experiment of the 9 wt% catalysts provided a similar selectivity profile, which suggested that the dispersion of the active metal sites for the 9D catalyst may provide a surface similar that that of the 9W catalysts. However, an isoconversion study of the 2 wt% catalysts showed 2 distinct selectivity profiles, indicating different surface characteristics for these catalysts.

This research endeavour found novelty in the usage of manganese oxide catalysts supported on SBA-15 for the oxidative dehydrogenation of *n*-octane. Coupling characterisation and catalytic data, the role of the support and catalytic behaviour of the metal oxide during the reaction was determined. The redox cycle of the catalyst was established and the reaction mechanism for the manganese oxide catalysts was found. Another distinctive aspect of this project was the alteration of the accessibility of the active site to influence catalyst performance. The 9W catalyst showed the highest conversion of *n*-octane, while the 9D catalyst had the greatest selectivity toward octenes. However, there are various other paths that could be taken to expand this research initiative and be carried out as part of future work for this study.

For instance, in order to substantiate the influence of the well ordered, mesoporous structure of the SBA-15 support structure, a first step for future work would be to prepare catalysts using amorphous silica of a similar surface area to that of the synthesized support. In this way, any changes in catalyst properties and catalytic testing results can be correlated to the difference between the well defined structure of the SBA-15 and the irregular structure of amorphous silica.

The SBA-15 support for this study was found to possess basic sites which resulted in the high selectivity toward octene isomers. However, it has been widely reported that SBA-15 modified with transition metals into the framework can alter the acid/base properties of the support. [77, 83-86]. This was done by direct synthesis or a post grafting method in order to incorporate the metal oxide into the support framework. Sun *et al.* [77] discussed the incorporation of various transition metals into SBA-15 such as

Fe and Al. This provided more acid sites present on the catalyst. The addition of acid sites to the already present basic sites on the support should provide a very different selectivity profile. This may lead to a greater formation of aromatic products or perhaps oxygenated compounds may begin to form. On the other hand, Vizcaino *et al.* [126] showed that incorporating Ca and Mg into the SBA-15 framework increased the basic character of the support. They used incipient wetness impregnation to incorporate these metals, after which Cu and Ni were supported on the modified SBA-15. The incorporation of metals into the framework also provided a better dispersion of Cu and Ni after impregnation. A modified support with increased basicity may provide even greater selectivity toward octenes.

The drawback to obtaining primarily octenes in a reaction product profile is that a mixture of octene isomers was obtained, with trans-2-octene found to have the highest selectivity for this project. A catalyst that can produce a single octene isomer instead or a mixture from *n*-octane would be very appealing for industrial use. The terminal octene isomer would be the most sought after isomer, as it is the most reactive of the isomers [27, 28] and hence difficult to produce as the single reaction product. A way to try and obtain terminal activation of the octane molecule could be by limiting the interaction between the feed and the pores of the support.

Zhao *et al.* [82] synthesized SBA-15 with different morphologies. Morphologies resembling fibers, rope, doughnuts and spheres were synthesized through the cosolvent, cosurfactant, and inorganic electrolyte approaches. Pitchumani *et al.* [112] also synthesized SBA-15 with morphologies in the form of films and cakes, with the dependant factor that determined the morphology during the synthesis being stirring rate. This might be a viable approach in order to limit the support and reactant interaction. Wang *etal.* [127] synthesized SBA-15 with varying pore diameters. Pore diameters were tuned using different synthesis conditions and by using trimethylbenzene as a swelling agent. This study shows that the pore sizes of SBA-15 can be tuned and this would be a more interesting route to try and obtain activation on the terminal position of the *n*-octane molecule.

Other innovative research ideas can be looked at in the future work for this project. Other higher linear alkanes such as *n*-decane can be investigated. Other metals can be supported on SBA-15 along with manganese to produce bimetallic catalysts. This research project provided a firm foundation upon which to build. The detailed insight into catalytic behaviour and performance previously discussed together with novel future plans provide a unique research endeavour that has the potential to be of great interest scientifically, as well as offering the possibility of having further industrial applications. With this in

mind, it would be beneficial to continue with the Masters research project based on the future work plans outlined and upgrade this project to transform this into a PhD research project.

References

[1] G. Ertl, Angewandte Chemie International Edition 47 (2008) 3524-3535.

[2] J.M. Thomas, W.J. Thomas, Principles and Practice of Heterogeneous Catalysis, VCHPublishers Inc., New York, 1997.

[3] M. Bowker, The Basis and Applications of Heterogeneous Catalysis, Oxford University Press, New York, 1998.

[4] J.W. Niemantsverdriet, Spectroscopy in Catalysis: An Introduction, 3 ed., Wiley-VCH, Weinheim, 2007.

[5] J. Hagen, Industrial Catalysis, Wiley-VCH, Weinheim, 2008.

[6] G. Ertl, H. Knozinger and J. Weitkamp, Handbook of Heterogeneous Catalysis, Wiley-VCH, Federal Republic of Germany, Vol. 1, 1997.

[7] BASF The Chemical Company, Heterogeneous Catalysts Yesterday, Today, Tomorrow, BASF SE Communication BASF Group, Ludwigshafen, 2008.

[8] A. Haynes, P. M. Maitlis, G. J. Sunley, M. J. Howard, Journal of the American Chemical Society 126(2004) 2847 – 2861.

[9] J. Chetty, PhD Thesis, University of KwaZulu-Natal, 2006.

[10] M.E. Davis, R.J. Davis, Fundamentals of Chemical Reaction Engineering, McGraw Hill, New York, 2003.

[11] G. C. Bond, Heterogeneous Catalysis: Principles and Applications, Oxford University Press, Oxford, 1987.

[12] J. T. Richardson, Principles of Catalyst Development, Plenum Press, New York, 1989.

[13] P. W. Atkins, J. de Paula, Physical Chemistry, Oxford University Press, Oxford, 8th edition, 2006

[14] T. Chetty, PhD Thesis, University of KwaZulu-Natal, 2013.

[15] J.G. de Vries, The Handbook of Homogeneous Hydrogenation, Wiley-VCH, 2007.

[16] F.R. Hartley, Supported metal complexes, D. Riedel Publishing Company, Holland, 1985.

[17] P. Gallezot, D. Richard, Catalysis Reviews: Science and Engineering 40 (1998) 81-126.

[18] A. Gervasini, S. Bennici, Applied Catalysis A: General 281 (2005) 199-205.

[19] W.H. Chen, Y.J. Syu, International Journal of Hydrogen Energy 35 (2010) 10179-10189.

[20] D. Stolten, Hydrogen and Fuel Cells: Fundamentals, Technologies and Applications, John Wiley & Sons, New York, 2010.

[21] L.Y. Sung, B.J. Hwang, K.L. Hsueh, F.H. Tsau, Journal of Power Sources 195 (2010) 1630-1639.

[22] M.M. Yung, Z. Zhao, M.P. Woods, U.S. Ozkan, Journal of Molecular Catalysis A: General 279 (2008) 1-9.

[23] O. Pozdnyakova, D. Teschner, A. Wootsch, J. Kröhnert, B. Steinhauer, H. Sauer, L. Toth, F.C. Jentoft, A. Knop-Gericke, Z. Paál, R. Schlögl, Journal of Catalysis 237 (2006) 1-16.

[24] F. Cipitì, V. Recupero, Chemical Engineering Journal 146 (2009) 128-135.

[25] R. Padilla, M. Benito, L. Rodríguez, A. Serrano-Lotina, L. Daza, Journal of Power Sources 192 (2009) 114-119.

[26] F. Mariño, C. Descorme, D. Duprez, Applied Catalysis B: Environmental 54 (2004) 59-66.

[27] J. Clayden, S. Warren, P. Wothers, N. Greeves, Organic chemistry, 6th edition, Oxford University Press, 2001.

[28] P.Y. Bruice, Organic Chemistry, 5th edition, Pearson Prentice Hall, New Jersey, 2007.

[29] B.Pillay, M. R. Mathebula, H. B. Friedrich, Applied Catalysis A: General 361 (2009) 57-64.

[30] V.D.B.C. Dasireddy, S. Singh, H. B. Friedrich, Applied Catalysis A: General 456 (2013) 105-117.

[31] S. Altwasser, C. Welker, Y. Traa, J. Weitkamp, Microporous and Mesoporous Materials 83 (2005) 345-356.

[32] B.B. Bhasin, J.H. McCain, B.V. Vora, T. Imai, P.R. Pujado, Applied Catalysis A: General 221 (2001) 397-419.

[33] S. Jongpatiwut, P. Sackamduang, T. Rirksomboon, S. Osuwan, D.E. Resasco, Journal of Catalysis 218 (2003) 1-11.

[34] V.D.B.C. Dasireddy, H.B. Friedrich, S. Singh, Applied Catalysis A: General 467 (2013) 142-153.

[35] B. Shi, B.H. Davis, Journal of Catalysis 157 (1995) 626-630.

[36] G. Rothenberg, Catalysis Concepts and Green Applications, Wiley-VCH, Weinheim, 2008.

[37] G. Neri, A. Pistone, S. De Rossi, E. Rombi, C. Milone, S. Galvagno, Applied Catalysis A: General 260 (2004) 75-86.

[38] N. Govender, MSc Thesis, University of KwaZulu-Natal, 2002.

[39] N. Govender, H.B. Friedrich, M. Janse Van Vuuren, Catalysis Today 97 (2004) 315-324.

[40] N. Govender, PhD Thesis, University of KwaZulu-Natal, 2007.

[41] N. Govender, H.B. Friedrich, M.R. Mathebula,Applied Catalysis A: General 297 (2006) 81-89.

[42] M. Ramdeen, MSc Thesis, University of KwaZulu-Natal, 2003.

[43] N. Masilo, MSc Thesis, University of KwaZulu-Natal, 2009.

[44] T. Naicker, PhD Thesis, University of KwaZulu-Natal, 2010.

[45] B. Pillay, M.R. Mathebula, H.B. Friedrich, Catalysis Letters 141 (2011) 1297-1304.

[46] A.S. Mahomed, PhD Thesis, University of KwaZulu-Natal, 2005.

[47] A.S. Mahomed, H.B. Friedrich, Applied Catalysis A: General 347 (2008) 11-22.

[48] M. Bux, PhD Thesis, University of KwaZulu-Natal, 2010.

[49] E.A. Elkhalifa, PhD Thesis, University of KwaZulu-Natal, 2010.

[50] E. Elkhalifa, H.B. Friedrich, Catalysis Letters 141 (2011) 554-564.

[51] T.C. Makatini, MSc Thesis, University of KwaZulu-Natal, 2012.

[52] M. Narayanappa, V. D. B. C. Dasireddy, H. B. Friedrich,Applied Catalysis A: General 447-448 (2012) 1343-1351.

[53] P. Botella, J.M. Lopez Nieto, A. Dejoz, M.I. Vazquez, Catalysis Today 78 (2003)507-512.

[54] J.M. Lopez Nieto, P. Botella, P. Concepcion, A. Dejoz, M.I. Vazquez, Catalysis Today 91-92 (2004) 241-245.

[55] G.J. Hutchings, J.K. Bartley, Y.H. Taufiq-Yap, S.N. Asrina, N. Dummer, Journal of Natural Gas Chemistry 20 (2011) 635-638.

[56] G.J. Hutchings, T.J. Hall, J.S.J. Hargreaves, R.W. Joyner, S.H. Taylor, Fuel Processing Technology 42 (1995) 151-178.

[57] G.J. Hutchings, G. Jin, W. Weng, Z. Lin, N.F. Drummer, S.H. Taylor, Journal of Catalysis 296 (2012) 55-64.

[58] G.J. Hutchings, B. Solsona, T. Garcia, C. Jones, S.H. Taylor, A.F. Carley, Applied Catalysis A: General 312 (2006) 67-76.

[59] G.J. Hutchings, B. Solsona, T. Garcia, S.H. Taylor, M. Makkee, Applied Catalysis A: General 365 (2009) 222-230.

[60] G.J. Hutchings, S.H. Taylor, Catalysis Today 49 (1999) 105-113.

[61] G.J. Hutchings, S.H. Taylor, M.L. Palacois, D.F. Lee, Catalysis Today 81 (2003)171-178.

[62] S. Pradhan, J.K. Bartley, D. Bethell, A.F. Carley, M. Conte, S. Golunski, M.P. House,R.L. Jenkins, R. Lloyd, G.J. Hutchings, Nature 4 (2012) 134-139.

[63] R. Lloyd, R.L. Jenkins, M. Piccinini, Q. He, C.J. Kiely, A.F. Carley, S.E. Golunski,D. Bethell, J.K. Bartley, G.J. Hutchings, Journal of Catalysis 283 (2011) 161-167.

[64] J.M. López Nieto, J. Soler, P. Concepción, J. Herguido, M. Menéndez, J. Santamaría,Journal of Catalysis 185 (1999) 324-332.

[65] A. Corma, C. Goberna, J.M. Lopez Nieto, N. Paredes, M. Perez, Studies in Surface Science and Catalysis 69 (1991) 409-416.

[66] J.M. López Nieto, A. Dejoz, M.I. Vazquez, W. O'Leary, J. Cunningham, Catalysis Today 40 (1998) 215-228.

[67] A. Dejoz, J.M. López Nieto, F. Márquez, M.I. Vázquez, Applied Catalysis A: General 180 (1999) 83-94.

[68] I. Ramli, P. Botella, F. Ivars, W. Pei Meng, S.M.M. Zawawi, H.A. Ahangar, S. Hernández, J.M.L. Nieto, Journal of Molecular Catalysis A 342–343 (2011) 50-57.

[69] F. Cavani, F. Trifirò, Catalysis Today 51 (1999) 561-580.

[70] A. Corma, Journal of Catalysis 216 (2003) 298-312.

[71] A. Corma, M. Boronat, Catalysis Today 169 (2011) 52-59.

[72] A. Corma, H. Garcia, Catalysis Today 38 (1997) 257-308.

[73] A. Corma, D. Kumar, Studies in Surface Science and Catalysis 117 (1998) 201-222.

[74] C.T. Kresge, M.E. Leonowicz, W.J. Roth, J.C. Vartuli, J.S. Beck, Nature 359 (1992) 710-712.

[75] J.S. Beck, J.C. Vartuli, W.J. Roth, M.E. Leonowicz, C.T. Kresge, K.D. Schmitt, C.T.W. Chu, D.H. Olson, E.W. Sheppard, S.B. McCullen, J.B. Higgins, J.L. Schlenker, Journal of the American Chemical Society 114 (1992) 10834-10843.

[76] D.Y. Zhao, J.L. Feng, Q.S. Huo, N. Melosh, G.H. Fredrickson, B.F. Chmelka, G.D.Stucky, Science 279 (1998) 548-552.

[77] B. Sun, L. Li, Z. Fei, S. Gu, P. Lu, W. Ji, Microporous and Mesoporous Materials 186 (2014) 14-20.

[78] A. Taguchi, F. Schüth, Microporous and Mesoporous Materials 77 (2005) 1-45.

[79] B. L. Newalkar, S. Komarneni, Chemistry of Materials 13 (2001) 4573-4579.

[80] B. Samran, T. J. White, S. Wongkasemjit, Journal of Porous Materials 18 (2011):167-175.

[81] M. Colilla, F. Balas, M. Manzano, M. Vallet-Regı Chemistry of Materials 19 (2007) 3099-3101.

[82] D. Zhao, J. Sun, Q. Li, G. D. Stucky,Chemistry of Materials 12 (2000) 275-279.

[83] A. Vinu, V. Murugesan, W. Böhlmann, M. Hartmann, Journal of Physical Chemistry B 108(2004) 11496-11505.

[84] A. Vinu, D.P. Sawant, K. Ariga, K.Z. Hossain, S.B. Halligudi, M. Hartmann, M.Nomura, Chemistry of Materials 17 (2005) 5339-5345.

[85] S.Y. Chen, C.Y. Tang, J.F. Lee, L.Y. Jang, T. Tatsumi, S. Cheng, Journal of Materials Chemistry. 21(2011) 2255-2265.

[86] M. Selvaraj, S. Kawi, D.W. Park, C.S. Ha, Microporous and Mesoporous Materials 117(2009) 586-595.

[87] E.S. Vasiliadoub, T.M. Eggenhuisenc, P. Munnikc, P.E. de Jonghc, K.P. de Jongc, A.A. Lemonidou, Applied Catalysis B: Environmental 145 (2014) 108-119.

[88] R. Huang, H. Yan, L. Li, D. Deng, Y. Shu, Q. Zhang,Applied Catalysis B: Environmental 106 (2011) 264-271.

[89] Y. Lou, H. Wang, Q. Zhang, Y. Wang, Journal of Catalysis 247 (2007) 245-255.

[90] T. Ressler, A. Walter, Z.-D. Huang, W. Bensch, Journal of Catalysis 254 (2008) 170-179.

[91] J.A. Meleroa, J. Iglesiasa, J. M. Arsuagaa, J. Sainz-Pardoa, P. de Frutosb, S. Blazquezb,Applied Catalysis A: General 331 (2007) 84-94.

[92] A. Dinse, S. Khennache, B. Frank, C. Hess, R. Herbert, S.Wrabetz, R. Schlögl, R. Schomäcker, Journal of Molecular Catalysis A: Chemical 307 (2009) 43-50.

[93] M. Sun, B. Lan, L. Yun, F. Ye, W. Song, J. He, G. Diao, Y. Zheng, Materials Letters 86 (2012) 18-20.

[94] T.L.F. Favre, P.J. Seijsener, P.J. Kooyman, A. Maltha, A.P. Zuur, V. Ponec, Catalysis Letters 1 (1988) 457-460.

[95] A. Maltha, S.C. van Wermeskerken, T.L.F. Favre, P.A.J.M. Angevaare, E.J. Grootendorst, C.A. Koutstaal, A.P. Zuur, V. Ponec, Catalysis Today 10 (1991) 387-391.

[96] K. H. Kung, M. B. Mcbride, Clay and Clay Minerals 36 (1998) 297-302.

[97] L. Lamaita, M. A. Peluso, J.E. Sambeth, H. J. Thomas,Applied Catalysis B: Environmental 61 (2005) 114–119.

[98] W.Wang, Y.Yang, J. Zhang,Applied Catalysis A: General 131 (1995) 189-206.

[99] L. A. Boot, M. H.J.V. Kerkhoffs , B. Th. van der Linden, J. van Dillen , J. W. Geus, F. R. van Buren, Applied Catalysis A: General 137 (1996) 69-86.

[100] L.E. Cadus, O. Ferretti, Catalysis Letters 69 (2000) 199-202.

[101] H. Zhou , J.Y. Wang, X. Chen, C. L. O'Young , S. L. Suib, Microporous and Mesoporous Materials 2I (1998) 315-324.

[102] R. Rosal, M. S. Gonzalo, A. Rodríguez, J. A. Perdigón-Melón, E. García-Calvo, Chemical Engineering Journal 165 (2010) 806-812.

[103] R. Zhang, D. Shi, N. Liu, Y.Cao, B. Chen, Applied Catalysis B: Environmental 146 (2014) 79-93.

[104] J. Tang, Y. Zu, W. Huo, L.Wang, J. Wang, M. Jia , W. Zhang, W.R. Thiel, Journal of Molecular Catalysis A: Chemical 355 (2012) 201-209.

[105] G. Satish-Kumar, M. Palanichamy, M. Hartmann, V. Murugesan, Microporous and Mesoporous Materials 112 (2008) 53-60.

[106] G. Satish-Kumar, M. Palanichamy, M. Hartmann, V. Murugesan, Catalysis Communications 8 (2007) 493-497.

[107] Q. Tang, S. Hu, Y. Chen, Z.Guo, Y.Hu, Y.Chen, Y.Yang, Microporous and Mesoporous Materials 132 (2010) 501-509.

[108] T.Tsoncheva, G. Issa, I. Genova, M. Dimitrov, Journal of Porous Materials 20 (2013) 1361-1369.

[109] P. Visuvamithiran, K. Shanthi, M. Palanichamy, V. Murugesan, Catalysis Science and Technology (2013) 2340 – 2348.

[110] M. Jin, J. H. Kim, J. M. Kim, J. K. Jeon, J. Jurng, G. N. Bae, Y. K. Park, Catalysis Today 204 (2013) 108-113.

[111] H. Pérez, P. Navarro, J. J. Delgado, M. Montes, Applied Catalysis A: General 400 (2011) 238-248.

[112] R. Pitchumani, W. Li, M. Coppens,Catalysis Today 105 (2005) 618-622.

[113] J. Lai, K. V. P. M. Shafi, A. Ulman, N. Yang, M. Cui, T. Vogt, C. Estournès, ACS Division of Fuel Chemicals 48 (2003) 729-730.

[114] M. Che, J. C. Vèdrine, Characterization of Solid Materials and Heterogeneous Catalysts, Volume 1, Wiley-VCH.

[115] M. Che, J. C. Vèdrine, Characterization of Solid Materials and Heterogeneous Catalysts, Volume 2, Wiley-VCH.

[116] H. Hattori, Chemical Reviews 95 (1995) 537-550.

[117] E. Heracleous, M.Machli, A. A. Lemonidou, I. A. Vasalos, Journal of Molecular Catalysis A: Chemical 232 (2005) 29-39.

[118] C. Perego. , S. Peratello, Catalysis Today 52 (1999) 133-145.

[119] M. A. Vannice, Catalysis Today 123 (2007) 18-22.

[120] U. Stienke, U. Kretzshmar, I. Ebert, H. P. Hennig, L. I. Barsova, T. K. Jurik, Reactivity of Solids 4 (1987) 1-21.

[121] C. Doornkamp, V. Ponec, Journal of Molecular Catalysis A: Chemical 162 (2000) 19-32.

[122] R. Burch, E. M. Crabb, Applied Catalysis A: General 97(1993) 49 – 65.

[123] V.D.B.C Dasireddy, S. Singh, H.B. Friedrich, Applied Catalysis A: General 421-422 (2012) 58-69.

[124] M. Laniecki, M. Wojtowski. Studies in Surface Science and Catalysis 158 (2005) 757-764.

[125] B. K. Hodnett, Heterogeneous Catalytic Oxidation: Fundamental and Technological Aspects of the Selective and Total Oxidation of Organic Compounds, 1st ed, John Wiley & Sons, 2000.

[126] A. J. Vizcaino, A. Carrero, J. A. Calles, Catalysis Today 146 (2009) 63-70.

[127] Y. Wang, M. Noguchi, Y. Takahashi, Y. Ohtsuka, Catalysis Today 68 (2001) 3-9.

Appendix

Table A1: Sample calculation for moles of 1-octene obtained

Mass of Organic Layer	2,09 g
Percentage Peak Area of 1-octene	0,78
Response Factor	0,91
Corrected Area = Percentage Peak Area/Response Factor	0,85
Normalised Peak Area = (Corrected Area/Sum of all corrected areas in product analysis) x 100	69,51
Mass of Product = (Normalised Area x Mass of organic layer)/100	1,46 g
Moles of Product = Mass of Product/Molar Mass of Product	0,013mol

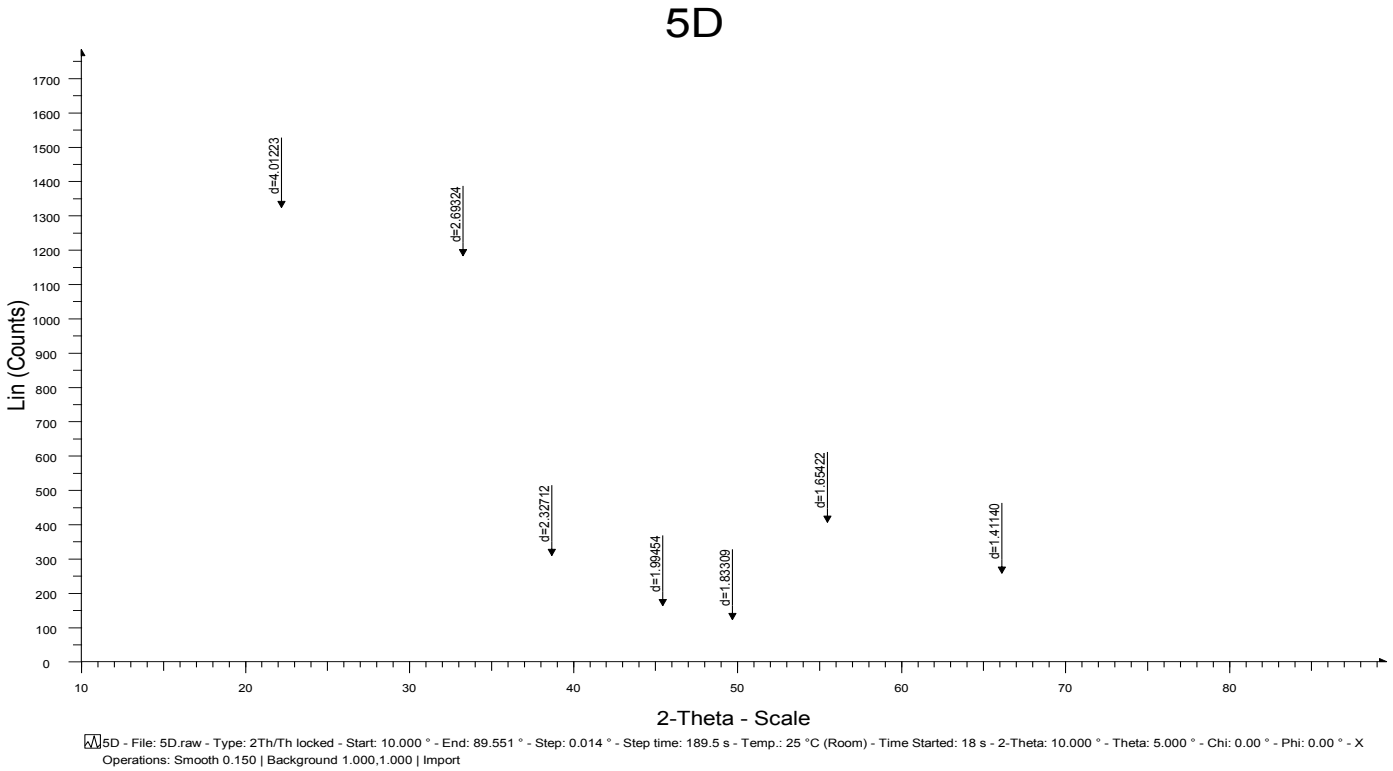

Figure A1 XRD pattern of 5D catalyst

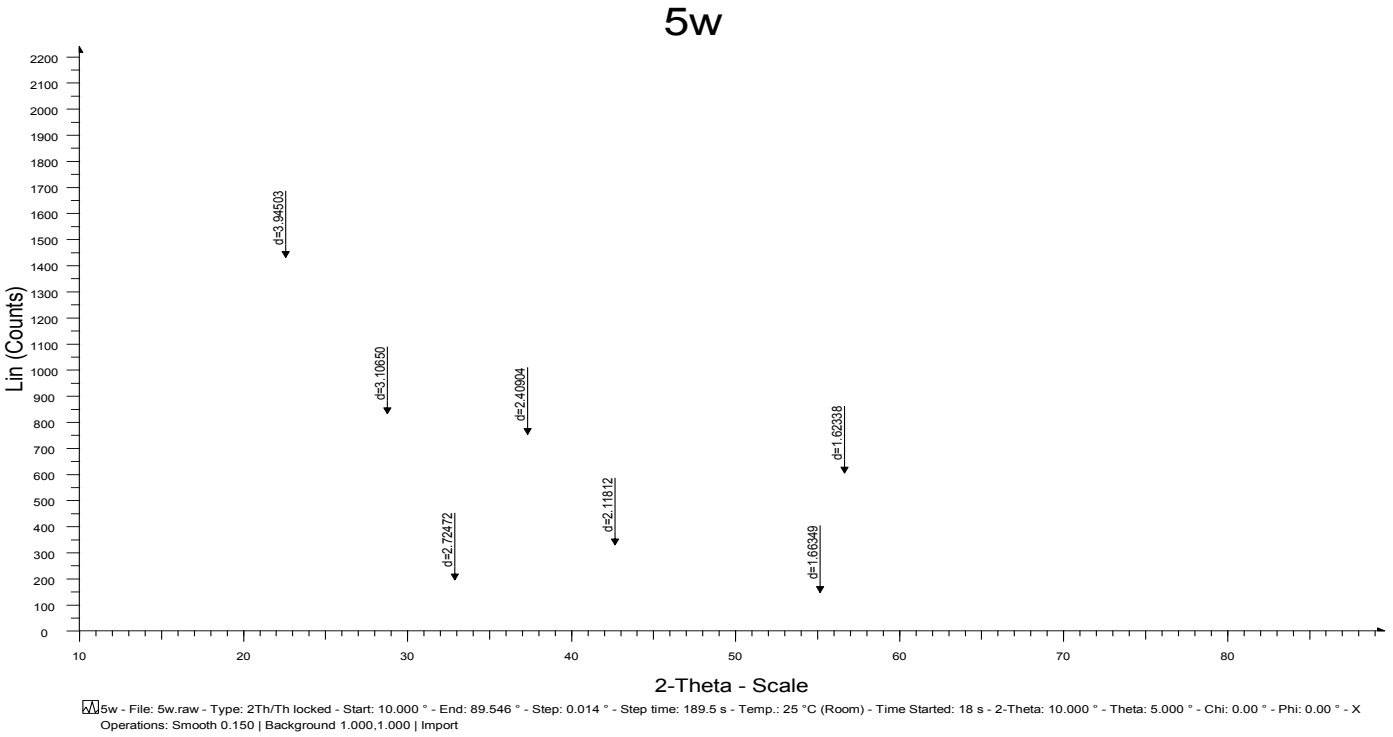

Figure A2 XRD pattern of 5W catalyst

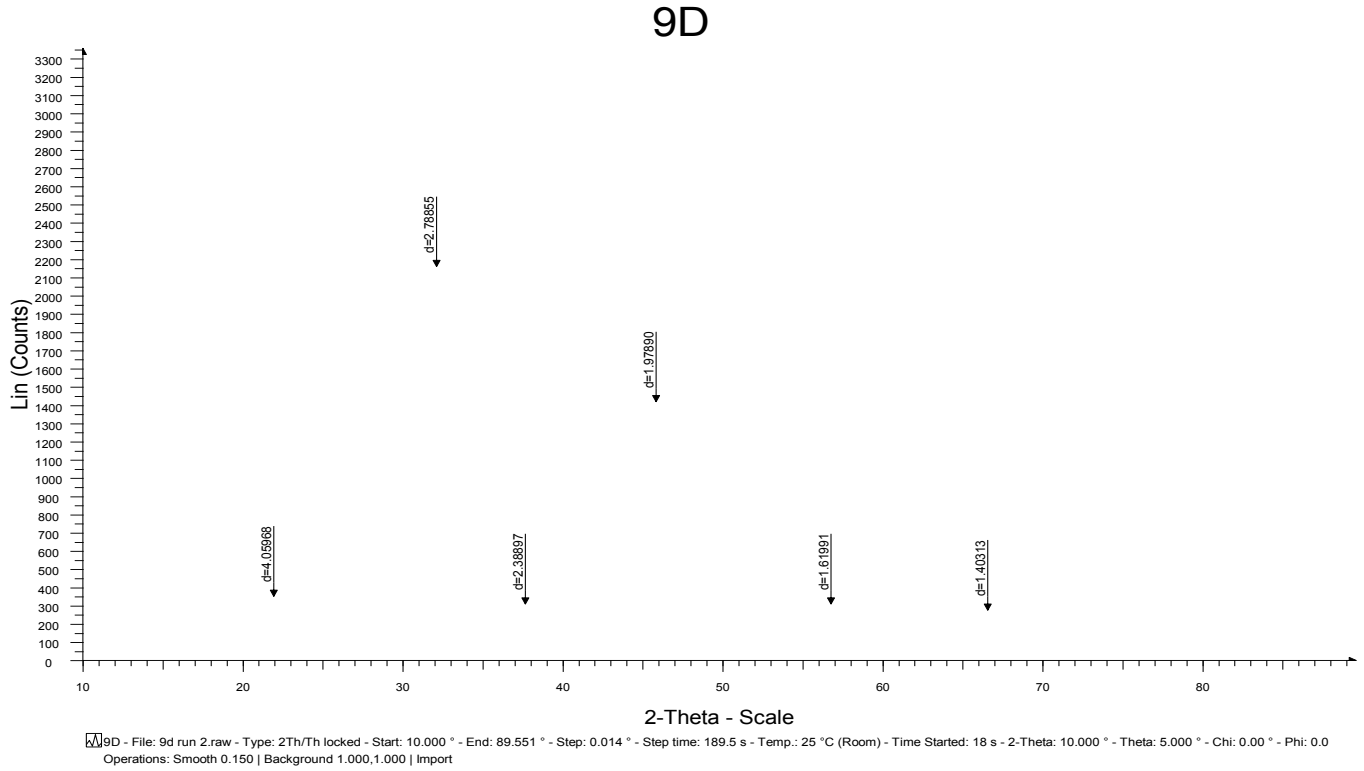

Figure A3 XRD pattern of 9D catalyst

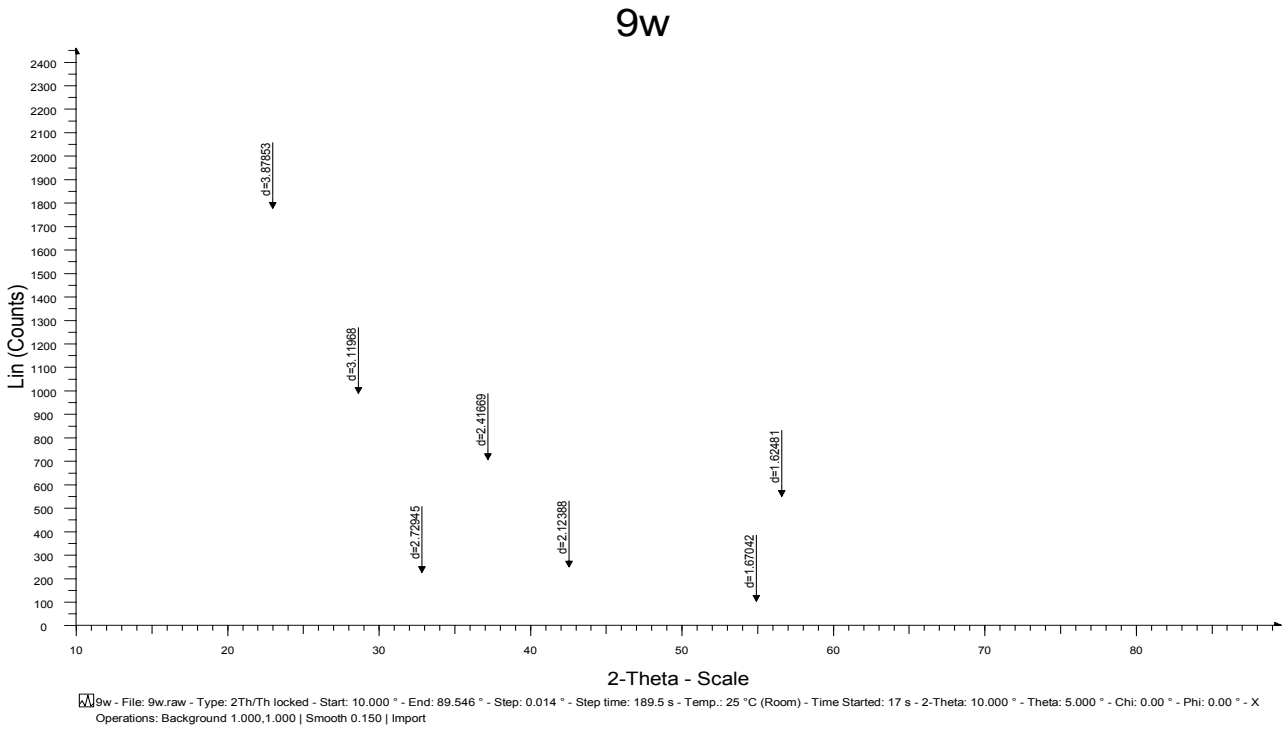

Figure A4 XRD pattern of 9W catalyst

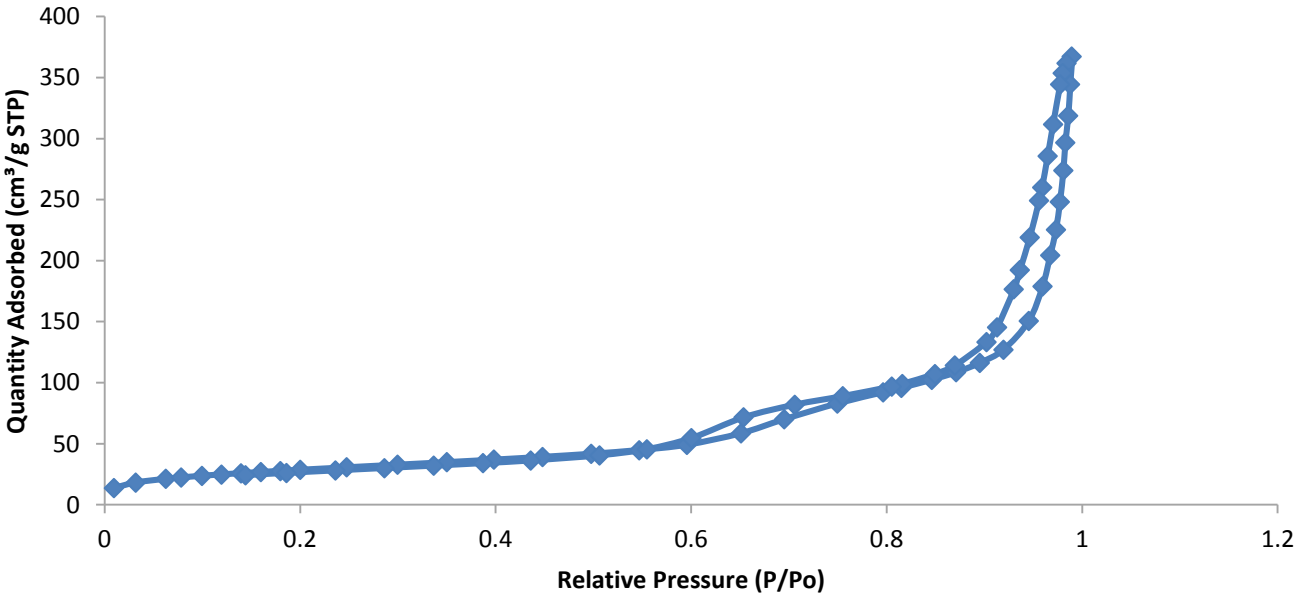

Figure A5 N_2 adsorption/desorption isotherm of 5D catalyst

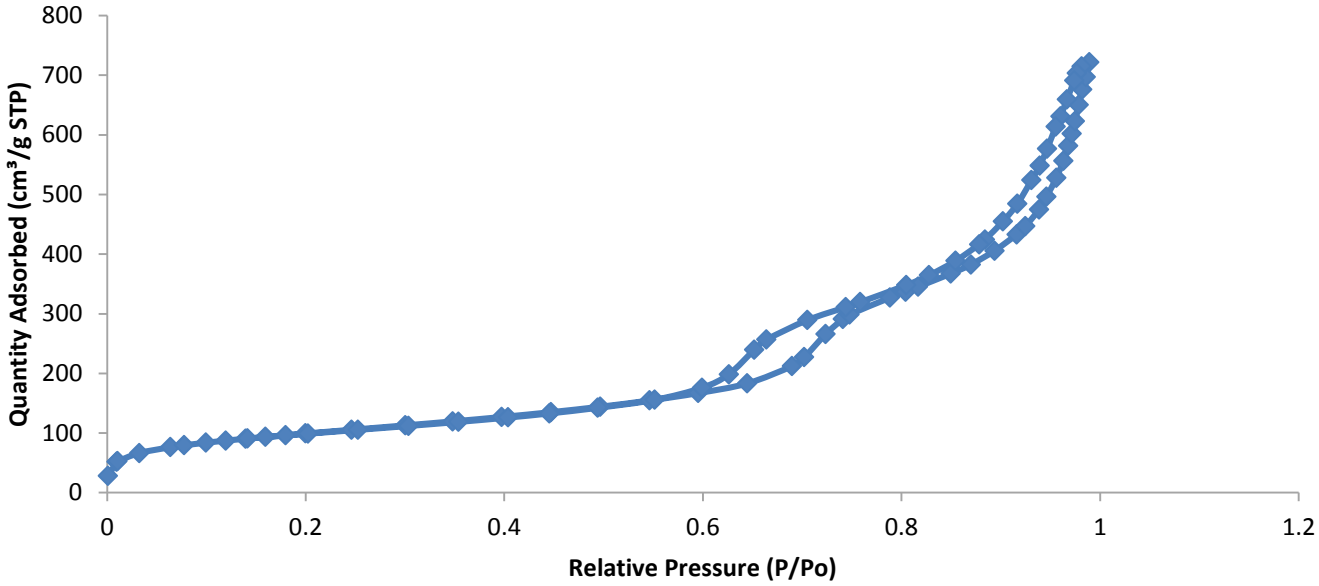

Figure A6 N_2 adsorption/desorption isotherm of 5Wcatalyst

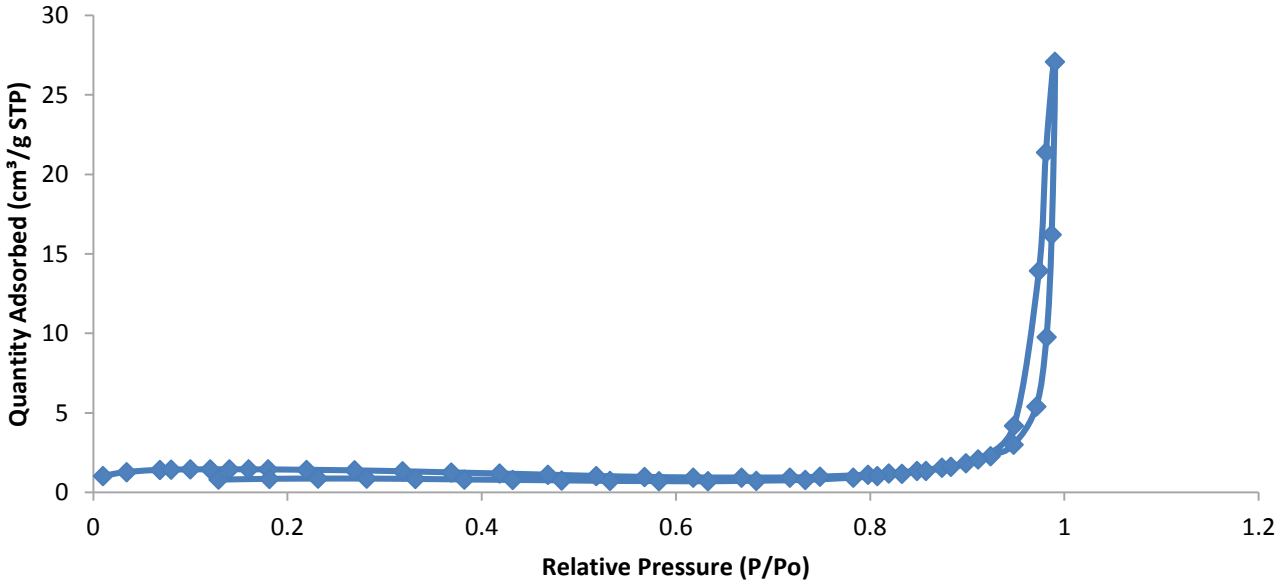

Figure A7 N_2 adsorption/desorption isotherm of 9D catalyst

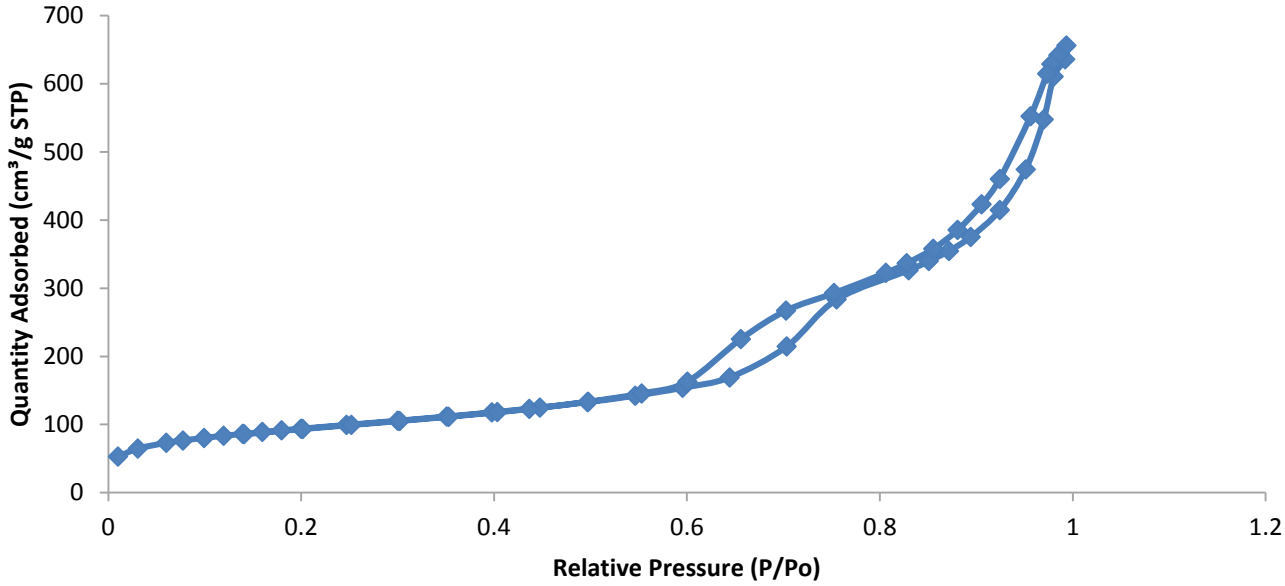

Figure A8 N_2 adsorption/desorption isotherm of 9W catalyst

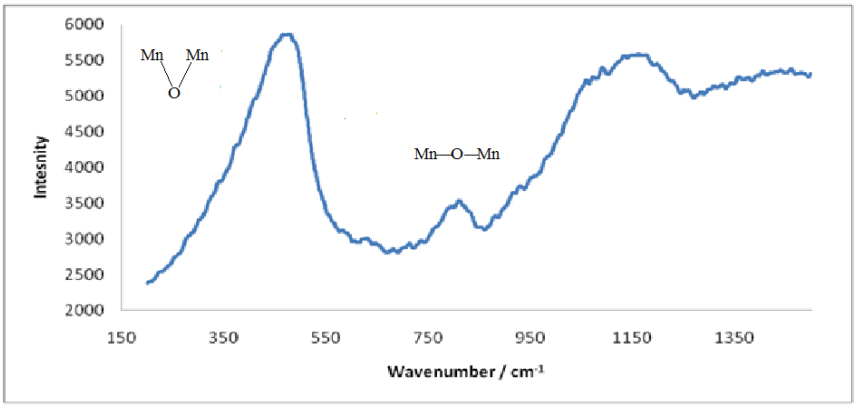

Figure A9 Raman spectrum of 2W catalyst

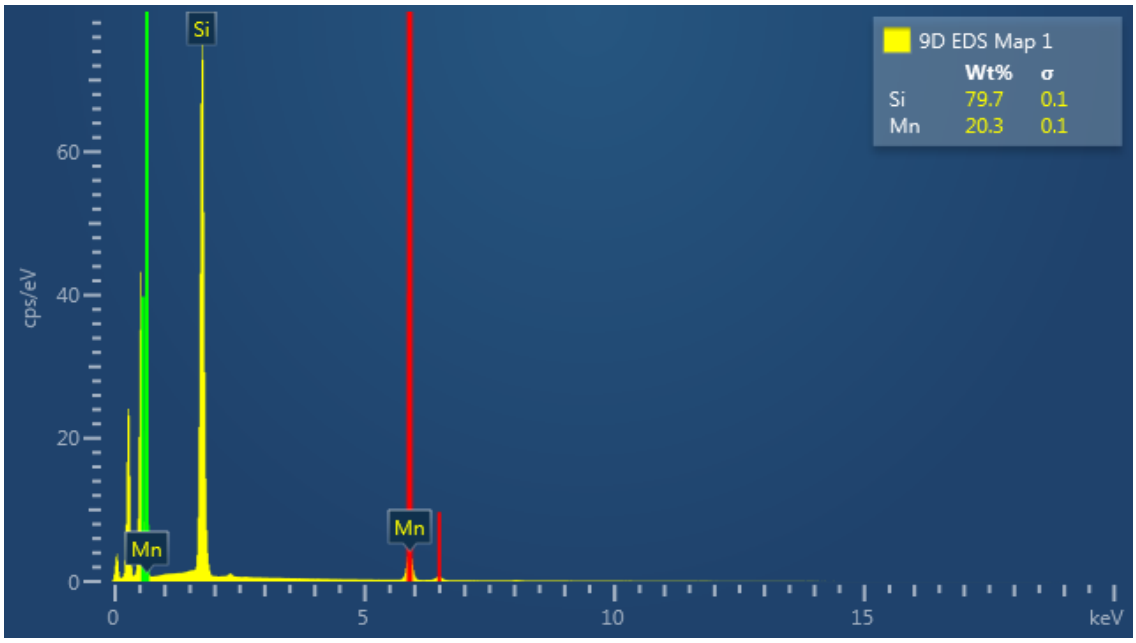

Figure A10 Electron mapping graph of 9D catalyst

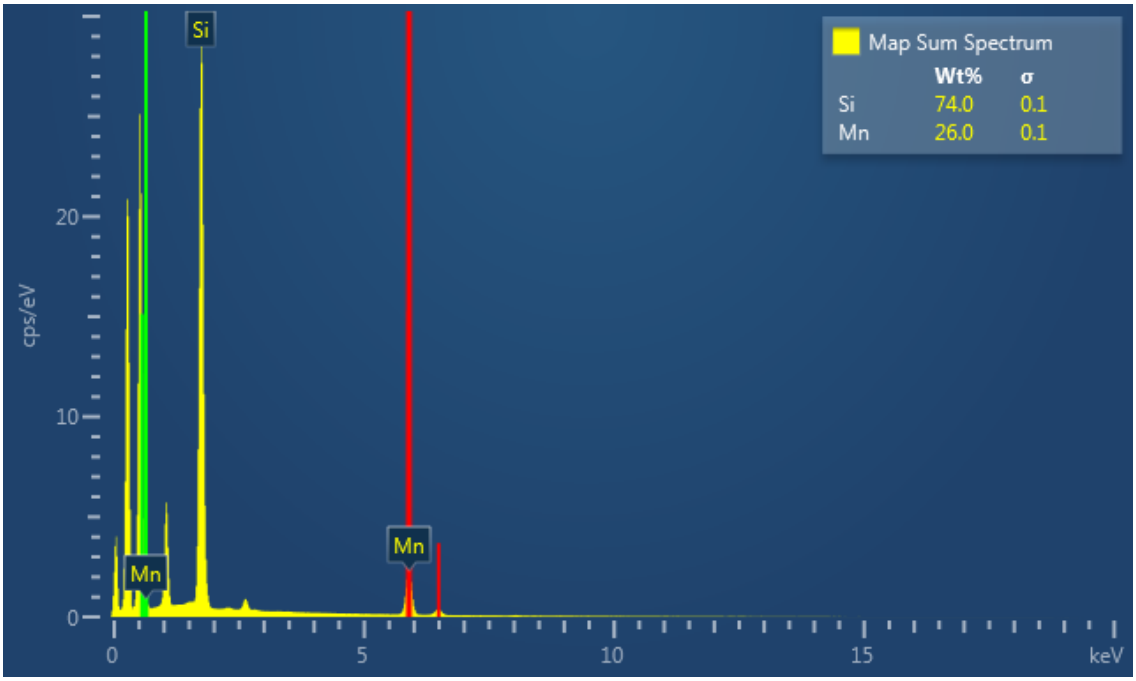

Figure A11 Electron mapping graph of 9W catalyst

Figure A12 Picture of micro-reactor set-up used

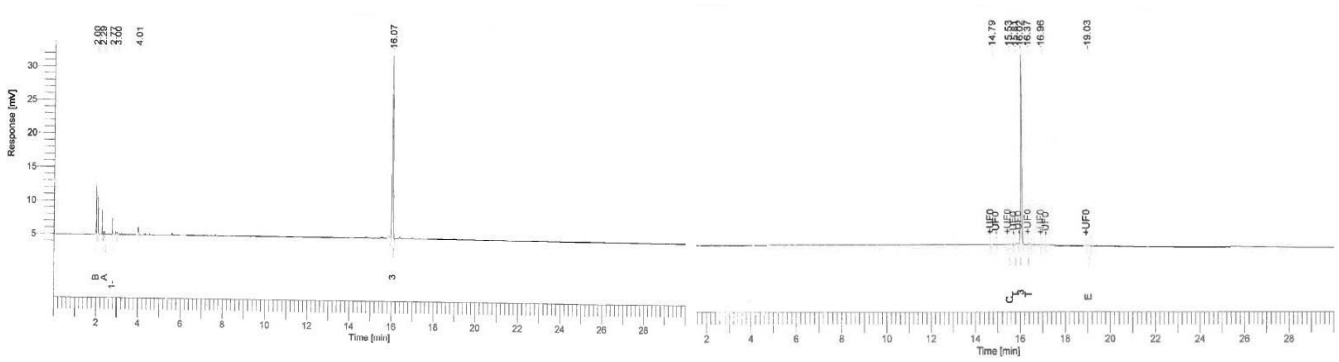

Figure A13 Sample chromatograms